TELESCOPIC IMAGING OF STREAMER AND DIFFUSE GLOW DYNAMICS IN SPRITES

A DISSERTATION
SUBMITTED TO THE DEPARTMENT OF ELECTRICAL ENGINEERING
AND THE COMMITTEE ON GRADUATE STUDIES
OF STANFORD UNIVERSITY
IN PARTIAL FULFILLMENT OF THE REQUIREMENTS
FOR THE DEGREE OF
DOCTOR OF PHILOSOPHY

Elizabeth Anna Gerken
July 2003

I certify that I have read this dissertation and that, in my opinion, it is fully adequate in scope and quality as a dissertation for the degree of Doctor of Philosophy.

Umran Inan
(Principal Adviser)

I certify that I have read this dissertation and that, in my opinion, it is fully adequate in scope and quality as a dissertation for the degree of Doctor of Philosophy.

Victor Pasko
(The Pennsylvania State University)

I certify that I have read this dissertation and that, in my opinion, it is fully adequate in scope and quality as a dissertation for the degree of Doctor of Philosophy.

Antony Fraser-Smith

Approved for the University Committee on Graduate Studies:

Dedication

to my mama,

Esther Ruth Gerken

Abstract

Telescopic imaging reveals that decameter-scale fine structures in luminous lightning-related discharges at high altitudes above thunderclouds (known as "sprites") exhibit a wide range of morphologies and time scales. Hundreds of sprites have been observed by the Stanford University telescopic imager with a field of view of $< 1°$, allowing the measurement of spatial scales of optical features as low as $\sim$10 m. Categories of observed structures include upward and downward branching, beading, propagating diffuse glow striations, transition regions between diffuse glow regions and highly structured shapes which are referred to as streamers. The telescopic imaging system used consisted of a $\sim$41 cm diameter, f/4.5 Dobsonian-mounted Newtonian reflecting telescope with an intensified CCD camera attached to its eyepiece and a bore-sighted wide field of view (FOV) camera mounted on its top. Both telescopic and wide field of view photometers were also used in some observations. The FOV of the telescope (0.5 inch CCD) was $\sim 0.7°$ by $\sim 0.92°$ while that of the bore-sighted camera (.33 inch CCD, 50 mm lens, f/1.4) was $\sim 9°$ by $\sim 12°$. The telescopic imaging system was deployed either in New Mexico or Colorado during the summers of 1998-2000. Electromagnetic signatures of causative lightning discharges, known as radio atmospherics (or sferics), were recorded simultaneously using crossed-loop magnetic antennas and ELF/VLF receivers located at Stanford and in Colorado. Telescopic images indicate that sprite structure can assume a wide variety of shapes, sizes, and time scales, but that certain structures appear repeatedly including beading, faint downward branching, bright upward branching, propagating diffuse glows, and columnar formations. Propagating diffuse glow striations are observed to move relatively slowly, exhibiting properties similar to phenomena observed in glow discharge tubes. While the sudden

appearance of highly structured formations suggest that the so-called streamers move at velocities greater than the time resolution of regular video rate imaging, some features have been determined to move at speeds as low as 10^4 m/s. Fine beading observed in many streamers may possibly be caused by meteoric dust particles in the upper atmosphere. Detailed analysis of telescopic images indicate that the so-called columniform sprites may originate from downward branching streamers. Beads at the base of columns are observed to glow for over 100 ms while slowly drifting upward. Faint downward branching streamers are found to occur at the base of large bright sprites. Some sprites which exhibit both downward branching streamers and upward propagating non-branching streamers may be double-headed streamers initiated from plasma enhancements. A transition region between streamer formation and diffuse glow is typically observed at $\sim$80 km altitude. Quantitative estimates of electrical charge moment (product of charge removed and height) in causative lightning discharges and exponential decay constants of sprite brightness are used to distinguish between diffuse glow and streamer mechanisms in a two-storm case study. Results indicate that storm geometry (e.g., the area the storm covers and cloud heights) plays a large role in the types of sprites produced.

Acknowledgements

In March 1997, at the dreary end of a long winter, I flew from university to university determined to select a graduate school. With the slush of Cleveland melting on my clothes, I arrived in the balmy greenery of Stanford. I strolled in amazement to the Durand Building through dappled sunlight dancing beneath tall slender palm trees. Once inside, I was greeted by the director of the VLF Group, Professor Umran Inan, with a broad smile and warm handshake. He immediately launched into detailing the research project he envisioned for me, namely to image high altitude lightning with a zoom lens in order to better understand the underlying physics. I could scarcely believe my ears - I could study lightning and other natural phenomena, play with video cameras, travel the world, *and* get a Ph.D.? Six years and many field trips later, I have indeed carried Umran's vision to fruition. These years at Stanford have been the most intense and grueling years of my life, but they have also been the most rewarding and I will always cherish my degrees from this institution. I didn't get to this point on my own, however, and I have so many to thank for assisting, advising and encouraging me on the way.

First and foremost I would like to thank my advisor Professor Umran Inan. His boundless enthusiasm, optimism, and energy have time and time again pushed me to reassess my perceived limitations and accomplish more than I thought I was capable of. At the same time, however, in the face of failure he has never been anything but understanding and instead of placing blame, he works to remedy the situation. I am immensely thankful for his constant support and encouragement throughout these years at Stanford. My second pillar of support at Stanford is Professor Antony Fraser-Smith who served on both my oral defense and reading committees. His door

has always been open for advice and help. The kind hospitality of Tony and Betsy Fraser-Smith helped me through many a homesick holiday on the West Coast.

I'd like to give special recognition to two ex-VLFers - Professors Victor Pasko and Steven Cummer. Victor Pasko's research has been a constant source of inspiration to me in my work (as evidenced by the numerous references to his work in this thesis). He has advised me on all my publications and has given excellent suggestions for improvement. I want to especially thank him for serving on both my oral defense and reading committees despite working a bazillion miles away as a professor at the Pennsylvania State University. The work of Steve Cummer played a major role in the interpretation of data presented in Chapter 5 of this thesis. Steve Cummer and Wenyi Hu, both of Duke University, checked the results from their charge moment model against mine and advised me on how to proceed. Both Steve and Victor have provided me with mentorship throughout my years at Stanford and I am very thankful for their kind advice and interest in my career.

My numerous field trips gathering sprites footage gave me the opportunity of being the guest at several laboratories. I spent two summers (1998 and 1999) at Langmuir Laboratory operated by New Mexico Institute of Mining and Technology in Socorro, New Mexico and am thankful to Prof. William Winn for hosting our experiment at this site. In the summer of 2000, I fielded our experiment at Yucca Ridge Field Station near Fort Collins, CO and received a great deal of support (and a bag of garlic to boot!) from our hosts Dr. Walt Lyons and Tom Nelson. In search of winter sprites, I traveled to Iitate Observatory near Sendai, Japan in the winter of 2000 with the kind support of the Tohoku University Sprites Group. I would like to especially acknowledge Prof. Yukuhiro Takahashi, Prof. Hiroshi Fukunishi, Mitsuteru Sato, and Rina Miyasato for their help in this campaign.

The skills necessary for successful field campaigns are not learned in books and papers and I have many to thank for sharing their knowledge with me. My steepest learning curve as a new graduate student was overcome primarily through the aid of Dr. Christopher Barrington-Leigh and Dr. Mark Stanley. It was from Chris that I learned the basics of low-light-level imagery and data analysis. Mark's coaching during my first summer of sprite hunting proved to be invaluable training and it was

from him that I learned the importance of patience and persistence in this field. Dr. Rick Rairden (Lockheed Martin) has been a constant source of support throughout my graduate career. He has supplied us with intensifier tubes, cameras, and monitors and has assisted in calibrating our equipment on multiple occasions. Dr. Stephen Mende (University of California, Berkeley) provided excellent advice in the design stages of our optical experiments and collaborated on data analysis. I am very grateful to Drs. Ken Cummins and John Cramer (Vaisala-GAI, Inc.) for supplying National Lightning Detection Network data on multiple occasions which allowed me to estimate the altitude of observed sprites.

I have been fortunate to work with an amazing group of people in STAR Laboratory - the VLF Group. This network of friends has celebrated my successes and comforted me in the face of failure. I can always count on a smile and a word of encouragement (tempered by a healthy bit of teasing) when I enter the office. I'd like to thank each and every member of the VLF Group. A number of VLFers assisted me on field campaigns and in data analysis and I would like to especially acknowledge Maria Spasojevic, Timothy Chevalier, Robb Moore, Troy Wood, and Bob Marshall. Bill Trabucco taught me how to use the tools in the machine shop, designed many a component for the telescopic imager and introduced me to Fort Collins' delectable Walrus Ice Cream. Jerry Yarbrough tirelessly searched through VLF antenna recordings to digitize sferics for me. Drs. Timothy Bell and Martin Walt graciously read through this dissertation. My anchor in the VLF Group is Ms. Shaolan Min. Not only has she come to my aid countless times in the office, but she also provided the social structure which knitted our group together by organizing numerous parties and events.

Last, but definitely not least, I'd like to acknowledge my dear friends and family across the country and around the world. Their support and encouragement kept me from giving up when the end of the tunnel seemed so far away. I'd like to thank my church family at St. Luke Lutheran in Sunnyvale for numerous prayers. As I prepared my defense and wrote this dissertation John Kendall stood by me with patience and understanding and even managed to sometimes coax me away from my computer for much needed breaks during times of great stress. My brother, Ted, has

been my sounding board throughout my college life and has listened with good humor to my venting through many a phone call. I cannot imagine what it would have been like to finish grad school without my sister and roommate, Millie. She assisted me in the field in both Colorado and Alaska. She machined components for the telescopic system, typed up customs forms, provided the refreshments for my defense, packed boxes with campaign equipment, sat through my practice talks and much more. And finally I want to thank my mother, Esther. I honestly cannot contain in words the importance of her love in my life. Not a day goes by when I don't share with her my worries, fears, hopes, and dreams. This dissertation is dedicated to my mama.

Solo Deo Gloria

Elizabeth Anna Gerken
Stanford, CA
July 31, 2003

This research was made possible through fellowships from the National Science Foundation (NSF) and the Stanford Graduate Fellowship Program. The telescopic system was built and fielded through the support of Office of Naval Research (ONR) Grant N00014-94-1-010 and NSF Grant ATM 9908766. ELF/VLF measurements at Stanford were supported by ONR Grant N00014-92-5-1576.

Contents

List of Figures

Chapter 1

Introduction

1.1 The role of lightning in Earth's environment

The spectacular electrical discharges that we know as lightning and which occur within thunderclouds or between clouds and the ground have captured human imagination throughout the ages. The roll of thunder and the flash of lightning demonstrate the might and power of the natural world we live in and reveal our frailty in its presence. Many cultures have historically viewed thunder and lightning as instruments of the gods. Horror stories and tales of woe are inevitably set in the midst of a raging thunderstorm. With the lore of lightning so firmly implanted in our society, it is rather remarkable that many properties of lightning are still not well-understood and that in fact, dramatic new discoveries continue to be made every year.

Lightning is the longest electrical spark discharge observed on Earth. Similar to the electrical spark one sees when reaching for a doorknob on a dry day, lightning results from the creation of a short circuit between a charged thundercloud and the ground. This short circuit effectively neutralizes the thundercloud and thus reduces the energy of its associated electric field. Lightning begins as a set of "leaders" reaching down from the charged thundercloud and up from the ground [*Uman,* 1969, pg. 5]. These leaders are channels of enhanced conductivity, which allow current to flow more freely than in the surrounding insulating air. When the leaders from the thundercloud and the ground meet, a short circuit is created and a "return stroke"

occurs in which a high current quickly travels through the channel. This current generates a high temperature causing a bright flash of light and an acoustic pressure wave (thunder). This return stroke can be rapidly followed by multiple other strokes, which the observer sees as a flickering within the channel. While it is the electrons that carry charge in a lightning channel, thundercloud charge can be effectively raised or lowered. The raising or lowering of the number of electrons in the cloud is known respectively as a positive cloud-to-ground lightning stroke (+CG) or a negative cloud-to-ground lightning stroke (−CG). For more detailed information on lightning, see *Uman* [1969].

Thunderstorms and lightning charge the atmosphere and counteract the "fair weather" electrical field between the ground and the electrosphere (DC conducting region of the upper atmosphere at 25 - 65 km altitude) [*Kraus,* 1992, pg. 98]. Under fair weather conditions, ions drift and a current flows from the upper atmosphere to ground. Large cumulo-nimbus thunderclouds act as huge wind-powered Van de Graff generators, which recharge the Earth-electrosphere capacitor through positive ion migration to the upper atmosphere and −CG's. Without thunderstorms, the fair weather field would drain the Earth-electrosphere capacitor in less than an hour [*Kraus,* 1992, pg. 211]. In this way lightning is an important contributor to the global circuit.

Lightning is observed not only by its optical flash and acoustic wave, but also by means of its electromagnetic signature. A lightning channel can be viewed as a large impulsive antenna radiating over a wide range of frequencies [*Uman,* 1969, pg. 61]. In the Very High Frequency (VHF) range, the antenna consists of a number of short dipoles generated by the tortuous path to ground of the leader. In the Very Low Frequency (VLF), Extra Low Frequency (ELF), and Ultra Low Frequency (ULF) range the antenna can be thought of as a simple vertical dipole that radiates impulsively. The electromagetic pulse (EMP) radiated by lightning discharges is often referred to as a radio atmospheric or simply as a "sferic". Sferics can be observed around the world as the VLF wave propagates with little loss in the Earth-ionosphere waveguide. Schumann resonances are observed in ULF range as the entire Earth-ionosphere waveguide cavity resonates in response to continued excitation by globally

occurring lightning discharges [e.g., *Füllekrug et al.,* 1996]. Lightning-generated VLF waves can also escape upward through the ionosphere and lightning-generated whistler waves interact with energetic particles of the radiation belts causing precipitation of energetic electrons out of the radiation belts [*Burgess and Inan,* 1993, and references therein].

Optical flashes and flickers over thunderstorms are frequently observed and can often be attributed to various types of Rayleigh scattering of light emitted in CG discharges. In the early 1990's, however, electrical discharge mechanisms that operate at high altitudes above thunderstorms were discovered [*Franz et al.,* 1990]. These luminous discharges have now been broadly categorized as "sprites", "elves", and "blue jets". If accumulated charge in a thundercloud is quickly lowered to the ground by a +CG, a quasi-electrostatic (QE) field can be set up between the thundercloud and the ionosphere, which can in turn produce a subsequent discharge at high altitudes (where the air is thin enough), referred to as a sprite produced by the heating of ambient electrons by the QE field [*Pasko et al.,* 1996]. The EMP from lightning can cause intense heating of ambient electrons when it reaches the lower ionosphere leading to the production of a rapidly expanding ring of brief flashes of light, or an elve [*Inan et al.,* 1997]. Inhomogeneities within a highly charged thundercloud can sometimes lead to the production of intense electric fields, causing streamers to form and propagate directly upward from the cloud top for tens of kilometers, referred to as blue jets. While substantial progress has been made during the past decade in advancing our understanding of these luminous phenomena, many properties of these high altitude discharges are still not explained by current theories and new phenomena continue to be discovered [*Pasko et al.,* 2002b; *Su et al.,* 2003].

1.2 Lightning-related transient luminous events

1.2.1 Sprites

Sprites are large luminous lightning-related discharges that appear in the altitude range of ∼40 km to 90 km above thunderstorms [e.g., *Sentman et al.,* 1995]. A

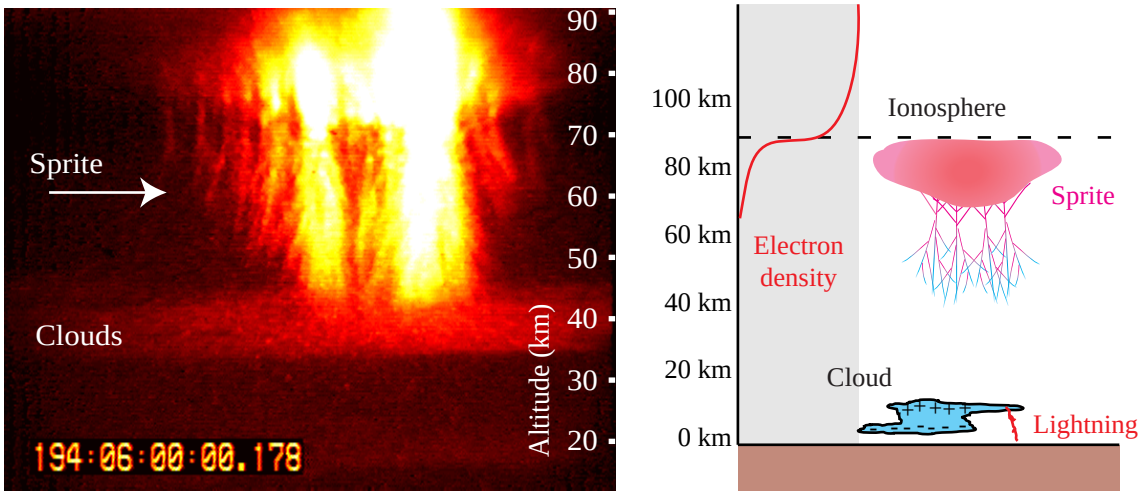

Figure 1.1: The lefthand panel shows an image of a large sprite over Northern Mexico. A schematic diagram of a sprite above a thundercloud is shown in the righthand panel. Sprites are electrical discharges that occur in the region between the lower ionosphere and the thundercloud.

large sprite observed over Mexico by a Stanford University camera in the summer of 1998 is shown in Figure 1.1. It is generally accepted that the dominant mechanism involved in sprite production is the quasi-static electric field between the clouds and the ionosphere, caused by the occurrence of a cloud-to-ground lightning stroke [*Pasko et al.,* 1997]. Sprite-producing thunderstorms are typically large meso-scale convective systems [*Lyons,* 1994] although it is also possible for a small thunderstorm to also produce sprites (see Chapter 5).

The majority of sprites are caused by positive cloud-to-ground lightning strokes (+CGs) with only a few documented examples of −CG sprites [*Barrington-Leigh et al.,* 1999]. The effective charge structure in a thunderstorm cloud is mainly that of an electrical dipole with net negative charge at the base and net positive at the top [*Uman,* 1969, pg. 2]. Since the negative charge is closer to the ground, most CGs in a storm are thus negative. As the storm decays, however, the top part of the cloud falls and positive charge is brought closer to the ground, resulting in the production of positive CGs at a higher rate. Sprites are generally observed at the end of a thunderstorm when the positive CG rate is higher. When charge is removed from

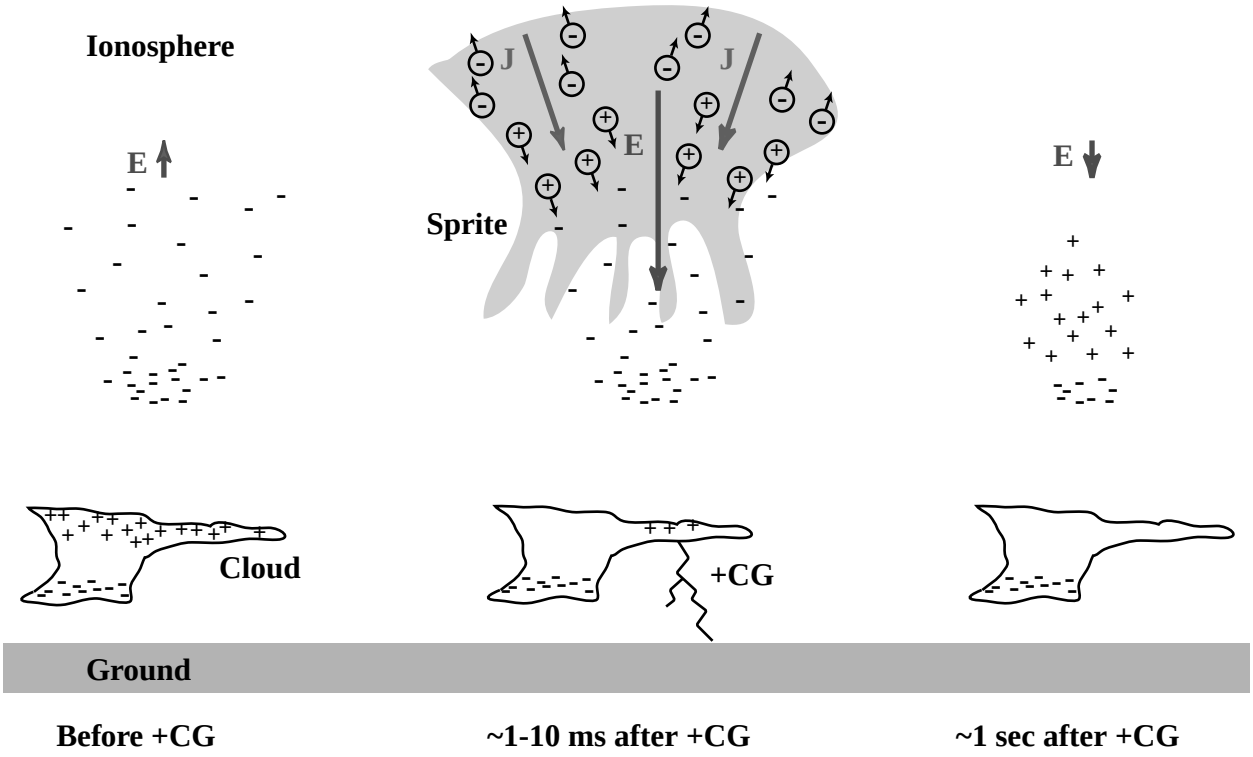

Figure 1.2: Schematic diagram of charge configurations in sprite-producing thundercloud [*Pasko et al.,* 1997]. Initially the thundercloud is effectively a vertical dipole with positive charge on top and negative charge on the bottom. The ions and electrons in the overlying mesosphere and lower ionosphere are distributed so as to cancel the electric field created by the thundercloud dipole. When a +CG occurs and positive charge is removed from the cloud, a subsequent breakdown, or sprite, can occur above the thundercloud. Following the sprite, the electrons and ions rearrange to once again reduce the electric field existing above the cloud.

the cloud during a positive CG discharge, a downward-directed electric field is set up between the cloud and the ionosphere. This electric field exists only temporarily and is essentially produced due to the fact that while the thundercloud is now in a monopole charge configuration, the polarization charge at higher altitudes is still distributed so as to shield the pre-discharge dipole configuration [*Pasko et al.,* 1997]. The imposed electric field persists until the polarization charge is rearranged, typically over tens to hundreds of milliseconds. If this field is strong enough, heating of ambient free electrons may occur above the thundercloud before the mesospheric electrons and ions have time to rearrange and neutralize this "quasi-static" electric field [*Pasko et al.,* 1997]. The heating of electrons can cause luminous glows and streamer discharges which are observed as a sprite (see the schematic diagram in Figure 1.2).

Global sprite campaigns show that properties of sprites are quite similar worldwide [*Neubert et al.,* 2001; *Hardman et al.,* 2000]. Observations using video recordings have revealed the existence of fine structure in sprites, including upward and downward branching and beads [*Sentman et al.,* 1996; *Taylor and Clark,* 1996; *Stanley et al.,* 1996; *Fukunishi et al.,* 1996b; *Gerken et al.,* 2000]. High speed imaging of sprites has captured the temporal development of some of the fine structures seen in sprites such as the upward and downward branching and slowly moving beads [*Stanley et al.,* 1999; *Stenbaek-Nielsen et al., 2000*], revealing that in general sprites are initiated as columns with downward branching at their bases followed by upward branching from the column. Spectral observations suggest that some sprites may exhibit strong ionization while others do not [*Armstrong et al.,* 2000] although this conclusion needs to be tempered by the fact that the ionization lines (e.g., the 487.2 nm line of N_2^+) are much harder to observe from the ground. The telescopic observations reported in this thesis show the prevalence of fine structure, which indicates the presence of streamers, and thus by implication ionization. Observations of the ionized and neutral N_2 (nitrogen) emissions show that there is a boundary at 55 km above which the characteristic electron energy in sprites is $\sim$1.75 eV while that below is $\sim$2.2 eV. Electromagnetic recordings show sprite-associated signatures in the VLF, ELF, and ULF frequency bands [*Cummer et al.,* 1998; *Reising et al.,* 1999; *Füllekrug et al.,* 1998] indicating that the electrical currents that flow within the body of the sprite

produce electromagnetic emissions.

A diffuse glow region has been observed to occur in the upper altitudes ($\sim 70-85$ km) of sprites [*Barrington-Leigh and Inan,* 2001; *Wescott et al.,* 2001; *Pasko and Stenbaek-Nielsen,* 2002; *Gerken and Inan,* 2002]. This diffuse glow region may exist independently or either precede or accompany the streamer formation region at lower altitudes. The diffuse glow region, or "sprite halo", and the streamer formation region are able to exist independently due to the strong altitude variation of the timescale for electrical relaxation of the post-lightning quasi-electrostatic field above thunderclouds [*Barrington-Leigh and Inan,* 2001].

Telescopic imaging of sprites reveals fine structure covering a wide range of features, which are primarily vertically-oriented but which are also sometimes slanted at varying degrees, including branching tree-like shapes and well defined but isolated columns [*Gerken et al.,* 2000]. Theoretical explanations of observed spatial fine structures and diffuse glow in sprites were put forth in the context of a streamer-based model of electrical breakdown above thunderstorms [*Raizer et al.,* 1998; *Pasko et al.,* 1998]. Characteristic structure widths for each altitude have been predicted, ranging from ∼10 m at 70 km to ∼100 m at 85 km [*Pasko et al.,* 1998]. It may also be possible to account for the fine structure in sprites by modeling the tortuous path of cloud-to-ground lightning as a fractal antenna resulting in a highly non-uniform radiation pattern at sprite altitudes [*Valdivia et al.,* 1997]. Fractal techniques have additionally been applied to streamers in sprites as a means of predicting general shapes of bulk sprite volumes [*Pasko et al.,* 2000; *Petrov and Petrova,* 1999].

1.2.2 Elves and blue jets

Considerations of lower ionospheric heating effects produced by intense EMP's radiated by lightning discharges led to the prediction of optical emissions at ionospheric heights above thunderstorms [*Inan et al.,* 1991; *Taranenko et al.,* 1992; *Taranenko et al.,* 1993]. The first observations of such an optical signature were reported in 1995 by Tohoku University using a vertical photometer array [*Fukunishi et al.,* 1996a]. Lasting less than 1 ms, these optical emissions, called "elves", followed the observation of

Rayleigh scattered light from the causative CG and preceded that of sprites. In 1996, a new horizontal photometer array was deployed by Stanford University. This horizontal array, called the Fly's Eye, provided the first measurement of the rapid lateral expansion of elves which was found to be consistent with that expected based on heating of the lower ionosphere by the EMP of a lightning discharge [*Inan et al.,* 1997]. Elves can be triggered by both positive and negative lightning discharges and may typically have lateral extents of $200 - 700$ km [*Barrington-Leigh et al.,* 1999]. A two-dimensional model combining the effects of the EMP and the quasi-electrostatic field has been used to predict the optical emissions of various lightning current waveforms [*Veronis et al.,* 1999].

In contrast to the elusive elve, which was first predicted and then searched for, "blue jets" emanating from cloud tops were sighted by ground-based observers and airline pilots for many years before a theory was developed [*Lyons et al.,* 2003]. Blue jets were captured serendipitously in video and classified as a lightning-related phenomenon during the Sprite94 airborne campaign over the central part of the U. S. [*Wescott et al.,* 1995]. Fifty-six blue jets were observed in a 22 min interval over a storm in Arkansas. Blue jets are primarily blue with a brightness of ∼500 kR, are highly collimated with a fan out near the top (40 - 50 km), propagate at ∼100 km/s, last for 200 - 300 ms, and are often observed to follow upward lightning strokes [*Wescott et al.,* 1995].

Pasko et al. [1996] model blue jets as positive streamers emanating from the thundercloud top, predicting an upward propagation velocity of ∼100 km/s and a stopping altitude of ∼50 km in good agreement with observations. A streamer model inherently accounts for the blue color of jets as emission from $N_2$2P excited by electron impact [*Pasko et al.,* 1996]. Blue jets can also be modeled as a negative streamer-like ionization wave propagating up from the cloud and initiated by an inhomogeneity such as a dendritic lightning channel [*Sukhorukov et al.,* 1996]. A negative streamer theory similarly predicts a height-independent velocity of ∼100 km/s and a terminal altitude of $40 - 50$ km. While *Sukhorukov et al.* [1996] requires a strong intracloud discharge to initiate the negative streamer, *Pasko et al.* [1996] proposes that positive streamers can be driven by a fast accumulation of positive charge in the top

of the thundercloud with no associated lightning discharge. Three-dimensional fractal modeling based on a phenomenological probabilistic approach to the modeling of streamer coronas predicts terminal altitudes, volumes, and cone angles which are consistent with blue jet observations [*Pasko and George,* 2002]. The fractal model additionally provides a means of distinguishing between blue jets and the so-called "blue starters" [*Wescott et al.,* 1995] (similar to blue jets but smaller and with lower terminal altitudes) based on the amount of charge accumulated at the thundercloud top [*Pasko and George,* 2002]. Blue jets are calculated to create a local perturbation of the content of nitric oxide and ozone by ∼10% and ∼0.5% respectively at 30 km [*Mishin,* 1997].

In September 2001, an unusual electrical discharge from a thundercloud top to the lower ionosphere was recorded near Puerto Rico [*Pasko et al.,* 2002b; *Lyons et al.,* 2003]. This event appears to be a combination of a sprite and a blue jet with a boundary observed at 42 km altitude. Thus far six of these so-called "gigantic jets" have been observed both from Puerto Rico and Taiwan [*Su et al.,* 2003]. Since all six were observed over oceans, it is likely that gigantic jets are a special feature of oceanic thunderstorms [*Su et al.,* 2003]. It may also be possible that this is a tropical phenomenon due to the typically lower conductivity profile at these latitudes that allows the quasi-electrostatic thundercloud fields to reach higher altitudes [*Pasko et al.,* 2002].

1.2.3 Geomagnetically conjugate effects

Observations of gamma ray bursts above thunderstorms [*Fishman et al.,* 1994; *Inan et al.,* 1996] have prompted the development of a theory of runaway electron production via electron acceleration by quasi-electrostatic fields above thunderstorms following strong lightning flashes [*Lehtinen et al.,* 2001]. The gamma ray bursts were recorded by the Burst and Transient Source Experiment (BATSE) detectors on the Compton Gamma Ray Observatory (CGRO), a low-earth orbit satellite [*Fishman et al.,* 1994]. It is proposed that free MeV electrons (possibly seeded by cosmic ray showers)

undergo runaway acceleration and avalanche to form a beam of relativistic electrons that then travel upward along the intense electric field at lower altitudes and along the earth's magnetic field lines at higher altitudes. When these electrons pass near the nuclei of the atmospheric constituents, gamma rays are generated through bremsstrahlung radiation which then reach the satellite after undergoing Compton scattering and attenuation [*Lehtinen et al.,* 2001]. The detection of gamma rays above thunderstorms is strong evidence of runaway processes occurring above the cloud. The runaway electrons can create optical emissions and contribute to sprite luminosity as they travel upward through the atmosphere. However, the levels of optical emissions are found to be much smaller than those generated through conventional breakdown processes leading to the heating of the much larger number of ambient electrons and thus would be indiscernible in the sprite optical data [*Lehtinen et al.,* 2001].

Once generated, the runaway electron beam travels along the magnetic field lines to the opposite hemisphere. Some of these electrons precipitate in the conjugate hemisphere and others bounce back along the field lines. The precipitated electrons generate detectable optical emissions through collisions with neutral atmospheric particles in the conjugate region [*Lehtinen et al.,* 2001]. These conjugate emissions have been termed "purple sprites" in reference to the fact that both blue and red nitrogen lines would be equally excited. Although geomagnetically conjugate optical emissions have not yet been detected, their observation would verify the model predictions and reveal a new type of a global impact of lightning discharges and sprites on the particle populations of the magnetosphere in the form of a source of trapped energetic electrons.

1.3 Scientific contributions

The purpose of the research described in this Ph.D. dissertation was to study the fine structure in luminous high-altitude lightning-related electrical discharges known as "sprites". The experiment on which the study is based is detailed in Chapter 2 and the scientific contributions resulting from the study are described in Chapters $3-5$. Specific contributions to knowledge can be summarized as follows:

- First telescopic images of fine structure in sprites.
- Quantitative measurements of streamer widths at sprite altitudes. Quantification of observed differences between positive and negative streamers in sprites.
- Identification of propagating diffuse striations in streamer regions.
- Comparison of charge moment estimates and photometry records for two storms. Utilization of optical decay constants to distinguish between diffuse glow and streamer processes.
- High-resolution observations of beads in sprites with lifetimes ranging from $\sim 17 - 240$ ms and $\sim 20 - 250$ m in radii.

Most of the results presented in Chapters 2-4 were previously published in *Gerken et al.* [2000], *Gerken and Inan* [2002], and *Gerken and Inan* [2003].

Chapter 2

Telescopic imaging of sprites

The initial observations of sprites were conducted using relatively wide field of view (FOV) low-light level cameras. Occasionally during these early observations sprite events happened to occur at close range, revealing the presence of fine structure down to the resolution of the video images, i.e., a few hundred meters [*Sentman et al.,* 1996; *Taylor et al.,* 1996; *Stanley et al.,* 1996; *Fukunishi et al.,* 1996]. In order to determine the nature of this fine structure, to measure its features at substantially higher resolution, and to verify predictions of smallest feature sizes of a few tens of meters, Stanford University developed a telescopic imaging system. Initially termed "The Dobsonian Sprite Experiment", this system allowed the acquisition of telescopic images of hundreds of events, recorded during the summers of $1998 - 2000$.

2.1 Instrumentation

2.1.1 System description

The telescopic imaging system initially consisted of two intensified low light level cameras - one having a wide field of view (FOV) and another having a telescopic FOV - but was enhanced in subsequent years of operation to also include wide FOV and telescopic photometers. A photograph of the system and a schematic diagram are shown respectively in Figures 2.1 and 2.2.

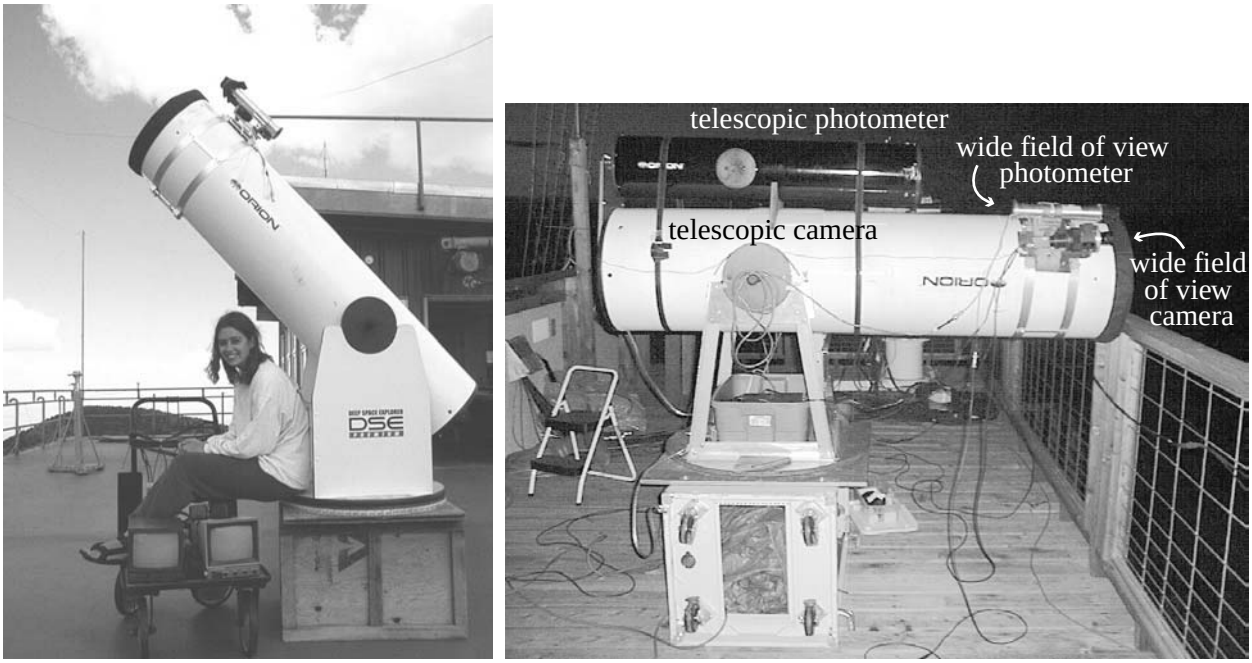

Figure 2.1: Stanford University telescopic imager. This system was used to record high-resolution images in four sprite campaigns between 1998 – 2001, the conduct of and the analysis of the data from which formed the basis for this dissertation.

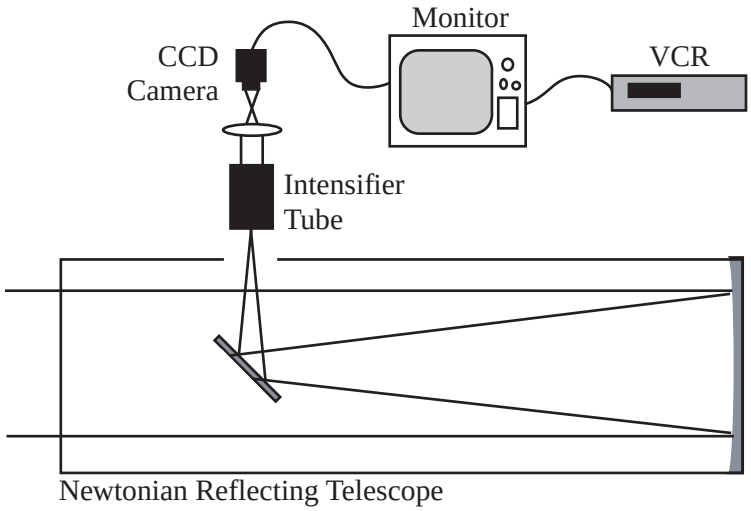

Figure 2.2: Schematic diagram of the telescopic imaging system.

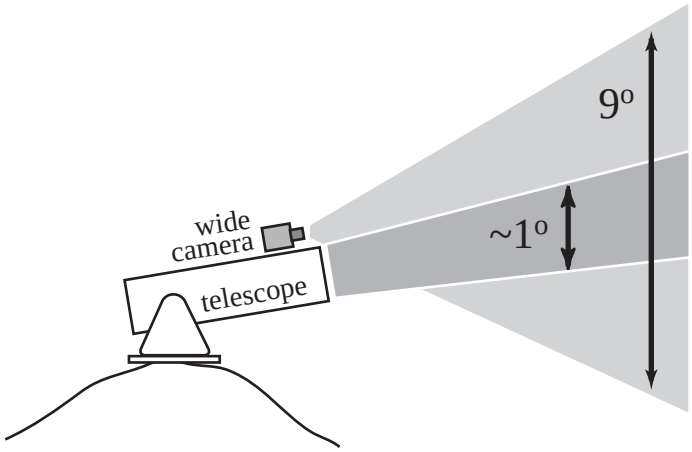

Figure 2.3: Fields of view (FOV) for the telescopic and wide FOV cameras.

Both of the video cameras used are intensified charge-coupled devices (ICCD's). In the first campaign (1998) the wide FOV camera consisted of an integrated ICCD system - purchased from S.T.A.N.O. Components, Inc - which consisted of an 18 mm second generation multi-channel plate and a 1/3 in CCD. The telescopic camera uses a Varo second generation (GenII) multi-channel plate intensifier tube and a Pulnix TM200 1/2 in CCD. After the first campaign the wide FOV camera system was replaced by the same Varo/Pulnix system as the telescopic camera. The Pulnix cameras are run in a field-selected mode, creating images exposed for ∼17 ms while the S.T.A.N.O. camera was run in interlaced frame mode creating images exposed for ∼33 ms.

An unfiltered 50 mm, f/1.4 lens is used for the wide FOV camera generating an angular viewing region of ∼9° by 12°. The narrow FOV camera is attached to the eyepiece of a ∼41 cm diameter, f/4.5 Dobsonian-mounted Newtonian reflecting telescope and has an angular viewing region of ∼0.7° by 0.92°. The wide FOV camera is strapped onto the telescope and bore-sighted as shown in Figure 2.3. Data from both cameras is stored on VHS or S-VHS video tapes using standard VCR equipment.

While the low light level telescopic ICCD can capture high spatial resolution images of transient phenomena, the ∼17 ms duration of the video fields does not allow the recording of images with high temporal resolution. Ideally, it would be desirable

to use the telescope together with a high-speed intensified camera (e.g. 1000 fps) however no such camera was available to Stanford during the period of observations. In lieu of having a high speed camera, two photomultiplier tubes (PMT's) were used in conjunction with the telescopic imager in the two most recent campaigns. These PMT's effectively act as single pixel high speed "imagers". The tubes are Hamamatsu HC-124-01 PMT's and have photocathodes, which are sensitive to photons between 185 nm and 800 nm wavelength. One PMT is encased in a metal tube with a single compound lens giving the tube an FOV of ∼3.3° by 6.6°. This wide FOV PMT is longpass filtered with a cutoff of ∼650 nm in order to provide a better signal-to-noise ratio for the observation of excitation in sprites, namely the N2 first positive band around 700 nm. The second PMT is used for telescopic view and is attached to the eyepiece of a Meade SkyQuest XT 8 inch diameter, f/6 telescope. Both PMT's are mounted on top of the 16 inch Dobsonian telescope and boresighted (see Figure 2.1). The telescopic FOV PMT records light signals from an angular viewing area of ∼1°. The gain on the PMT's is variable and controlled by an external voltage signal. The electrical signal output from a single PMT is low-pass filtered to frequencies below 25 kHz and recorded on VHS video tapes using one of the audio inputs of a VCR. An encoded IRIG-B GPS signal is normally stored on the other audio channel for timing information. This type of recording limits the time resolution to the 1 ms resolution of the IRIG-B signal, in spite of the much higher sampling rate available, but it is convenient and does not require interfacing with a separate computer.

2.1.2 Calibration

For quantitative interpretation of the recorded images, the camera on the telescope was calibrated for brightness, edge-sharpness, and phosphor persistence [*Gerken et al.,* 2000]. The brightness levels of the images were calibrated using a light source of a known radiance at 600 nm, which was covered by a narrow band (7 nm) Melles-Griot filter. The spectral response of the telescopic images is limited to the wavelength range $\sim 450-850$ nm by the intrinsic bandwidth of the GenII image intensifier tube. The camera system was determined to saturate at ∼3 MegaRayleighs (MR) or $3\text{x}10^{12}$

photons-cm^{-2}-s^{-1}-str^{-1}. Reported brightness values represent a simple average over one exposure (i.e. $\sim$17 ms).

An edge-sharpness calibration was performed by imaging scenes with adjacent black and white blocks. Transitions from the maximum white value to half of the maximum value occurred over four camera pixels. In order to estimate the lateral widths of filamentary features in sprites, a cross section is first taken across the width of the filament (Figure 2.4). In accordance with the above description of edge calibration, filament edges which fade into the background in 4 pixels are taken to have a "sharp" boundary and thus have a total lateral width of 4 pixels less than that seen in the image (i.e., 2 per boundary). Widths of sprite features as reported in later chapters are half maximum widths as observed in image cross sections. Uncertainties quoted therein are based on the width of one pixel.

The persistence of the phosphor in the intensifier tube of the camera was examined by imaging a bright light streaked in front of the camera. Illumination from a relatively dim light with intensity less than the saturation threshold (i.e., less than 3 MR) was found to decay before the onset of the next frame, thus representing the ideal desired response for an imaging system. [*Burke,* 1996]. This property allows sprite durations (to within $\sim$17 ms) to be determined from the video footage. However, illumination from very bright lights did cause persistence in the intersifier tube which lasted for as many as 11 frames.

2.2 Observation campaigns

The Stanford University telescopic imaging system was deployed in several campaigns to observe both sprites and other atmospheric luminous phenomena. These campaigns were conducted in locations around the world ranging from New Mexico and Colorado to Alaska, Japan and France.

Langmuir Laboratory is a dedicated lightning laboratory operated by the New Mexico Institute of Mining and Technology. It is located in the Magdalena mountains of central New Mexico near Socorro, NM [34.0 N, 107.2 W]. The telescopic system was deployed at this facility during the summer months (July - August) of 1998 and

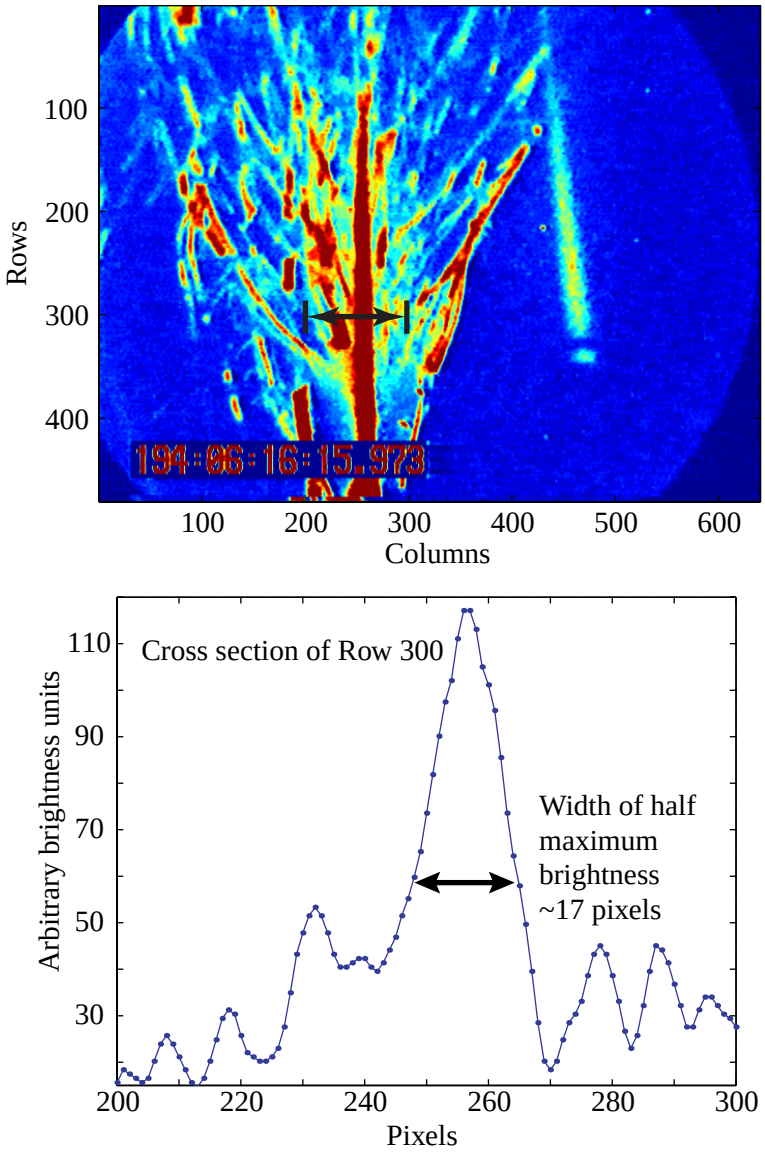

Figure 2.4: Streamer cross section. The upper panel displays a representative sprite recorded by the telescopic imager. The black ad white images are false-colored to better illustrate the dynamic range of luminosity. The black arrow marks the region shown in the cross section below (lower panel). The half maximum width of one streamer is marked on the cross section in the lower panel.

1999 with observations primarily focused on large storms over northern Mexico.

During May - July, 2000, the telescopic system was deployed at Yucca Ridge Field Station. Operated by FMA, Inc., this facility is located to the east of Fort Collins, Colorado [40.5 N, 105.0 W] and has excellent viewing conditions for storms over the Great Plains.

The Stanford telescopic imager was also used in Japan and France in connection with campaigns aimed at observations of the predicted "conjugate" sprites [*Lehtinen et al.,* 2001]. A photometric array (the Wide-Angle Sprite Photometer array) was deployed to observe brief flashes of light in the geomagnetically conjugate regions while the telescope was used to look at sprites occurring above the parent lightning flashes. These campaigns were conducted at the Observatoire Midi-Pyrenees (France), and Iitate Observatory (Japan). Analysis of data from these campaigns is beyond the scope of this dissertation.

In addition to sprites observations, the Stanford telescopic system has been used to measure optical emissions generated by HAARP (High Frequency Active Auroral Program), a powerful high-frequency (HF) transmitter used for ionospheric heating and modification experiments. The HAARP facility, located near Gakona, Alaska [62.4 N, 145.2 W], consists of a 48-element, 8x6 antenna array with a maximum radiated power of 960 kW and an operational frequency range of 2.8 - 10 MHz. Artificial airglow emissions in the F2 layers (∼300 km altitude) have been detected [*Pedersen et al.,* 2001]. Kilometer-scale fine structure in this airglow was imaged for the first time by the Stanford telescopic system in February 2002 [*Gerken et al.,* 2003].

2.3 Observational techniques

Meteorological tools such as the Geostationary Operational Environmental Satellites (GOES) infrared imagery and the National Lightning Detection Network are instrumental in locating and tracking potential sprite-producing thunderstorms. The GOES weather satellites are a joint development of the National Oceanic and Atmospheric Administration (NOAA) and the National Aeronautics and Space Administration (NASA). GOES spacecraft operate as a two-satellite constellation in geosynchronous

orbit above the equator and typically observe 60% of the earth. They measure the earth's atmosphere, its surface, cloud cover, and the solar and geosynchronous space environment (see http://www.goes.noaa.gov/ for further details). The National Lightning Detection Network (NLDN) is an array of more than 100 sensors covering the continental United States, which utilizes time-of-arrival and magnetic direction finding to detect and record cloud-to-ground lightning strokes with high accuracy in time ($\sim$1 μs) and location ($\sim$500 m) [*Cummins et al.*, 1998].

Each night of a typical sprite observation campaign, the GOES satellite infrared images of the United States are closely watched for storm activity (Figure 2.5). The infrared images are color-scaled by temperature. When a large storm forms within the viewing area of the field station (typically a $\sim$900 km radius), the optical instruments are aimed in that direction. The National Lightning Detection Network (NLDN) data is then used to determine if regions of the storm are producing the large positive CGs typically associated with sprite initiation (Figure 2.6) [*Boccippio et al.,* 1995]. These large +CG's frequently occur in decaying (or trailing stratiform) regions of large mesoscale convective systems [*Lyons,* 1994] although they can also be observed in much smaller storms (see Chapter 5).

After the optical instruments are aimed in the direction most likely to produce sprites, the wide FOV camera is monitored until an event occurs. The probability of detecting a transient event such as a sprite in a telescopic imager, with such a narrow FOV, is extremely low. Nevertheless, telescopic observations were successfully conducted due to the known property that successive sprites tend to occur in near proximity to each other for an extended period of time. Thus, once one sprite is observed in the wide FOV camera, the telescope is re-oriented to the position of that sprite and then typically another sprite occurs in close enough proximity to be imaged by the telescope. As the storm drifts throughout the night or different parts of the storm become active, the telescope can be easily adjusted accordingly based on observations in the wide FOV camera.

GOES Satellite Near-Infrared Images

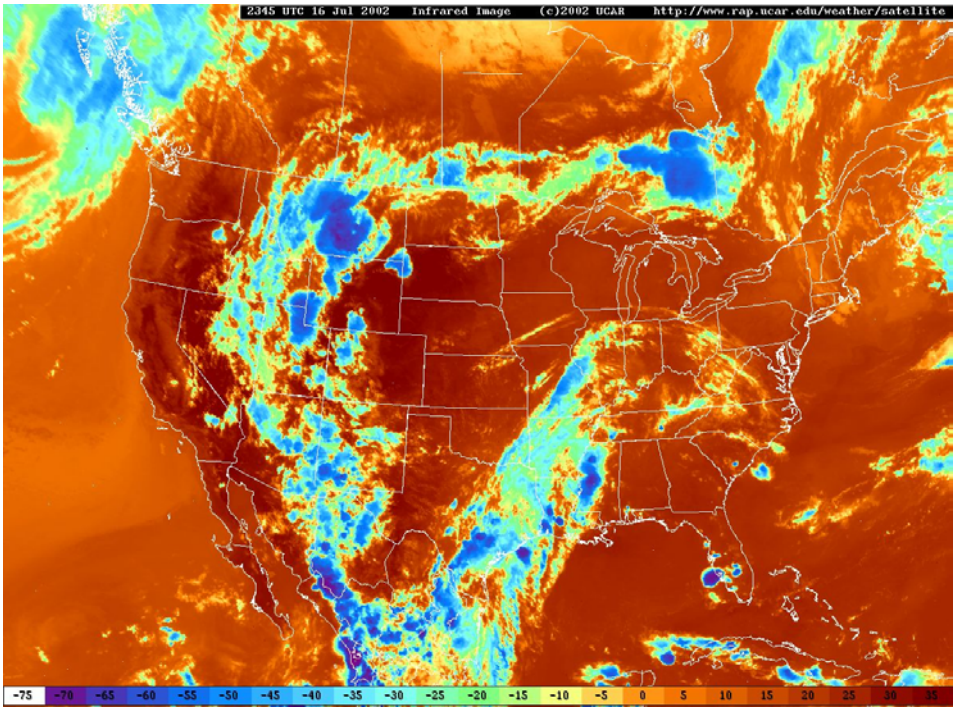

http://www.rap.ucar.edu/weather/satellite/latest_US_ir.jpg

Figure 2.5: GOES satellite infrared image of the United States. The color scale corresponds to temperature. In this example storms are located over the Rocky Mountains, stretching up from Mexico into eastern Texas.

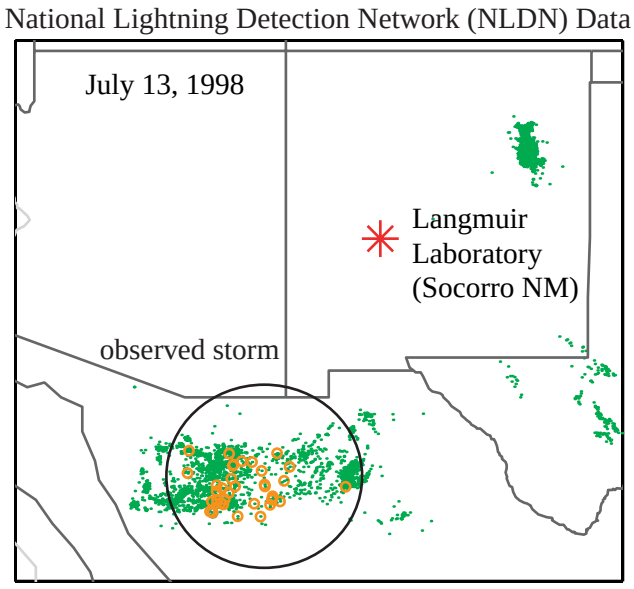

Figure 2.6: NLDN data for storm observed on July 13, 1998. The green dots show all of the cloud-to-ground (CG) strokes recorded during the storm while the orange circles indicate only those CGs associated with observed sprites.

2.4 Telescopic images of sprites

Hundreds of sprites have been observed by the Stanford telescopic imager throughout the various campaigns since 1998. Just as no two cloud-to-ground lightning strokes look exactly alike, different sprites are also not alike and in fact the fine structure in sprites exhibits a high degree of variability. Unlike CG discharges, however, the electrical breakdown mechanism observed in sprites also exhibits high variability, primarily due to the rapid height variation of atmospheric properties at high altitudes (i.e., neutral density, electron density). Streamer breakdown (see Section 3.1) prevails at lower altitudes while diffuse glow is dominant at higher altitudes. The altitude of transition from one regime to the other is not always the same [*Pasko and Stenbaek-Nielsen,* 2002]. Telescopic images of sprites thus reveal the complex and dynamic environment and phenomenology of high altitude electrical discharges. Some of these processes are now fairly well-understood while others still remain a mystery. In this section we show a selected sample of telescopic images of

sprites.

On July 13 and August 6, 1998, ∼50 sprites were observed over northwestern Mexico, at a range distance of ∼450 to 580 km from Langmuir Laboratory. The moon was nearly full on the night of August 6, increasing the background light level. Lightning location and peak current data from the NLDN [*Cummins et al.*, 1998] were used to determine the range of the sprites from Langmuir Laboratory on the basis of the largest +CG stroke recorded in temporal proximity to each sprite, which by implication is assumed to be the "causative" lightning discharge. The altitudes of the sprites (and associated uncertainties) were determined by assuming them to be roughly (within ∼ 40 km) centered above the causative +CG stroke [*Winckler et al.,* 1996; *Lyons et al.,* 1996; *Wescott et al.,* 1998] and using the recorded starfields to determine the elevation angle and azimuth of the telescope.

Figure 2.7 shows a large sprite observed on July 13 at 06:00:00 UT, which lasted a maximum of ∼50 ms (one video frame). The upper panel displays the wide FOV while the lower panel shows the narrow (telescopic) FOV. The white rectangle on the upper panel outlines the position of the narrow FOV within the wide FOV. The images have been false-colored and are made to artificially saturate at 685 kR in order to better represent intensity and bring out dimmer features (see colorbar). Time stamps correspond to the beginning of the exposure time for each image. The broadband VLF sferic recorded at Yucca Ridge Sprite Observatory in Colorado (40°40′06″ N, 104°56′24″ W) is shown below the two images with an arbitrary linear intensity scale. The current amplitude (in kA) of the sprite-associated sferics as recorded by the NLDN is indicated. The respective propagation delays for the sferic in the Earth-ionosphere waveguide from the sprite regions shown to Yucca Ridge and Langmuir Laboratory are ∼4 ms and ∼2 ms. This type of very large sprite has been previously observed [*Winckler et al.,* 1996] and is believed to occur in response to very rapid removal of a large quantity of charge, consistent with the relatively large peak current (+128 kA) of the associated CG discharge [*Bell et al.,* 1998]. It is evident from the narrow FOV image that such sprite structures consist of densely-packed branching filaments. The transverse scale of filamentary structures in this image ranges from 60 to 145 m (±12 m) in the altitude range of 60–64 km (±4.5 km).

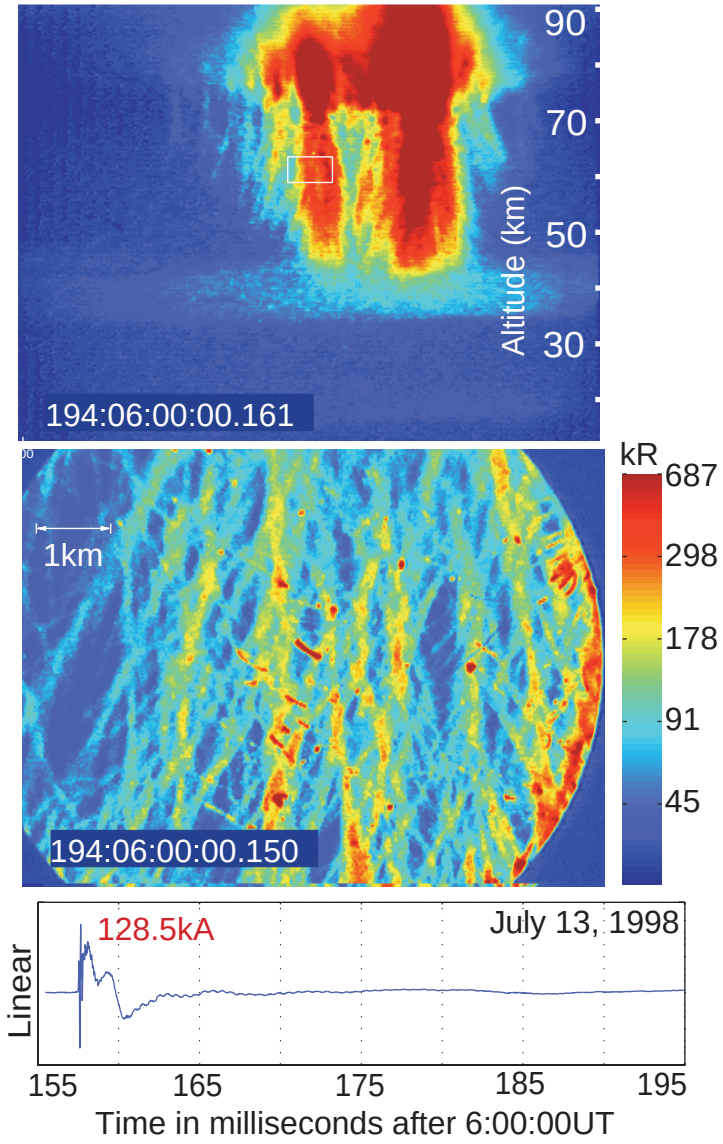

Figure 2.7: The wide (top panel) and narrow (lower panel) FOV images of a bright sprite event. Time-stamping (GPS) corresponds to the beginning exposure time for each image. The narrow FOV in the wide FOV is outlined by a white rectangle in the top panel. Altitude scaling shown in the wide FOV panel corresponds to the location of the causative CG as recorded by the NLDN. Format and colorcoding in subsequent figures of this section are the same as shown here unless otherwise noted. This telescopic image demonstrates that while the sprite appears to be amorphous in the wide FOV image, the lower portion of this sprite in fact consists of a volume of densely-packed filaments.

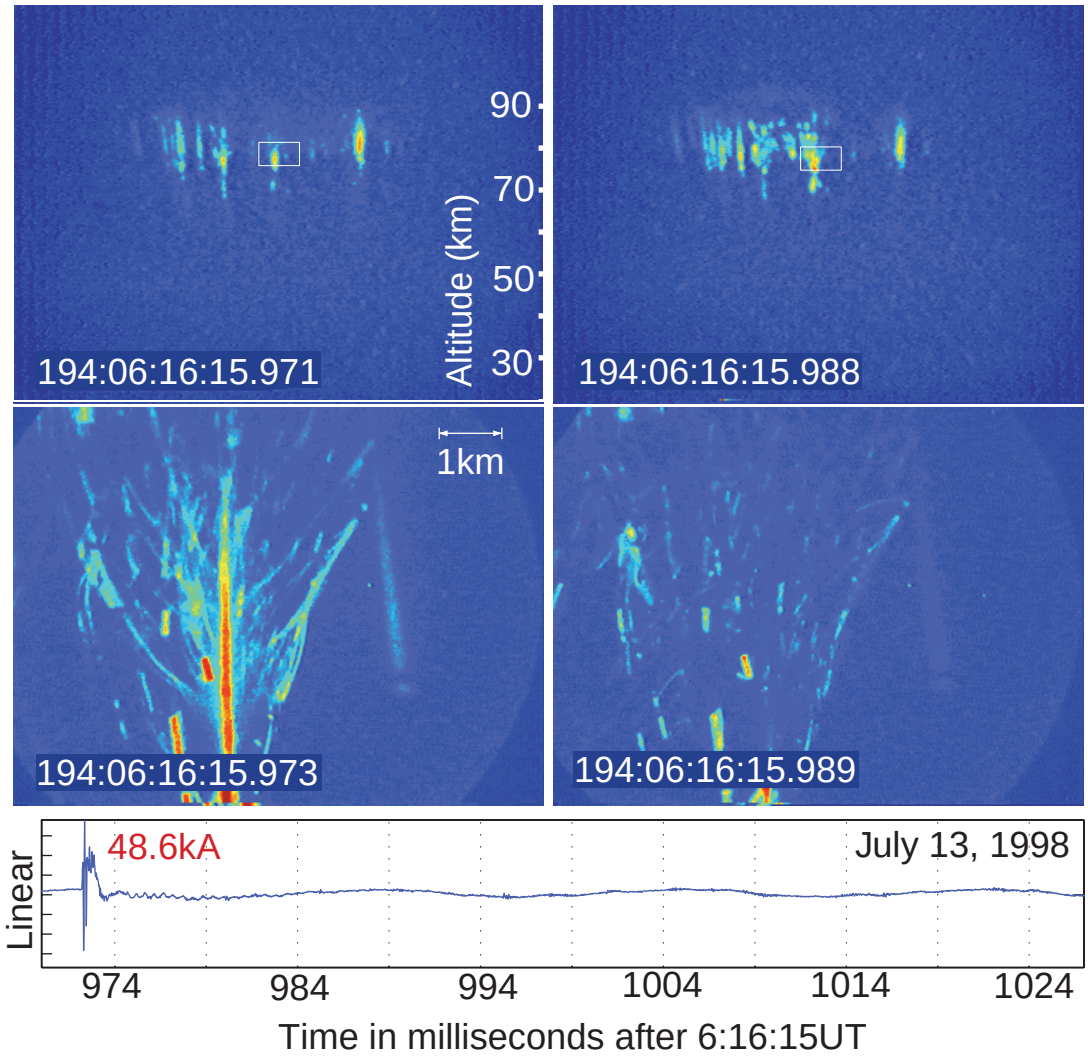

Figure 2.8: Images of a sprite exhibiting a branching tree-like structure.

For the sprite event shown in Figure 2.8 the telescopic image reveals a bright central column with branches that appear to emanate from it at ∼45°. The central column is 650 kR at its brightest point while the branches are ∼90 kR. A "columniform" sprite [*Wescott et al.,* 1998] is evident in the background. As shown in Figure 2.8, some "hot spots" in the sprite persist into the next field. Sprites with such unusual tree-like morphology similar to that shown in Figure 2.8 had not been reported prior to the observations of *Gerken et al.* [2000] but were confirmed in several other cases during the July - August 1998 campaign. The tree-like branching may be due to the horizontal electric field emanating from the intensely ionized bright column, creating a local distortion in the largely vertical primary quasi-static field.

Figure 2.9 shows a so-called "carrot" sprite [*Winckler,* 1995]. The telescopic view indicates that the upper part of the sprite appears to branch upward while the lower part branches downward. The brightest portion of the telescopic image is 1.6 MR and lasted 5 video fields. No NLDN stroke was associated with this sprite and thus range data for altitude determination is unavailable.

Figure 2.10 shows a columniform sprite event observed on August 6, 1998. The columns first appear in the very first field shown, apparently initiated by a 77 kA CG stroke and appear subsequently to extend downward and to fade by the fourth and fifth field. In the sixth field another sprite event occurs just below the FOV of the telescope, apparently in response to the 26 kA CG flash, which also leads to the slight re-brightening of the columnar forms and in particular the beads at the bottom. Remarkably, these columnar forms have relatively sharp edges (5 pixels) and lack fine structure. The widest of the columns is 196±13 m across in the altitude range of $81 - 85 \pm 6$ km.

Figure 2.11 shows a sprite apparent in the first wide FOV image which is produced in response to a 145 kA +CG discharge occurring during the last few milliseconds of the telescopic field shown. This occurrence indicates that the sprite formation was relatively rapid (i.e., it occurred during the remaining time period of the field of ∼17 ms), consistent with the high peak current of the discharge [*Bell et al.,* 1998]. The sferic waveform of the +CG discharge exhibits a "slow-tail" typical of many sprite-producing lightning discharges [*Reising et al.,* 1996; *Cummer et al.,* 1998]. Apparent

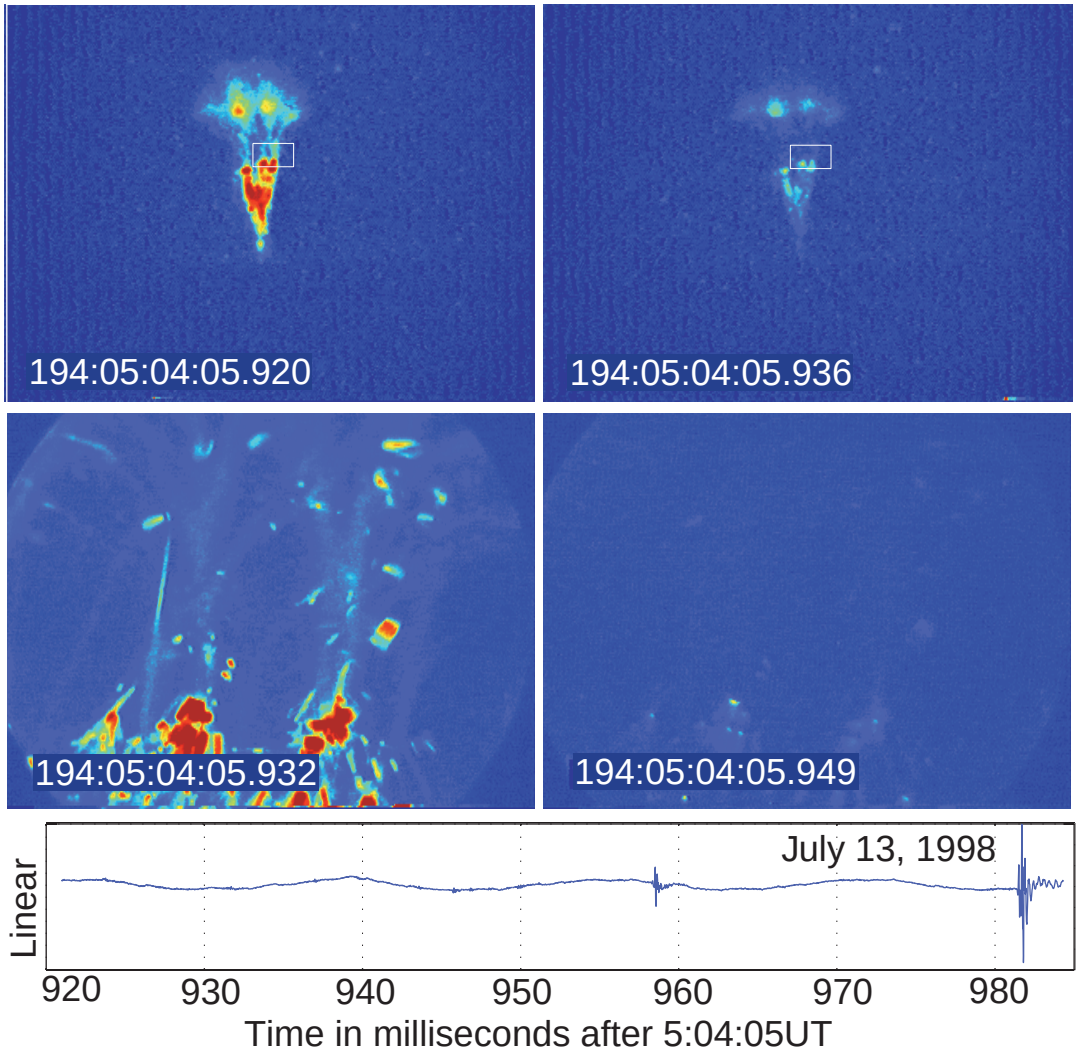

Figure 2.9: Images of a carrot sprite.

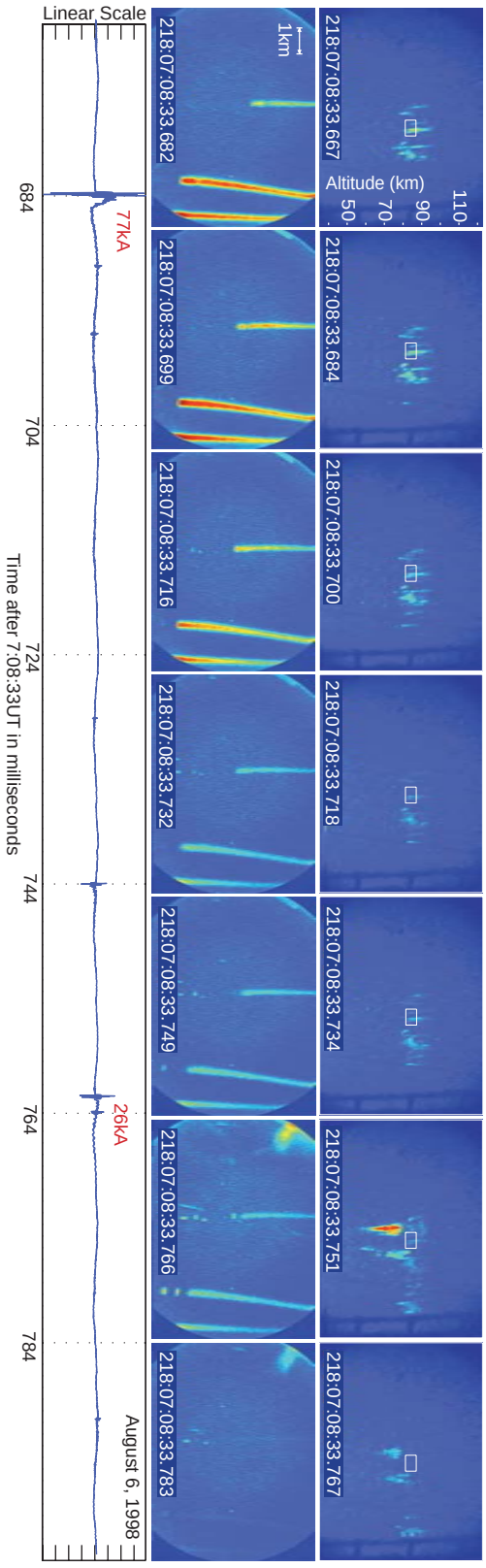

Figure 2.10: Successive images showing time evolution of isolated columnar structures observed on August 6, 1998.

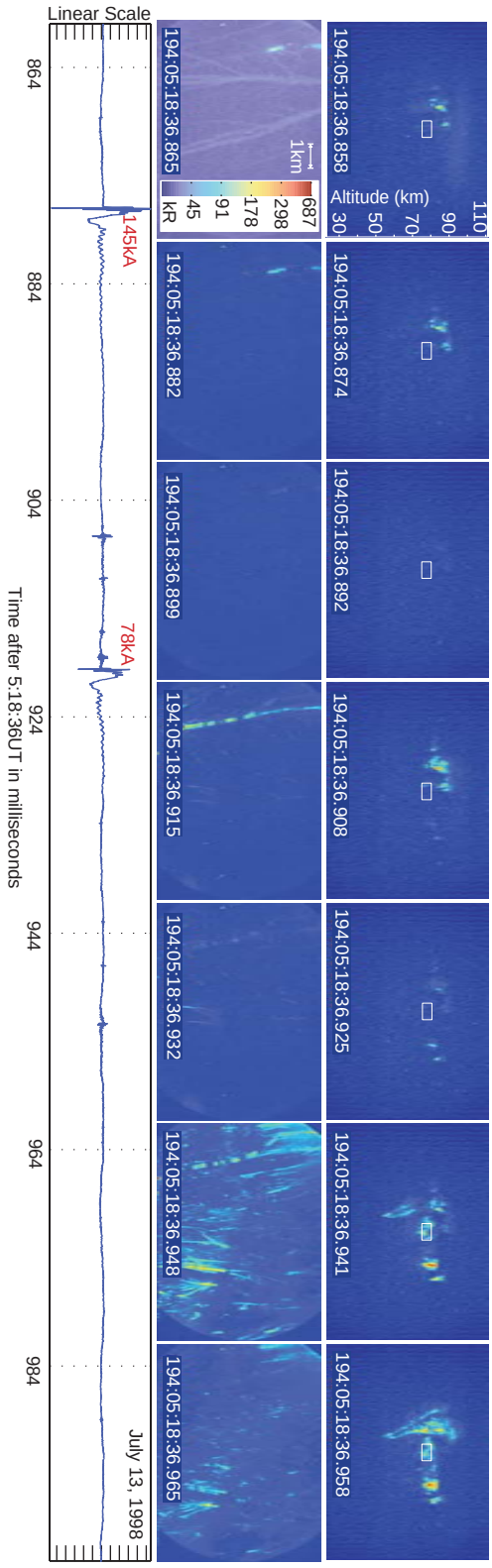

Figure 2.11: Successive rexcitation of columnar forms observed on July 13, 1998. Format and color coding of brightness levels are modified in the lower left-most panel as indicated.

in the narrow FOV shown below is a near-vertical column of illumination consisting of bands of high and low intensity. The lateral extent of this luminous column is 150 ± 13 m over the altitude range of $76 - 80 \pm 5$ km. Note that both the overall sprite and the narrow column fade away in the next two video fields but are re-excited in the fourth frame, apparently in response to a CG discharge with peak current $\sim$78 kA. The re-excitation of a previously bright but faded away column indicates that this preconditioned region of the atmosphere was primed for excitation with respect to its immediate surroundings. This result is most likely due to the persistence of ionization from the first sprite, which is expected to chemically dissipate in several tens of seconds in the altitude range of $\sim 76 - 80$ km [*Pasko and Inan*, 1994]. The re-excited column appears to fade away in the next field, followed by a dramatic explosion of luminosity, in spite of the apparent lack of any large associated sferics occuring between the 5th and 6th fields. This brightening may well be an example of delayed sprites of the type reported by *Bell et al.* [1998], and are believed to occur due to continuing currents, which may flow for up to 100 ms or more following the initial discharge [*Cummer and Füllekrug,* 2001]. It is interesting to note (from the 6th narrow FOV image) that the singular column is once again re-excited, but is now accompanied with a host of other narrow near-vertical forms, ranging in lateral size from 27 to 54 ± 13 m in this altitude range of 76–80 ± 5 km.

Chapter 3

Streamer dynamics in sprites

3.1 What is a streamer?

A streamer is a transient filamentary plasma structure that propagates as an ionization wave with charge separation and an enhanced, localized electric field in its wavefront (streamer "head" region). As shown in Figure 3.1 [*Bazelyan and Raizer,* 1998, pg. 45] the electric field induced in this wavefront is highly nonuniform, allowing for a large enhancement in field strength to occur in the vicinity of the streamer head. In order for a streamer to be initiated, a high-energy electron must be accelerated in the presence of an electric field. This electron gains energy from the field and collides with other particles causing further ionization and avalanche multiplication of electrons. In this way an ionization wave is propagated either parallel or antiparallel to the driving electric field depending on the geometry of the electrodes at initiation. For example, steamers initiated on a sharp metal tip that is positively charged propagate along the electric field lines while those initiated on a negative tip propagate against the field lines. For further discussion the reader is referred to *Bazelyan and Raizer* [1998] and *Raizer* [1991]. The streamer mechanism of carrying electron current occurs in ionized gases under high pressure and with low ambient free electron densities.

There are two conditions that can cause streamer termination. A streamer may be terminated when it travels into a region of increased electron density such that the

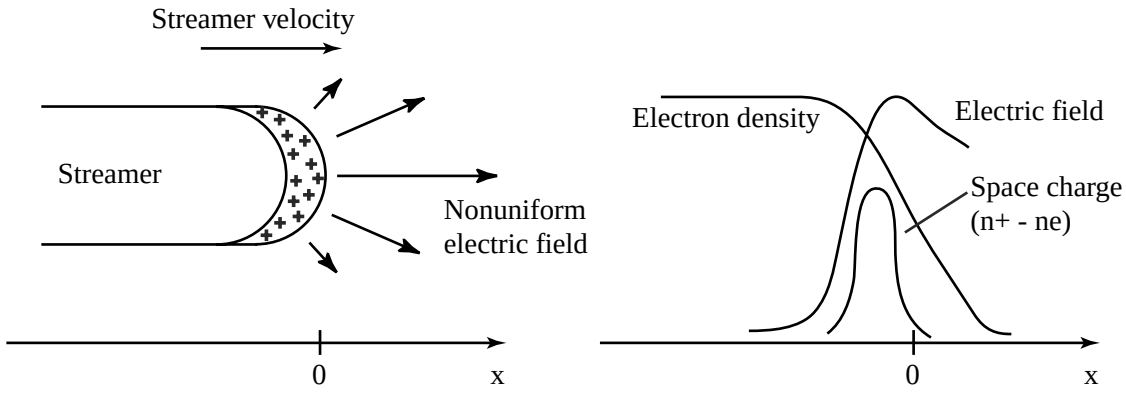

Figure 3.1: Diagram of a streamer [*Bazelyan and Raizer,* 1998, pg. 45]

density in the streamer body is equal to that of the ambient density. In this case the streamer expands and develops into a diffuse glow (see Chapter 4). The reason for this behavior is that the increased ambient electron density causes increased conductivity and the electrons no longer need to remain in the streamer channel in order to carry current. The second condition of streamer termination occurs when a streamer reaches an increased neutral density such that the ambient electric field is no longer high enough to sustain streamer breakdown and propagation [*Raizer et al.,* 1998]. The electric field required for streamer propagation is lower than that of the conventional electric breakdown field [*Raizer,* 1991, pg. 355]. This means that once a streamer is initiated it is possible for it to travel into regions of higher neutral density where initiation of breakdown would not have been possible. However if the neutral density becomes too large the ambient electric field may fall below that which is needed for streamer propagation and the streamer is terminated.

3.2 Streamer models and laboratory measurements

The polarity of a streamer is determined by the charge in the streamer head as illustrated in Figure 3.2. A positive streamer accelerates electrons into its head and travels in the direction of the external electric field while a negative streamer expels electrons from its head and travels in the opposite direction (see *Raizer* [1991]).

Due to the fact that positive and negative streamers travel in opposite directions

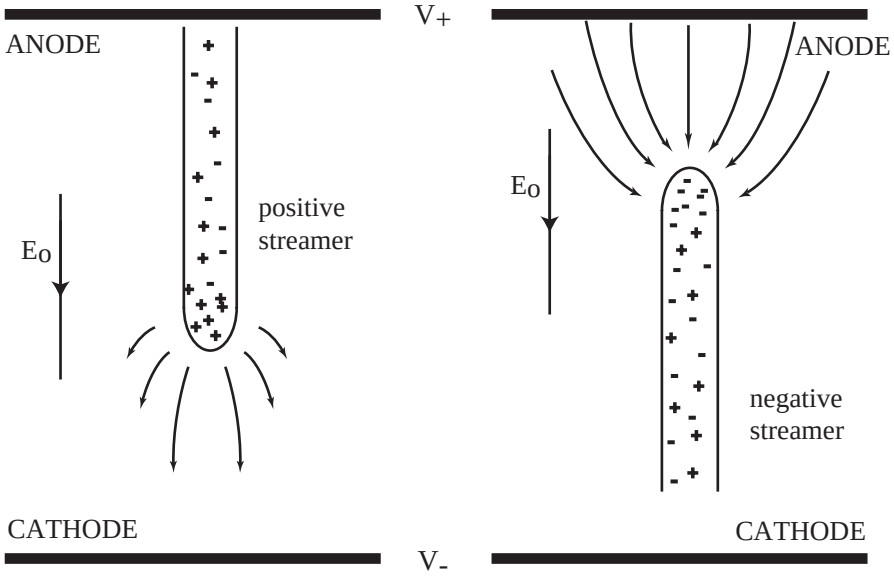

Figure 3.2: The polarity of a streamer is determined by the charge in the streamer head [*Raizer*, 1991, pg. 335 – 338]. The curved lines indicate the electric field emanating from the streamer head.

with respect to the ambient electric field, there is an inherent asymmetry between the two types of streamers [*Dhali and Williams,* 1987]. This asymmetry has been observed in various streamer properties determined by modeling and laboratory measurements [*Vitello et al.,* 1994; *Babaeva et al.,* 1997; *Dhali and Williams,* 1987; *Kulikovsky,* 1997; *Yamada et al.,* 1990; *Massala and Lesaint,* 2001]. A summary of these properties is given in Figure 3.3.

Several models have been developed to study the differences between positive and negative streamers [e.g., *Babaeva et al.,* 1997; *Dhali and Williams,* 1987; *Kulikovsky,* 1997]. Since positive streamers travel in the direction of the ambient electric field, electrons are continually added to the streamer in the head region. This property allows the positive streamer to have a higher electric field in the head region and to typically travel at a higher velocity than the negative streamer [*Babaeva and Naidis,* 1997]. On the other hand, positive streamer velocity is dependent on the external electric field to a higher degree than that of negative streamer velocity [*Dhali and Williams,* 1987]. Positive streamers have a higher electron density in their bodies, which allows for

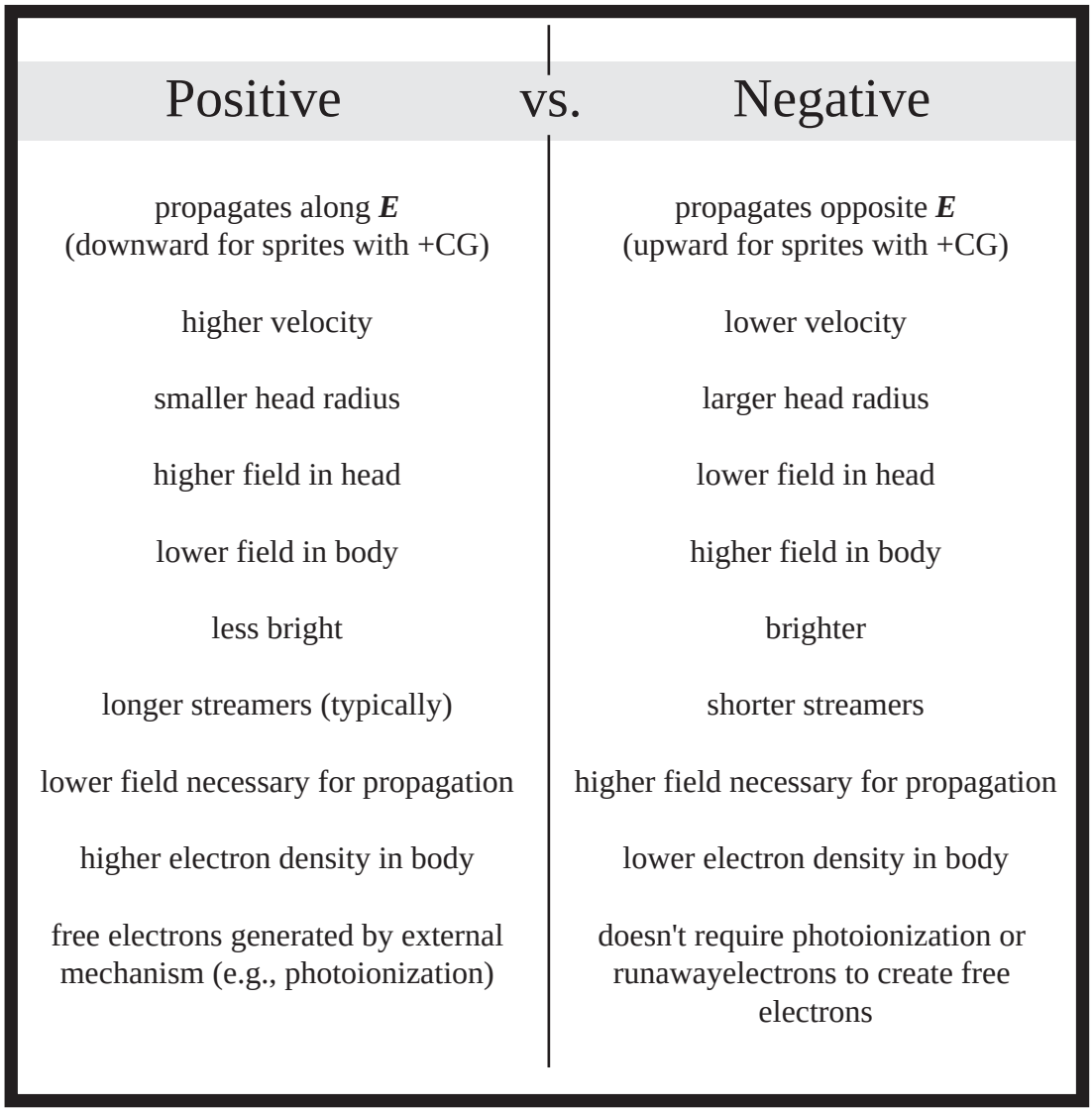

Figure 3.3: Summary chart of typical differences between positive and negative streamers as determined by modeling and laboratory measurements. References are detailed in the text (Section 3.2).

a higher degree of shielding and thus a lower electric field within the body region [*Babaeva and Naidis,* 1997]. Unlike negative streamers, positive streamers require a pre-existing background free electron density in order to propagate [*Kulikovsky,* 1997], because they draw electrons into their body while negative streamers expel electrons. The pre-existing free electrons which are needed for streamer initiation could be created by photoionization, cosmic rays, or some other such preionizing mechanism [*Vitello et al.,* 1994].

Laboratory experiments of streamers in dielectric liquids reveal similar differences between positive and negative streamers. *Yamada et al.* [1990] found that positive streamers appear with a lower voltage (i.e., lower electric field) and propagate faster than negative steamers. Positive streamers were also found to be more filamentary than negative streamers and were more likely to develop along electric field lines. At high electric fields, however, negative streamers had velocities on the same order as that of the positive streamers [*Yamada et al.,* 1990]. Similar results were obtained by *Massala and Lesaint* [2001] in laboratory experiments involving streamers in mineral oil. Negative streamers observed in these experiments required a higher voltage (i.e., electric field) for initiation, had a lower velocity and emitted more light than their positive counterparts. It was found that when a lower voltage was applied, the streamers were shorter in length. Negative streamers were generally composed of a bright main trunk with a few lateral branches while the positive streamers formed a larger volume of thin luminous filaments [*Massala and Lesaint,* 2001]. The work of *Devins et al.* [1981] also shows that negative streamers are much less filamentary than positive streamers. Laboratory experiments in N_2/O_2 mixtures by *Yi and Williams* [2002], however, show that positive streamers travel longer distances before branching. Positive streamers measured in these experiments were found to have about half the diameter of the more diffuse negative streamers [*Yi and Williams,* 2002]. Positive streamers require a lower external electric field than negative streamers and are observed to frequently travel longer distances [*Yi and Williams,* 2002].

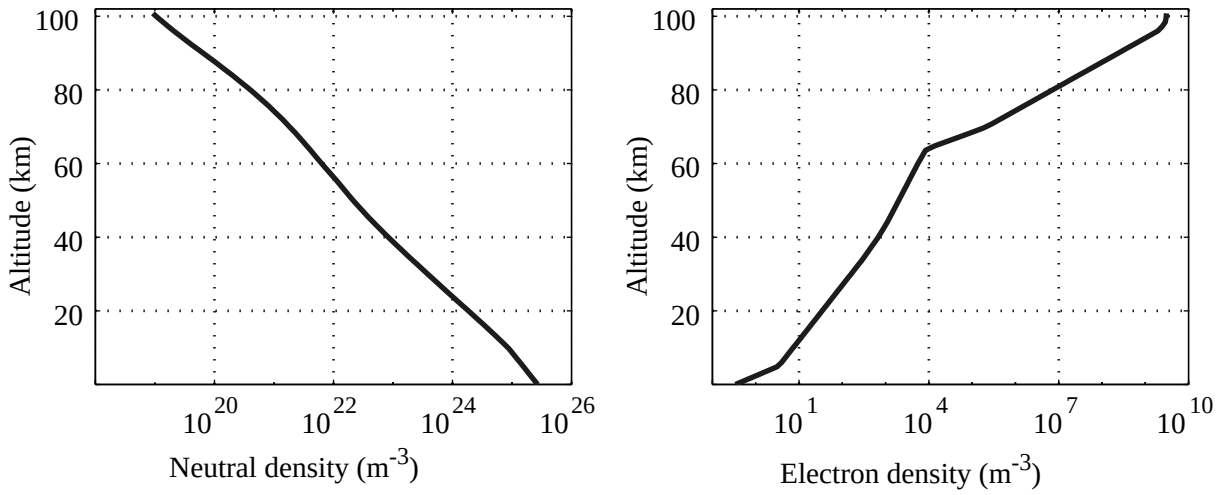

Figure 3.4: The lefthand panel displays neutral atmosphere density derived from the U.S. Standard Atmosphere (U.S. Standard Atmosphere, U.S. Government Printing Office, Washington, D.C., 1976). The righthand panel shows a typical nighttime background electron density profile [*Pasko and Inan,* 1994, Figure 4, Profile 1]

3.3 Parameter scaling with altitude

As discussed in the previous section, streamer properties are highly dependent on the polarity of the streamer. Streamer properties also depend on the background electron, ion and neutral densities. In high altitude discharges such as sprites, which may extend over an altitude span of 50 - 100 km, the atmospheric neutral density decreases exponentially with altitude while the electron number density exponentially increases with altitude as shown in Figure 3.4. Consequently, streamer properties are observed to vary throughout the altitude extent of a sprite. Theoretically, it should be possible to use observed streamer properties to gain insight into the natural background densities in the vicinity of a sprite. Since this region of the atmosphere is particularly difficult to study by other methods, sprites may thus serve as a useful tool in collecting data on the atmospheric composition at mesospheric altitudes.

3.3.1 Neutral, electron, and ion density

Neutral atmospheric density decreases exponentially with altitude. Various models can be used to describe atmospheric parameters in the mesosphere. In the following analysis the neutral particle density is based on the U.S. Standard Atmosphere model (U.S. Standard Atmosphere, U.S. Government Printing Office, Washington, D.C., 1976) as shown in Figure 3.4. This model is based on rocket and satellite data as well as ideal gas theory and represents atmospheric densities and temperatures from sea level to ∼1000 km.

The electron density increases nearly exponentially up to the lower regions of the ionosphere (∼95 km) as shown in Figure 3.4. The background nighttime electron density is highly variable in the D-region of the ionosphere. Large-scale variations occur diurnally and seasonally and are greatly affected by solar activity and geomagnetic storms. Small-scale ionospheric variations can be caused by events such as lightning-induced electron precipitation [*Inan et al.,* 1985]. Ionospheric perturbations can last from a few minutes to many days [*Davies,* 1965, pg. 257]. In order to constrain variables in the following streamer calculations, a typical electron density profile has been selected [*Pasko and Inan,* 1994; Figure 4, Profile 1].

The atmospheric altitude profile of total conductivity is found by summing the electron and ion components. The electron component can be found using the previously-discussed electron density profile and the relation:

$$\sigma_e = q_e N_e \mu_e \tag{3.1}$$

where σ_e is the electron conductivity in units of Siemens/m (S-m^{-1}), q_e is the electron charge, N_e is the electron density, and μ_e is the electron mobility. Electron mobility has a complicated dependence on electric field. Throughout this chapter we use a functional dependence of electron mobility on electric field based on experimental data developed by *Pasko et al.* [1997]. The effects of the magnetic field of the earth on conductivity are neglected since at these altitudes the ionospheric plasma is highly collision dominated [*Pasko et al.,* 1997].

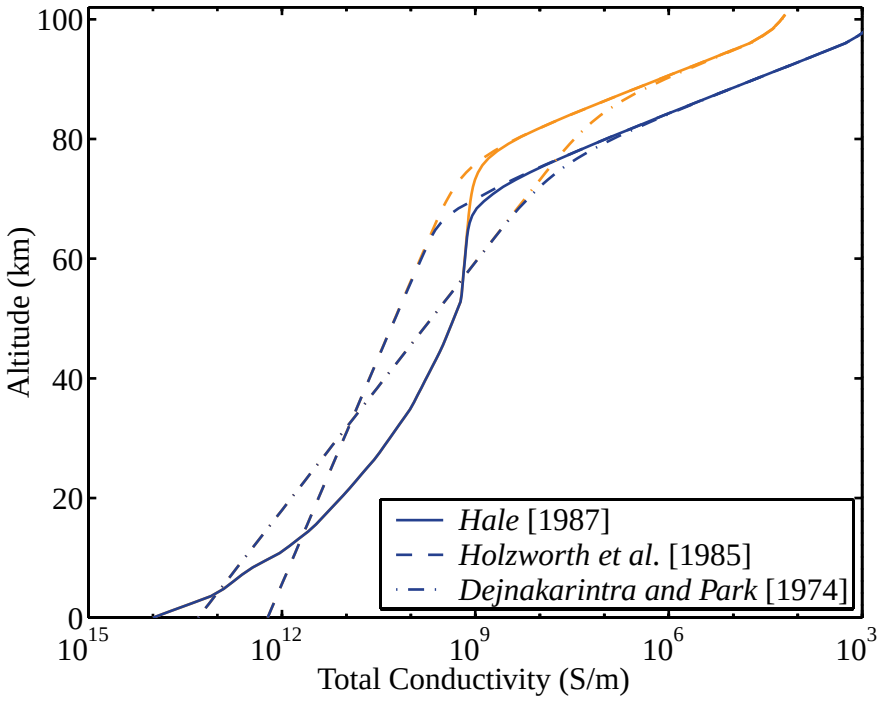

Figure 3.5: Nighttime conductivity versus altitude. The three plots display altitude profiles from three different sources and are used throughout this chapter. The blue lines represent conductivity profiles with the ambient electric field set to zero while the orange lines show the profiles for a breakdown electric field level (32 kV/cm at ground).

At high altitudes electron density plays a dominant role in the total electrical conductivity of the atmosphere. Below ∼60 km, however, the total conductivity is largely determined by ion conductivity [*Pasko et al.,* 1997]. Just as there is variability in the electron density profiles, the ion compositions (and thus the ion conductivity) also exhibit a high degree of variability, especially at nighttime. Ion conductivity profiles have been determined both experimentally [*Holzworth et al.,* 1985; *Hale,* 1994] and by theoretical modeling [*Dejnakarintra and Park,* 1974]. Figure 3.5 shows total conductivity for three different ion conductivity profiles. Both ambient conductivity with the electrons assumed to be cold (blue lines) and "breakdown" electron conductivity (orange lines) are displayed in order to demonstrate the dependence of conductivity on the electric field. The cold conductivity is defined as that corresponding to the case when the electric field equals zero while the breakdown conductivity is that when the electric field is equal to the breakdown electric field. If the external electric field applied to a gas exceeds the breakdown electric field, the gas is transformed into an ionized conducting state, or "breaks down" [*Raizer,* 1991, pg. 128]. Breakdown electric field values at ground level can range from $26 - 56$ kV-cm^{-1} depending on the gap being studied, but for the purposes of this figure we used the value of 32 kV-cm^{-1} cited in *Raizer* [1991]. Heating of the ambient electrons by the electric field increases the collision frequency and decreases the mobility and thus the conductivity as shown in Figure 3.5.

3.3.2 Streamer time scales

The dynamics of a high altitude electrical discharge is governed by several different time scales that vary with altitude as shown in Figure 3.6. The most important time constant is that of dielectric relaxation. The dielectric relaxation time constant is defined as:

$$\tau_\sigma = \frac{\epsilon_0}{\sigma} \tag{3.2}$$

where ϵ_0 is the permittivity of vacuum and σ is the isotropic conductivity as defined in the previous section. As can be seen in Figure 3.6, this time constant rapidly decreases with altitude and is highly dependent on the conductivity profile. The

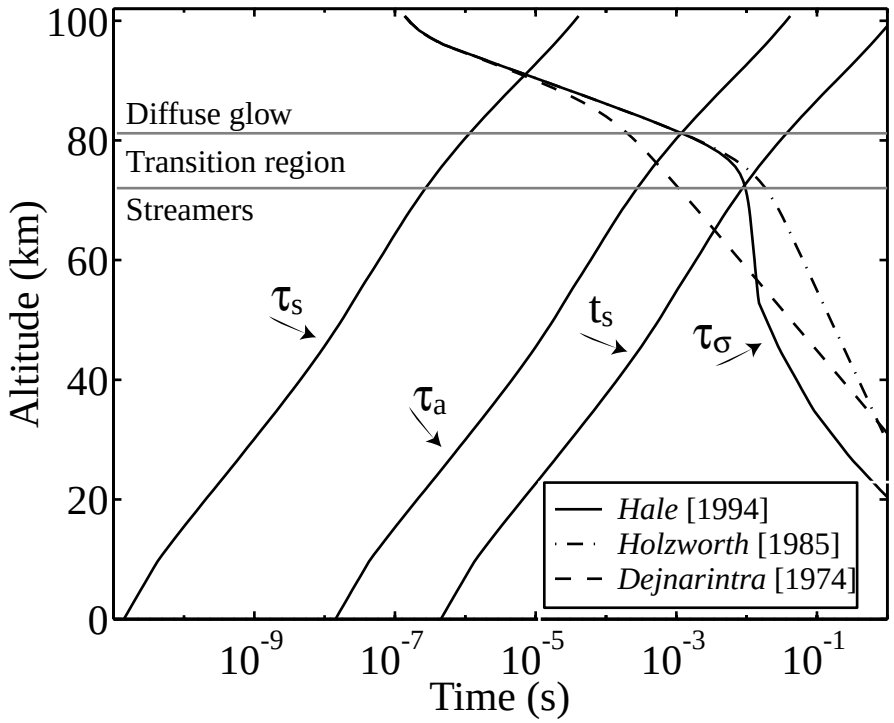

Figure 3.6: Several altitude-varying time constants determine the dynamics of high altitude electrical discharges. t_s is the time scale for streamer formation, τ_a is the attachment time constant, τ_s is the dielectric relaxation time constant inside the streamer, and τ_σ is the ambient dielectric relaxation time constant. At low altitudes streamer processes dominate while at high altitudes, where the dielectric relaxation time constant is very small, diffuse glow occurs. Note that the boundaries between streamer and diffuse glow processes are highly dependent on the conductivity profile [*Pasko et al.,* 1998].

dielectric relaxation time constant is essentially an indication of how long it takes for free charge to be redistributed so as to expel an imposed electric field from a region. At high altitudes where the conductivity is high (due largely to the high electron density) free charge can quickly rearrange such as to rapidly expel an electric field.

A second time constant important in atmospheric discharges is that of attachment. Attachment is the process whereby free electrons are "attached" to nearby neutrals and are thus removed from participation in streamer and diffuse glow processes. As shown in Figure 3.6, the attachment time constant increases rapidly with altitude as the neutral density drops and thus has less and less of an impact on the production and maintenance of electrical discharges. The attachment time scale in this figure refers to the two-body attachment of electrons to O_2 molecules with dissociation ($e^- + O_2 \rightarrow O + O^-$) [*Pasko et al.,* 1997]. The characteristic attachment time scale is:

$$\tau_a = \frac{1}{\nu_{a\,\max}} \tag{3.3}$$

where $\nu_{a\,\max}$ is the maximum attachment coefficient. *Pasko et al.* [1997] derived a functional dependence of $\nu_{a\,\max}$ on electric field and neutral particle density based on experimental data. We use the relation $\nu_{a\,\max} \simeq 7\times10^7 N/N_0$ as derived in *Pasko et al.* [1998].

The third significant time scale in high altitude discharges is the time needed for the evolution of an individual electron avalanche into a streamer. This time scale is defined as:

$$t_s = \frac{z_s}{v_d} \tag{3.4}$$

where z_s is the distance required for an avalanche to generate a space charge field comparable to the ambient electric field and v_d is the electron drift velocity. The variable z_s depends on the breakdown electric field, streamer radius, and the ionization and attachment coefficients as discussed in *Pasko et al.* [1998].

The final time scale displayed in Figure 3.6 is that of the dielectric relaxation within the streamer head. As for the ambient dielectric relaxation time constant, this time constant $\tau_s = \epsilon_0/\sigma_s$, where σ_s is the conductivity within the streamer. Following the discussion in *Pasko et al.* [1998], τ_s varies inversely with neutral particle density

($\tau_s \sim N^{-1}$).

At altitudes below ~70 km, t_s is much smaller than τ_σ and the discharge is dominated by streamer processes. Between $\sim 70 - 85$ km, however, t_s exceeds τ_σ. In this region, labeled "Transition region" in Figure 3.6, streamer dynamics and sprite behavior are dominated by strong attachment prior to the onset of electrical breakdown. The altitude of the transition region is a sensitive function of the atmospheric parameters since this is the altitude range where the t_s, τ_a, and τ_σ time scales overlap. This sensitive dependence allows the transition region to potentially be used as a means of assessing the accuracy of modeled conductivity and electron density profiles [*Pasko and Stenbaek-Nielsen,* 2002]. Above ~85 km, the dielectric relaxation time constant is faster than either the attachment or streamer time scales, and diffuse glow discharges are typically observed (see Chapter 4 for further discussion of diffuse glow).

3.3.3 Critical electric fields

In order for an electrical discharge process to be initiated and sustained, the local electric field must exceed a certain critical level. In the case of sprites, this electric field is imposed by the occurrence of a cloud-to-ground lightning stroke. The magnitude of the field is highly dependent on the geometry of the charge in the thundercloud (height, distribution, etc.) as well as the quantity of charge removed from the cloud during the cloud-to-ground lightning stroke. These parameters are not well-known due to their high variability from thundercloud to thundercloud and due to the difficulty of making measurements of the altitude and quantity of charge in a thunderstorm. Figure 3.7 shows possible quasi-static electric field configurations due to varying amounts of charge removal and cloud heights as modeled by *Pasko et al.* [2001].

The critical electric fields in streamer formation are the electrical breakdown field and the minimum fields required for positive and negative streamer propagation. Electrical breakdown can be thought of as the process that turns a nonconducting

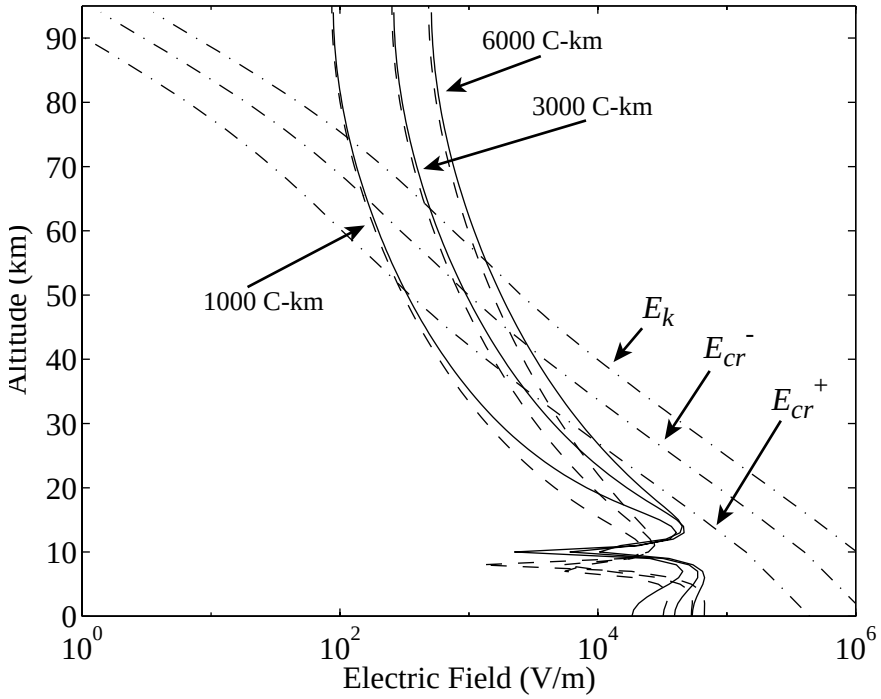

Figure 3.7: Critical electric fields for streamer breakdown [*Pasko et al.,* 2001]. The dot-dashed lines show the critical breakdown and streamer propagation fields scaled with neutral density. E_k is the breakdown electric field, E_{cr}^- is the critical electric field for negative streamer propagation, and E_{cr}^+ is the critical electric field for positive streamer propagation. The solid lines show the electric field set up by a lightning stroke of varying charge moments for a charge source at 10 km altitude. The dashed lines show the corresponding fields for a charge source at 7 km altitude, a more reasonable approximation for a CG channel length [*Marshall et al.,* 2001]. The altitudes at which the electrostatic field of the thundercloud exceeds the critical electric fields depends on the thundercloud charge geometry and charge moment.

material into a conducting material by applying a strong field. The minimum threshold field required to initiate this process is the electrical breakdown field [*Raizer,* 1991, pg. 324]. Once initiated, however, a streamer head has a high enough electric field (created by the roughly spherical charge distribution) that it is able to propagate into regions of lower electric field. The critical electric fields for atmospheric electrical discharges as shown in Figure 3.7 are based on those measured in laboratories at ground pressure and are then scaled to sprite altitudes. Breakdown voltages depend on the ratio of electric field to atmospheric density, thus the critical fields scale proportionally with atmospheric pressure (or density) [*Raizer,* 1991, pg. 324].

Figure 3.7 from *Pasko et al.* [2001] shows that the critical electric fields are only exceeded by the electrostatic field of the thundercloud at higher altitudes. An extremely large charge moment of 6000 C-km for the lightning stroke allows streamers to be initiated at altitudes as low as ∼55 km while a 1000 C-km stroke can only initiate streamers above ∼75 km. This figure also shows the obviously expected fact that charge deposition at 7 km altitude (dashed lines) is expected to create a lower field at sprite altitudes than that of charge deposition at 10 km (solid lines).

3.3.4 Streamer radius

Predicted radial scaling with altitude

Vitello et al. [1994] derived an approximate relation involving the streamer radius, electric field, electron density and velocity by setting the conduction current in the streamer body equal to the displacement current in the streamer head. By simplifying the streamer geometry to a cylindrical body and spherical head, the conduction and displacement currents can be approximated as:

$$I_c \simeq q_e \pi r_s^2 n_{e_b} \mu_e E_b \tag{3.5}$$

$$I_d \simeq \frac{\epsilon_0 \pi R_h^2 E_h v_s}{R_h} \tag{3.6}$$

where r_s is the streamer radius, n_{e_b} is the electron density in the body, E_b is the electric field in the body, μ_e is the electron mobility, R_h is the radius of curvature of

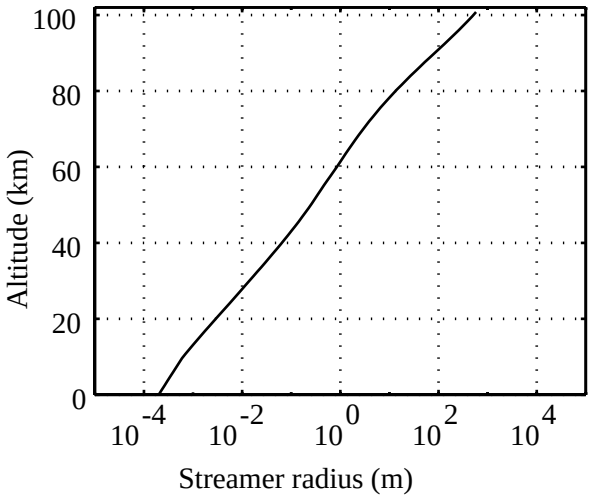

Figure 3.8: Streamer radius scales inversely with neutral density following the discussion in *Pasko et al.* [1998]. A typically observed value of 0.02 cm was used for the ground level radius value.

the streamer head, E_h is the electric field in the head, and v_s is the streamer velocity. By setting the conduction and displacement currents equal to each other (for stable streamer propagation) and substituting in the dielectric relaxation time constant $\tau_s{=}\epsilon_0/\sigma_s$ where $\sigma_s{=}q_e n_{e_b} \mu_e$, the following relation is derived [*Vitello et al.*, 1994]:

$$\frac{E_b}{E_h} = \left[\frac{R_h}{r_s}\right] \left[\frac{v_s \tau_s}{r_s}\right] \tag{3.7}$$

Following the discussion in *Pasko et al.* [1998], if it is assumed that both E_b/E_h and R_h/r_s remain constant with altitude, that $\tau_s{\sim}N^{-1}$, and that v_s is invariant with altitude, this relation shows that streamer radius $r_s{\sim}N^{-1}$. Figure 3.8 shows a plot of the variation of the characteristic streamer radius with altitude for a typically observed ground level radius of 0.02 cm.

Telescopic observations of streamer radii

Many sprites were observed by the telescopic imager during a large storm on July 13, 1998. Case studies of selected sprite events during this storm are discussed in the next section. In order to study the altitude dependence of streamer radius, the

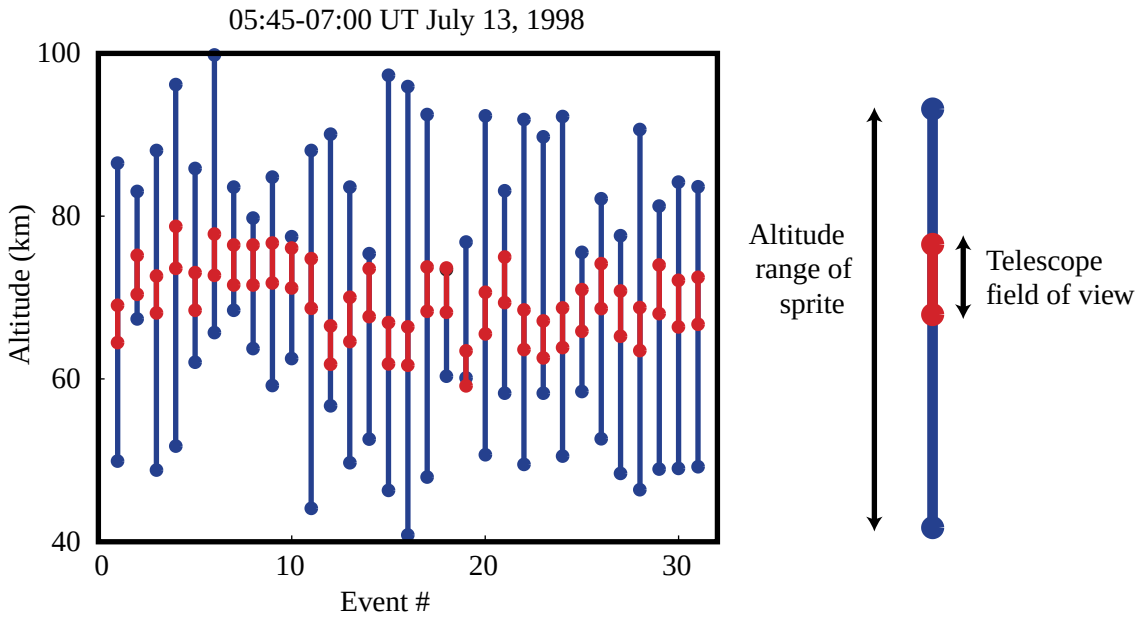

Figure 3.9: The altitude range covered by the telescopic system during a large storm on July 13, 1998. The blue bars represent the altitude range of the entire sprite (as observed in the wide FOV imager) and the red bars show the altitude range covered by the telescopic images ($\sim 60 - 80$ km)

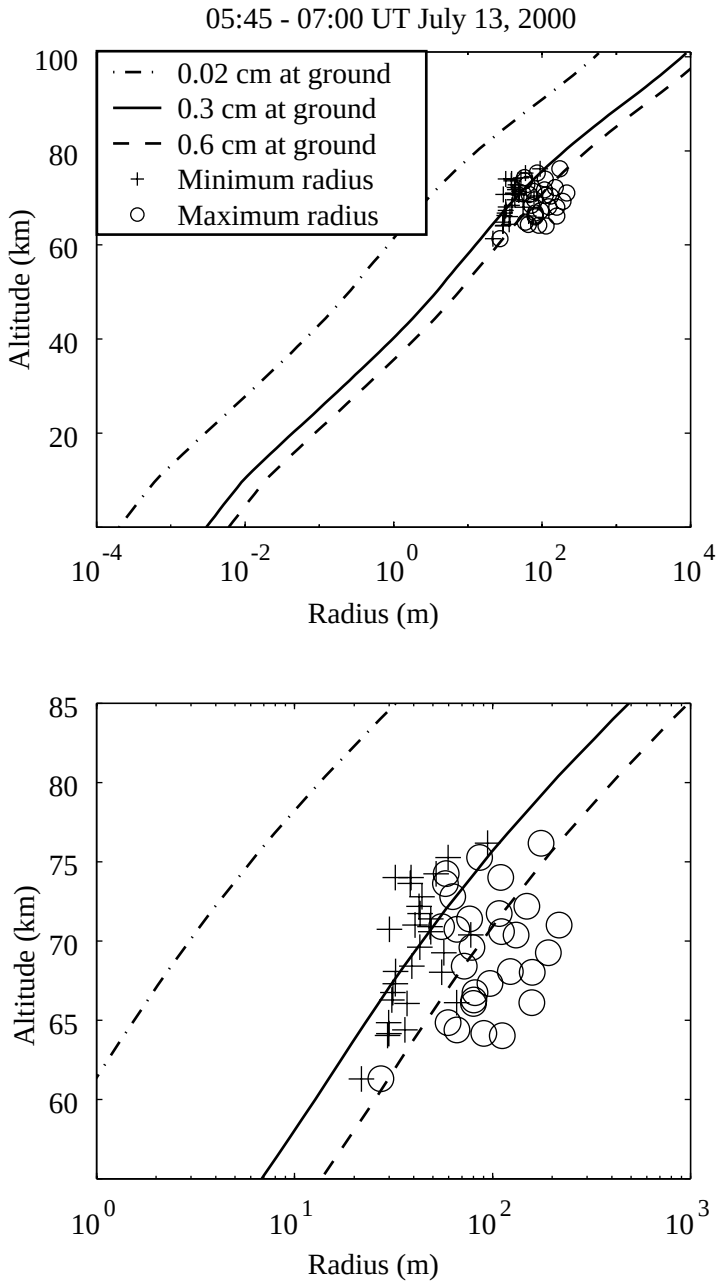

Figure 3.10: Sprite streamer widths measured in telescopic images taken during the July 13, 1998 storm. The lines relate predicted values of streamer radii for various ground level values extrapolated to sprites height. The plus signs show the minimum streamer radii measured in each sprite event while the circles show the maximum radii. It can be seen that the measured streamer radii exceed that of the predicted value for ground level streamer width of 0.02 cm.

streamer widths in 31 sprites from this storm were measured. The streamer width in the telescopic images is defined as the half-maximum width of brightness. Figure 3.9 shows that the telescopic images from this storm cover an altitude range of $\sim 60-80$ km.

The measured streamer widths are plotted in Figure 3.10. The dot-dash line shows the predicted streamer widths obtained using a value at the ground level of 0.02 cm and scaling inversely with neutral density. The corresponding streamer widths for ground level values of 0.3 cm and 0.6 cm are shown respectively with solid and dashed lines. The plus signs (+) plot the minimum streamer width measured for each sprite event while the circles (o) indicate the maximum streamer width. As can be seen, ground-level streamer width values of 0.3 cm and 0.6 cm (scaled inversely with neutral density to sprite altitudes) provide a better fit to the observed data during this particular storm. Although 0.02 cm is commonly used as the streamer radius in air at atmospheric pressure, laboratory measurements do show a range of radii; for example, *van Veldhuizen et al.* [2002] measure atmospheric streamer diameters to be 0.016 ± 0.003 cm. *Yi and Williams* [2002] find the streamer radius to be highly dependent on the ratio of N_2 to O_2 as well as on the polarity of the streamers. At ground level, the atmosphere contains $\sim$20% O_2 [*Davies,* 1965, pg. 5]. In general higher percentages of O_2 lead to higher streamer radii due to the role of photoionization and negative streamers are typically wider than positive streamers [*Yi and Williams,* 2002]. *Yi and Williams* [2002] measured streamer radii to range from $0.2 to 0.8$ cm. In light of such measurements, the streamer radii observed by the telescope fall within the values of other observations when extrapolated to ground level. It may be possible to extract information about neutral atmospheric composition by using sprite streamer data and by studying storm-to-storm variability.

3.4 Telescopic observations of high altitude streamers

Hundreds of cases of fine structure in sprites were documented with the Stanford telescopic imager. Selected cases from July 13, July 19, and August 6, 1998 are used to illustrate various streamer properties observed in these high altitude electrical discharges.

3.4.1 Case I: 05:15:00 July 13, 1998

This event illustrates the rich diversity of morphologies possible in the fine structure of a single sprite event. Faint downward branching streamers, also referred to as "sprite tendrils" [e.g. *Wescott et al.,* 1998; *Stanley et al.,* 1999; *Stenbaek-Nielson et al.,* 2000], are frequently observed in the telescopic images. They occur either at the base of the sprite or prior to a bright sprite event. Both types occur in the 05:15:00 UT July 13, 1998 event shown in Figure 3.11.

As in previous video images shown in Chapter 3, the monochromatic (black and white) digitized video images presented in this and subsequent figures of this and later chapters have been false-colored in order to better show the dynamic range of the data. The false-color scale ranges from blue at minimum brightness to red at maximum brightness (e.g., refer to the colorscale in Figure 1, *Gerken et al.* [2000]). None of the narrow field images presented here were saturated in the camera; however, the dynamic ranges have been scaled (in brightness and contrast) in order to enhance relatively dim fine-scale features. In the first narrow FOV panel (N1) faint downward-branching streamers precede the main sprite event and are not evident in the wide FOV image. The second narrow FOV panel (N2) similarly has a downward-branching structure but this one is at the base of a bright sprite as can be seen from the corresponding wide FOV image. It should be noted, however, that each video frame corresponds to 17 ms of photon accumulation, which means that in fact both sets of downward streamers could have preceded the bright sprite structures. Sprite features observed with high-speed imagers have been seen to develop within a few

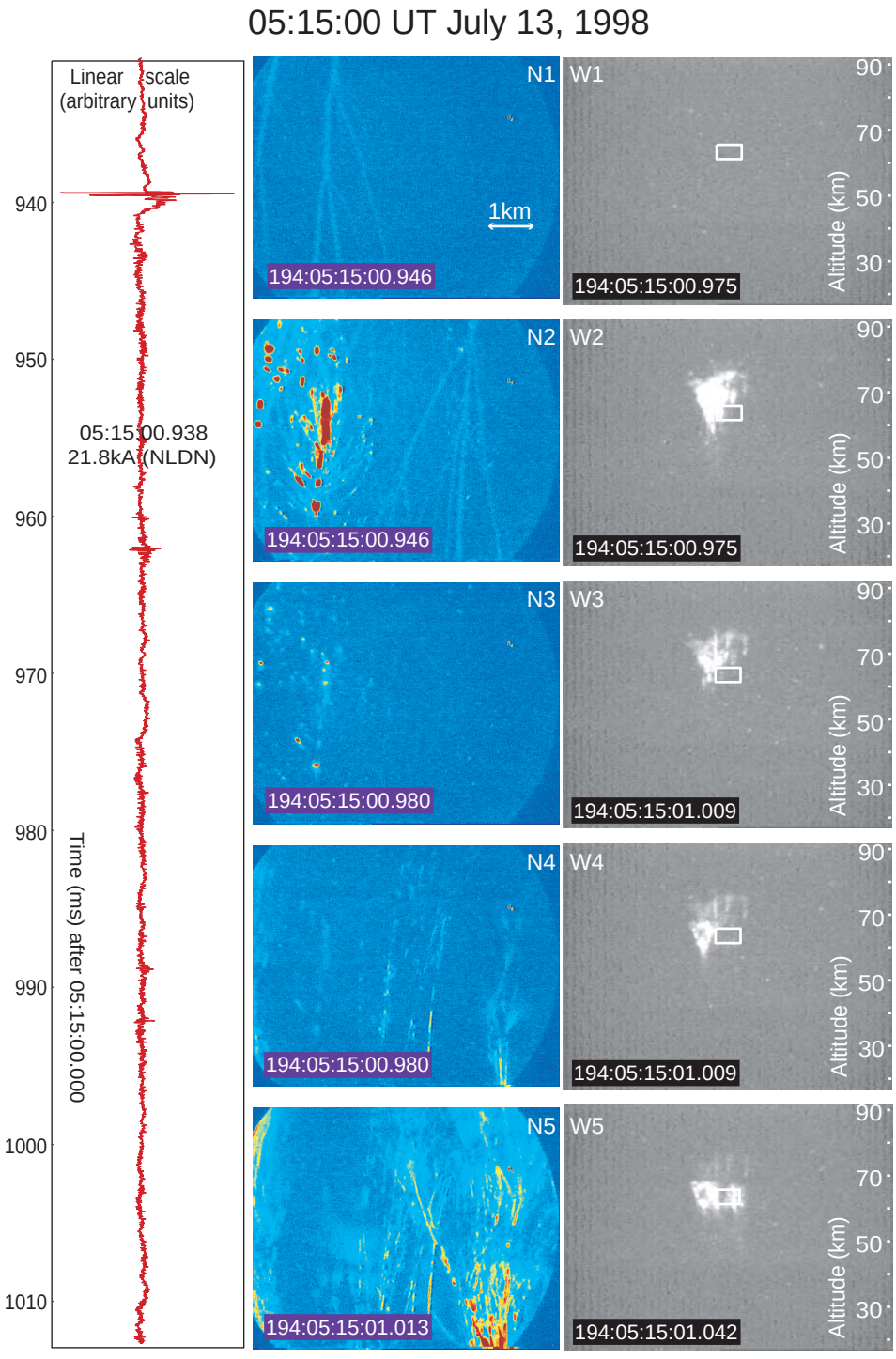

Figure 3.11: This sprite event exhibits several types of features including faint downward positive streamers, bright upward negative streamers, beading, and a propagating diffuse glow. The leftmost panel contains the Stanford ELF recording during the event. The middle column shows the telescopic FOV (panels N1-N5) and the rightmost column shows the wide FOV (panels W1-W5). The narrow FOV with respect to the wide FOV is depicted by a white rectangle in the wide FOV images. Images presented are de-interlaced NTSC TV images and time-stamping occurs at the end of the first field of each frame.

milliseconds [*Stanley et al.,* 1999; *Stenbaek-Nielsen et al.,* 2000]. In both the first and second frames the streamers maintain a fairly constant half-maximum width of $\sim 120 - 130$ m ($10 - 11$ pixels) as predicted in theoretical models of the filamentary stage of streamers [*Vitello et al.,* 1994]. The brightness of the filamentary feature remains fairly constant and is ∼10 kR as determined by the camera calibration described in *Gerken et al.* [2000]. No beading is apparent. Relatively little branching is observed in these structures with the streamers apparently propagating several kilometers before splitting. The streamers appear to bifurcate at close to the same angle each time with two primary streamers continuing to create a fractal-like pattern. Streamer bifurcation was modeled by *Pasko et al* [1998] who proposed that the streamers split when their radius exceeds that necessary for stable propagation. The regular branching may imply that the local electric field (external to the streamer) is uniformly vertical and that the branches follow the field lines created by the superposition of the local electrostatic field and the electric field of the streamer head (as illustrated in *Raizer,* [1991, pg. 332]). Although it should be possible to reconstruct these field lines from the streamer images, triangulation with stereo images is necessary since the angle of branching cannot be determined from a single two-dimensional image.

An upward-branching structure can be seen in the second narrow FOV panel (N2) where the downward branching had occurred in the previous panel (N1). The downward branches were likely initiated above the field of view and propagated downward (and out of the field of view) while the apparent upward branching structures may have been initiated below the field of view and have propagated into it. Since the associated sferic was produced by a positive cloud-to-ground (CG) lightning stroke, the primary electric field set up at high altitudes above the thunderstorm following the CG is expected to be directed downward. The downward branching structures are thus likely to be positive streamers while the upward branching structures are negative streamers.

The field of view of the telescope covers $\sim 60 - 65$ km altitude range in these images. As described in *Gerken et al.* [2000], the altitude range for each sprite is calculated using the elevation ad azimuth as determined from the background starfield

and the range of the associated +CG as determined by the National Lightning Detection Network (NLDN). The greatest source of error in altitude determination is due to an imprecise knowledge of the range of the sprite since a sprite could be laterally displaced up to 40 km with respect to the causative CG [*Winckler et al.,* 1996; *Lyons et al.,* 1996]. The spatial resolution of the system is determined by the range of the object being imaged (e.g., at a range of 500 km, each pixel maps to ∼12.5 m by ∼12.5 m).The charge moment for the sferic associated with this sprite is calculated to be ∼1000 C-km using the model of *Cummer and Inan* [2000]. Figure 3.7 shows the calculated electric field versus altitude for CG discharges of varying charge-moments as well as the conventional breakdown electric field and critical electric fields for stable positive and negative streamer propagation. According to these calculations, even for a relatively large discharge involving the removal of 100 C from 7 km altitude, the electric field only exceeds the breakdown field at an altitude of 75 km or higher. This results is consistent with the images of positive streamers presented in this example, which appear to have been initiated at an elevation greater than 65 km. However, the negative streamers appear to have been initiated at an altitude below 60 km where the breakdown field is not exceeded. Since the positive streamers precede the negative streamers it is possible for them to have played a role in the initiation of the negative streamers due to the enhanced electric field in the vicinity of the streamer head [*Dhali and Williams,* 1987]. Such a circumstance is consistent with high-speed camera images [*Stanley et al.,* 1999] showing that sprites begin as downward branching forms and subsequently develop into upward branching structures.

The upward branching filaments (i.e., negative streamers) found in the second telescopic panel (N2) have much higher peak brightness (average value of ∼240 kR over the duration of a video field) than the positive streamers preceding them. Streamer emission intensity has an exponential dependence on the electric field in its head [*Kulikovsky,* 1997]. For a given streamer radius and velocity, the electric field found in the streamer channel is higher in a negative streamer whereas the field in the streamer head is higher in a positive streamer [*Babaeva and Naidis,* 1997]. Tree-like structures similar to the ones shown in this example are probably the time-integrated images of an upward-moving streamer with many streamers emanating from its tip.

Extensive beading is also observed. As opposed to the positive streamers discussed previously, in general, beads persist for one or more frames, either remaining stationary or drifting slowly as was reported by *Stenbaek-Nielsen et al.* [2000].

In the third panel (N3) of telescopic images in Figure 3.11, some of the beads continue to glow. The only other structure present is a faintly glowing portion of the negative streamer that continues to glow in the fourth and fifth panels (N4 and N5). By the time of the fourth panel (N4), most of the beaded structure has faded away. New and almost vertical filaments are formed with no branching. These bright filaments are ∼60 m wide and have a brightness of ∼50 kR. The direction of propagation is not evident. The filaments consist of a number of long luminous segments with dark spaces in between. In the following panel (N5), these filaments remain present and grow brighter with some of the segments merging to form long channels. The rightmost group of filaments diverge from vertical in a cone expanding with altitude, indicating upward propagation. These filaments may be in close proximity to each other and are therefore repelled by one another by electrostatic forces as would be expected in the case of charged conductors.

3.4.2 Case II: 04:07:48 July 19, 1998

This event (Figure 3.12) is an example of a very slowly propagating upward (negative) streamer structure preceding a bright sprite. As opposed to Case I where a sferic was recorded in ELF at the same time as the initial streamers (to within the 17 ms resolution of a video field), the closest sferic recorded prior to this sprite was 30 ms before the start time of the telescopic video field in which the event was first observed (N1). No CG lightning strokes are reported by the National Lightning Detection Network (NLDN) for the associated storm within the full second during which the sprite was observed so that the delay between causative sferic and sprite initiation is in this case ambiguous. The first three panels of the wide FOV camera (W1 - W3) show that initially a very small and dim sprite occurred and was followed by the sudden development of a large bright sprite in the fourth panel (W4). The subsequent frames show further development of this bright sprite. There is a large ELF pulse

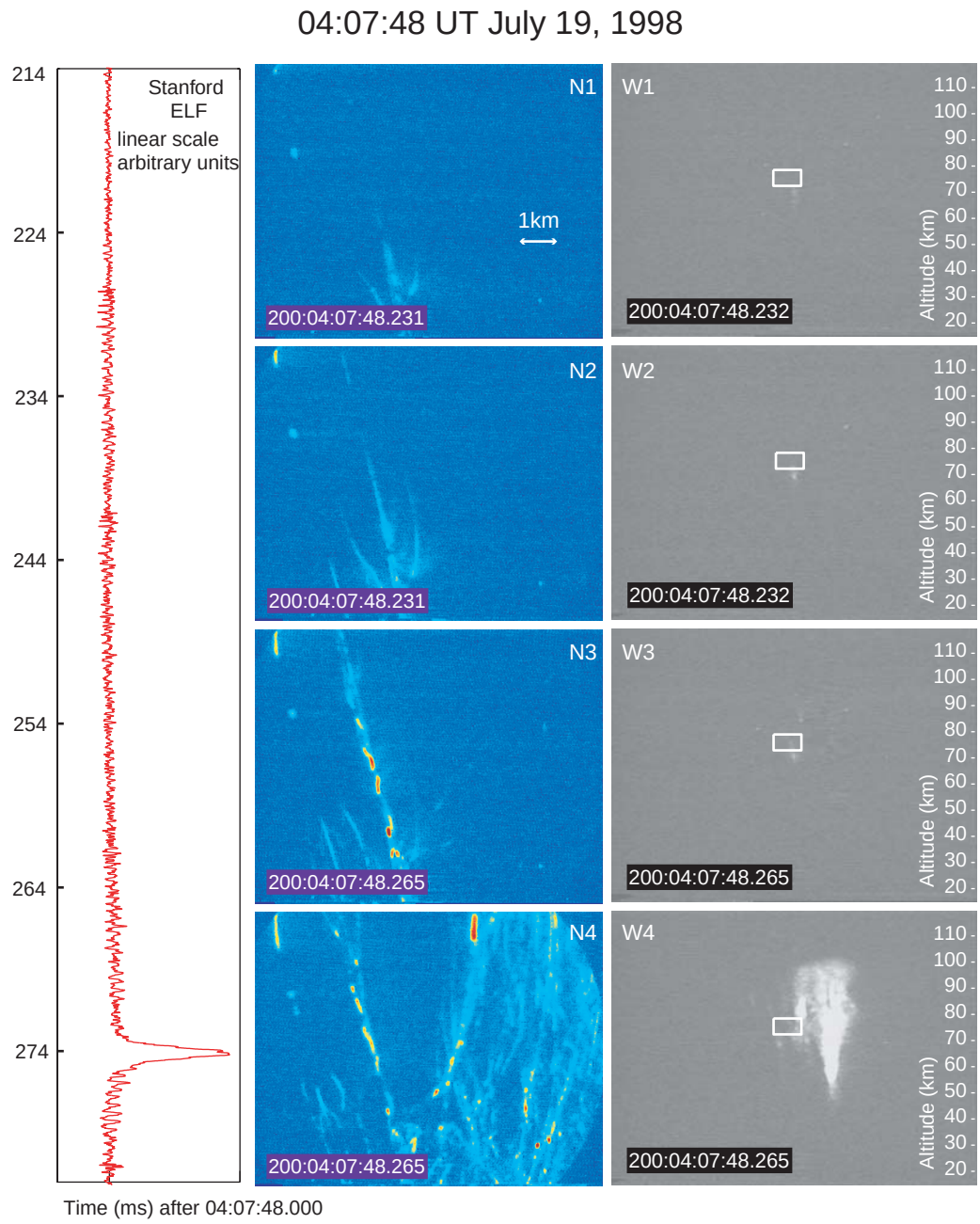

Figure 3.12: Slowly propagating streamers preceding a bright sprite event at 04:07:48UT July 19, 1998. No sferic signature is observed in the Stanford ELF recording for 30ms prior to the appearance of the bright sprite and no CG is reported by NLDN during the second of this event. An ELF peak is observed in conjunction with the bright sprite. Images presented are de-interlaced NTSC TV images and time-stamping occurs at the end of the first field of each frame.

recorded at Stanford simultaneous (within the ∼17 ms resolution of a video field) with the bright sprite event that appears to have been radiated by the sprite itself [*Cummer et al.,* 1998].

The telescopic images capture two streamer structures in this event that develop very slowly prior to the bright sprite. The first narrow FOV panel (N1) shows a forked structure in the middle bottom portion of the field. The middle branch of this forked structure has a width of ∼120 m as seen in the second panel (N2). Based on the measurements from two successive video fields, the middle branch propagates upward at a velocity of $\sim 10^5$ m/s, two orders of magnitude less than the velocities measured by *Stanley et al.* [1999], and at the lower limit of that predicted by *Raizer* [1998]. Observations have shown that there is a minimum velocity possible for streamer propagation that is of the order of magnitude corresponding to the electron drift velocity [*Raizer et al.,* 1998]. Simulations indicate that lower ambient voltages (i.e., electric field) result in lower streamer velocities [*Dhali and Williams,* 1987], and such may be the case for the example in hand. The electric field between the clouds and the ionosphere may be initially low (thus causing lower velocity streamers) but may be increasing in time in response to a continuing current flow to ground from a previous lightning stroke.

Simultaneous to the upward development of the forked structure, another streamer appears to start at the top of the field of view and extends down towards the middle branch. It is possible that this extension is actually a part of the upward streamer with a dark space in the middle. In such a case, the velocity of this streamer would be higher than that stated in the previous paragraph. Finally, in the third panel (N3), the middle branch reaches its maximum brightness and beading occurs. It appears that the middle branch may have reached a charge source (i.e., a region of available free charge) that caused a "return stroke" to propagate downward following the path of the original streamer. Typically, this sort of a process appears in the form of a reversed streamer at a much higher ionization than the original streamer [*Raizer,* 1991, pg. 343]. If the causative CG lightning has slow charge removal (≥1 ms) then the time dependence of the effective boundary separating lower ionospheric regions dominated by displacement and conduction currents begins to play a significant role

in streamer dynamics [*Pasko et al.,* 2000]. This effective boundary can be used as a dynamic reference for the boundary of the lower ionosphere. If the lower ionosphere has a high conductivity, the effective boundary is able to quickly descend to 80 km altitude [*Pasko et al.,* 1999; *Pasko et al.,* 2000]. The upper edge of the field of view in this example is in fact at ∼80 km so that it is possible that the upward going streamer encountered the lower boundary of the highly conducting ionosphere, leading to the initiation of a "return stroke" from the ionosphere. A return stroke is an ionization wavefront which travels in the reverse direction along the path previously forged by a streamer and is associated with high currents and bright optical emissions [*Uman,* pg. 7, 1969].

The second slowly developing feature present in this sprite event is a downward propagating streamer that begins at the upper left-hand corner of the narrow FOV. The streamer expands downward over the four fields shown with a speed of $\sim 10^4$ m/s and is much brighter than the upward going streamers. There is a small bead below the streamer that brightens and moves upward in the direction of the bright downward streamer. In the third panel (N3) a dim streamer reaches upward beneath the bead and continues to propagate in the fourth panel (N4). Although these features appear to be along the same channel, such is not necessarily the case since only two dimensions are imaged. Columnar structures have been observed in other sprite events but beads are generally found in closer proximity to the base of the column [*Wescott et al.,* 1998; *Gerken et al.,* 2000].

3.4.3 Case III: 04:44:07 UT July, 19 1998

This case is an example of faint positive streamers found at the base of a small carrot sprite on the side of a large bright sprite event as shown in the wide FOV panel (W1) of Figure 3.13. Faint positive streamers are frequently observed either preceding a bright sprite or at the base of a bright sprite. These streamers can occur in a dense filamentary structure [*Gerken et al.,* 2000] or as more isolated tendrils with fewer bright spots. As was also the case in Figure 3.11, bifurcating branching angles seen in this example are similar to that modeled by *Pasko et al.* [1998]. The streamers

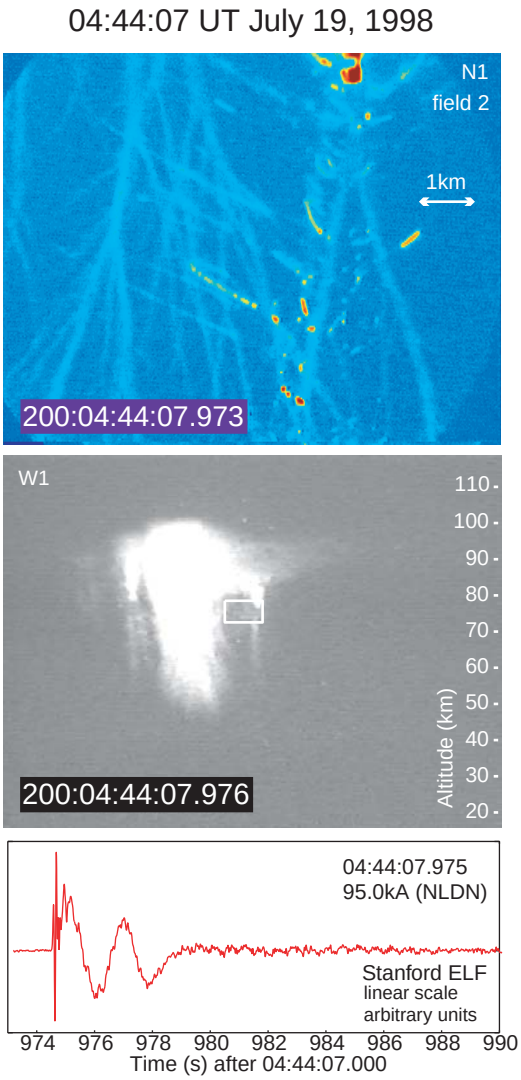

Figure 3.13: Faint downward branching positive streamers during a large bright sprite event at 04:44:07 UT July 19, 1998. Faint positive streamers are frequently observed either preceding a bright sprite or at the base of a bright sprite.

observed in the telescopic image (N1) range in width from ∼80 to 145 m. Some beading does occur and appears to follow an upward branching path. This upward branching path may be part of another sprite structure in front of (i.e., closer to the observer) the tendrils or alternatively may be a negative streamer traveling back up the original positive streamer channel and branching upwards. The top portion of the rightmost tendril group is in the base of the bright region of the carrot sprite and is much brighter than the faint downward branches.

3.4.4 Case IV: 05:53:46 UT July 13, 1998

Figure 3.14 shows an example of an unusual sprite structure exhibiting only downward branching. The upper non-branching columns expand with altitude as predicted [*Pasko et al.,* 1998; *Raizer et al.,* 1998]. This sprite develops over several fields. It is initiated with a downward "wishbone" shape that then grows an upward column and develops further downward branching around the "wishbone". The upward columns range in width from ∼200 to 210 m and the downward branches range in width from ∼71 to 100 m. Lasting for over 100 ms, the columns are seen in subsequent fields (not shown) to move upward at a speed of $\sim 10^4$ m/s and are therefore assumed to be negative streamers. There appears to be a different threshold radius between the positive and negative streamers since the positive streamers branch while the negative streamers expand although they presumably originating from the same point. It has been shown that a streamer that starts with a radius below some critical threshold expands while those with too large a radius contract [*Vitello et al.,* 1994] or branch [*Pasko et al.,* 1998]. This sprite event may be a grouping of double-headed streamers initiated by some sort of plasma density enhancement such as that which would be caused by heated dust particles [*Zabotin and Wright,* 2001]. In theoretical models, double-headed streamers have been found [*Vitello et al.,* 1994] to evolve slower with lower streamer propagation velocities, and lower peak electric fields than the corresponding values for single-headed streamers.

The negative streamer columns have abrupt termination points that slowly move upward in subsequent fields (not shown). There is a less luminous broader segment

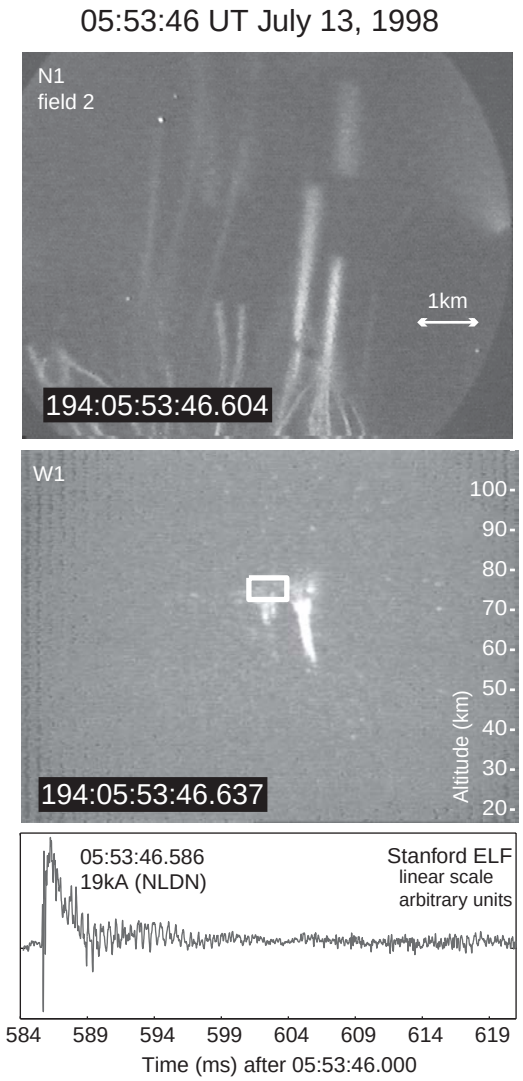

Figure 3.14: Bi-directional streamers in a small sprite event at 05:53:46 UT July 13, 1998. The positive streamers branch while the negative streamers expand indicating that this bi-directional streamer may have been initiated with a radius below that necessary for negative streamer propagation but above the critical radius for positive streamer propagation.

above the rightmost column that may be part of the same channel. It is interesting that there are several structures in the telescopic image with the same morphology (i.e., branching on the bottom, column on top) indicating that in this case, streamer morphology is not a random process but rather is one that corresponds to a particular atmospheric and/or ionospheric condition. A localized plasma enhancement may have been present in this region and may have caused several double-headed streamers to form.

Chapter 4

Diffuse glow and beading

As shown in the previous chapters, numerous morphologies and time scales are observed in telescopic images of sprites. After our discussion of the streamer discharges in Chapter 3, we consider in this chapter other features observed in sprites, namely diffuse glow and beading. At low altitudes the streamer mechanism dominates (see Chapter 3), while at upper altitudes diffuse glow is generated. As implied by the name, diffuse glow is observed as a dim homogeneous glowing region with no fine structure present. Frequently beading is also observed in sprites. While both sprite streamers and diffuse glow can be accounted for using the physics of gas discharges, the beading phenomenon is not well-understood and currently no theory fully explains the underlying physical mechanisms. Beads observed by the telescopic imager either remain stationary or travel and can last for over 100 ms.

4.1 Diffuse glow in sprites

It was pointed out earlier (Section 1.2.1) that a diffuse glow region usually occurs at the upper altitudes ($\sim 70 - 95$ km) of sprites. This diffuse glow may exist independently or either precede or accompany the streamer formation region at lower altitudes. The diffuse glow region (also called "sprite halo") and the streamer formation region can exist independently due to the strong altitude variation of the timescale for electrical relaxation of post-lightning quasi-electrostatic field above thunderclouds

[*Barrington-Leigh and Inan,* 2001].

A diffuse glow can occur in regions of low neutral density and/or high electron density in the presence of an applied electric field. The glow is initiated by energetic electrons (possibly seeded by background cosmic rays), which are accelerated in this electric field and then collide with neutral particles. These collisions can result in additional electrons and/or photons being emitted through ionization and excitation. The electrons regain their energy by acceleration in the electric field. These electrons can then suffer further collisions and if the electric field is high enough the process continues in an avalanche fashion. A schematic depiction of this process of electron avalanche is shown in Figure 4.1. If only a few electrons were available as in the streamer region discussed in Chapter 3, then these avalanches could form double-headed streamers. In the diffuse glow region of high ambient electron density, however, the conductivity is so high that the electric field is quickly expelled before streamers are able to form. A diffuse glow is thus observed throughout the volume [*Raizer,* 1991, pg. 2].

4.1.1 Transition between streamer and diffuse glow regions

Figure 4.2 shows an example of the transition region between streamer formation and glow discharge in a sprite. The diffuse glow/streamer transition altitude can be used (in combination with a theoretical model) to identify the ambient mesospheric/lower ionospheric conductivity profile and the observation of this transition altitude potentially provides a new means of remotely sensing the lower ionosphere [*Pasko and Stenbaek-Nielsen,* 2002]. Unlike the examples shown in the previous chapter in which streamers abruptly terminated, the streamers evident in Figure 4.2 fade to broadly expanding, less luminous diffuse glows. The transition region only exists over a narrow region of $1-2$ km in height at an elevation of $\sim$80 km, consistent with model predictions by *Pasko et al.* [1998] that the transition region should exist between $75-85$ km. Since no branching is evident, the polarity of the streamers is ambiguous. However, one possible clue may be the fact that the tips are tapered. As previously

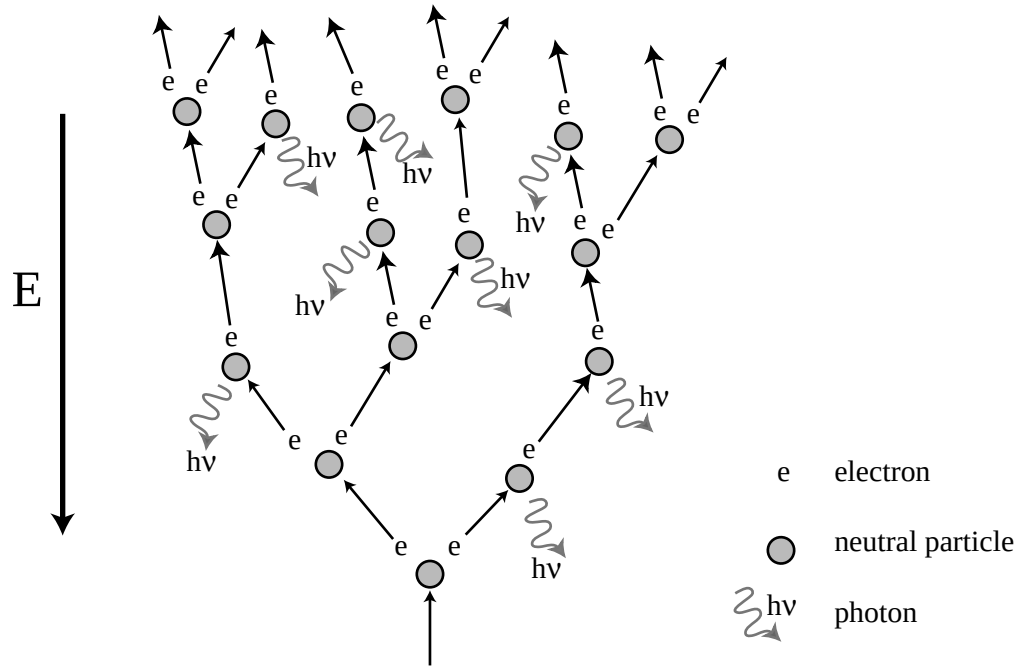

Figure 4.1: Schematic description of the process of electron avalanche initiated by a single electron in the presence of a large electric field.

mentioned, numerical models indicate that streamers initiated with too small a radius should expand until they reach their critical radius [*Vitello et al.,* 1994]. It may be that the diffuse glow was initiated first at high altitude and that streamers were initiated by seed electrons as the glow expanded to lower altitude regions where the driving electric field persists so that the streamer regime becomes possible. These streamers would then be positive downward propagating streamers that expanded to a stable radius. Diffuse glow regions of this type have been identified as the "sprite halo" [*Barrington-Leigh and Inan,* 2001] as discussed in greater detail in the following section (Section 4.1.2). If the streamers were negative and upward propagating they would be expected [*Vitello et al.,* 1994] to expand into the glow region smoothly. It is thus more likely that these structures are indeed positive streamers.

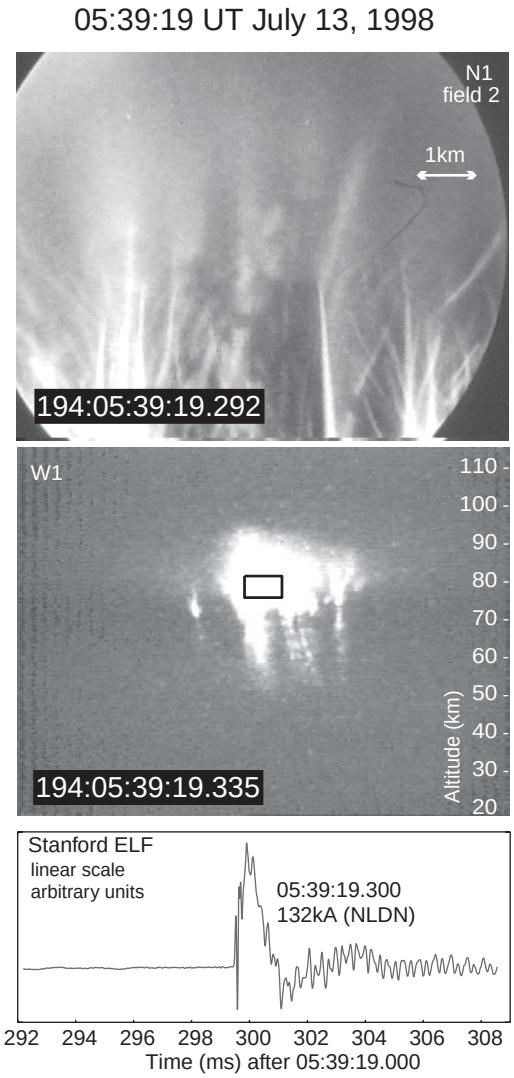

Figure 4.2: Transition between the streamer region and the diffuse glow region as seen in a large sprite event at 05:39:19.335 UT. The transition region only exists over a narrow region of $1-2$ km in height at an elevation of $\sim$80 km, consistent with model predictions that the transition region should exist between $75-85$ km.

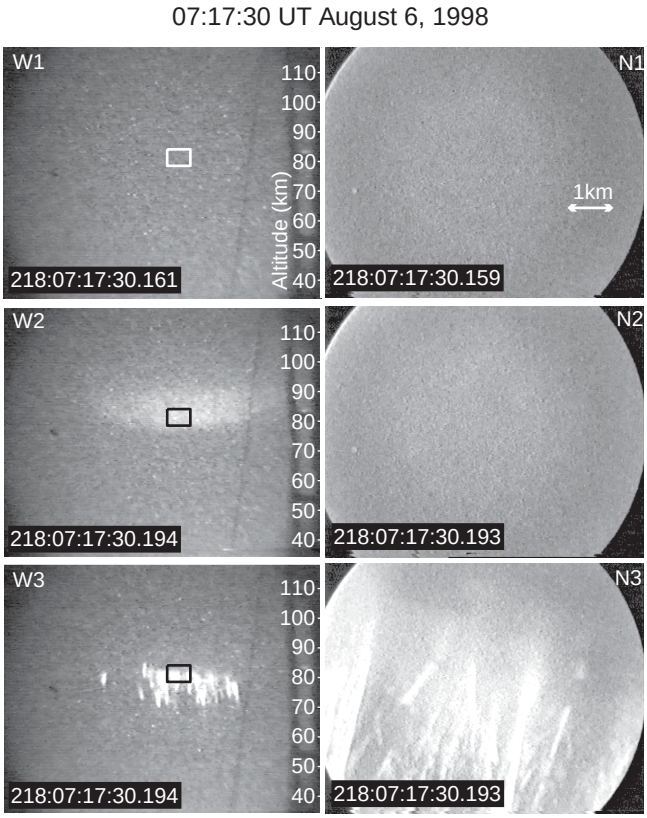

Figure 4.3: Diffuse glow region (or "sprite halo") observed during an event at 07:17:30UT August 6, 1998. As expected, no structure is observed in the telescopic image - only a faint overall brightening.

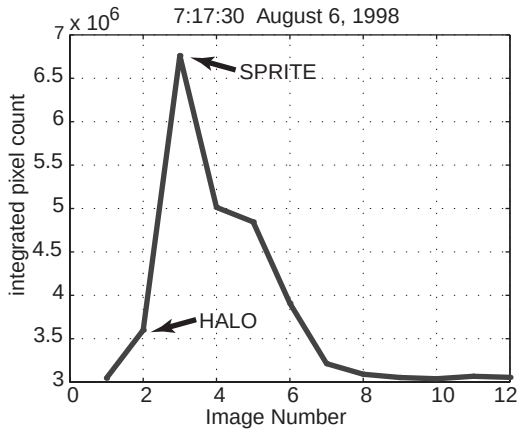

Figure 4.4: Integrated pixel count during the sprite halo event shown in Figure 4.3. Pixel counts were summed over each image for 12 successive images. It is apparent that the telescopic images do brighten at the time of the sprite halo although no structure is seen.

4.1.2 Sprite "halos"

Figure 4.3 displays an example of the diffuse glow region in sprites - the so-called "sprite halo". As previously mentioned, this diffuse glow region may exist by itself or may either precede or accompany streamer activity (at lower altitudes) and generally occurs at an altitude of ∼70 to 85 km. The diffuse glow region is believed to be produced by a relatively large charge moment change occurring over a relatively short timescale [*Barrington-Leigh and Inan,* 2001]. Triangulation shows that while sprites can be displaced by up to 50 km from the causative CG, halos tend to be centered directly over the lightning stroke [*Wescott et al.,* 2001].

Figure 4.3 shows a sequence of three fields of a sprite event. The wide FOV images, on the left, display first one field prior to the event, then a sprite halo between $\sim 80-90$ km altitude, and finally a structured sprite below at $\sim 70-85$ km altitude. Subsequent images (not shown) contain further development of the structured sprite. The field of view of the telescope is positioned in altitude such that it observes the lower half of the sprite halo and the top of the structured sprite. As expected, the telescopic images (on the right) show no fine structure in the sprite halo. The overall brightness level does however increase at the time of the sprite halo. This faint

diffuse glow is difficult to detect visually on the images but if the pixel counts are integrated over each image and plotted versus time, the brightening due to the sprite halo is readily observable. A plot of integrated pixel counts for several images of this sequence is shown in Figure 4.4. The first three images correspond to those shown in Figure 4.3 while the rest are subsequent images displaying sprite development and decay. As can be seen, the integrated count for the image containing the sprite halo is significantly greater than that of the image preceding or following the sprite event but much less than that of the structured sprite.

Sprite halos are often observed to have upwardly concave shapes, due to the enhanced ionization of the descending space charge region [*Barrington-Leigh et al.,* 2001]. The enhanced ionization leads to higher electric fields outside the diffuse glow region and thus affects streamer formation. Sprite halos account for streamer initiation at elevations below that predicted by models which do not take into account the effects of a descending enhanced ionization region.

4.1.3 Propagating diffuse glow patches

In the fifth panel (N5) of Figure 3.11 beading as well as faint broad diffuse glow was observed to be present. A glowing region near the middle of the panel proceeds to move upward in the six subsequent fields, lasting over 100 ms. The movement of this diffuse glow is shown in Figure 4.5 with a superimposed stationary dashed white line for reference. Note that the brightness and contrast in these images (N1-N6) have been adjusted to enhance the diffuse glow. The glowing region covers an area of $\sim 4.80 \times 1.75$ km and propagates at a velocity of $\sim 10^4$ m/s, three orders of magnitude less than streamer velocities reported by *Stanley et al.* [1999]. Other examples of this type of glow were also found in telescopic images of sprites. The glow generally occurs in the presence of many fine filaments as is the case here. These filaments and other preceding ionization channels are likely to temporarily raise the local electron density to the level where a glow discharge is maintained instead of a streamer structure as is often observed at higher altitudes ($\sim 70 - 85$ km). Each example of this type of propagating diffuse glow has been found to propagate upward. Frequently, multiple

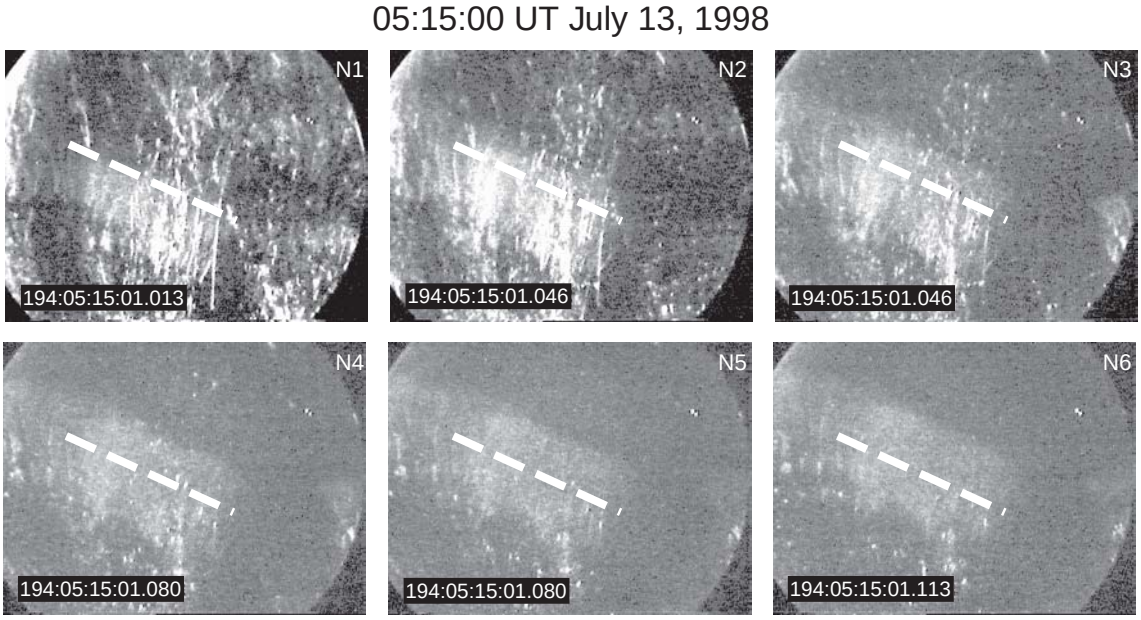

Figure 4.5: Propagating diffuse glow during the 05:15:00 UT July 13, 1998 event. The dashed white line has been superimposed for reference. The glowing region covers an area of $\sim 4.80 \times 1.75$ km and propagates at a velocity of $\sim 10^4$ m/s, three orders of magnitude less than streamer velocities previously reported. Note that N1 in this figure corresponds to the fifth panel (N5) of Figure 3.11 but the brightness and contrast in the images (N1-N6) of this figure have been adjusted to enhance the diffuse glow.

horizontal striations are observed in the glowing region.

Propagation of this horizontally-striated diffuse glow may be due to a diffusion-dominated mechanism similar to that observed in striated glow discharges [*Stewart,* 1956; *Raizer,* 1991, pg. 230]. A striated state is preferable in a glow discharge, due to the fact that it is more likely for an electron to gain enough energy for ionization without losses through excitation in a short distance with a steep potential gradient than over a longer distance with a slowly increasing potential gradient. Additionally, excitation losses are low in the flat potential region between striations [*Allis,* 1976], resulting in a striated glow discharge having a lower average electric field than a homogeneous one.

Raizer [1991, pg. 234] gives the following interpretation of the striated state sometimes observed in a diffuse glow discharge. If an instability is triggered such that striations are set up, the charge density becomes arranged sinusoidally in the direction of the ambient electric field lines. Although there is a high degree of charge neutrality, the electrons diffuse somewhat and charge separation occurs (refer to Figure 9.5 and page 235 of *Raizer* [1991]). This charge separation enhances the ambient field on one side of the charge density peaks while diminishing it on the other side. Electron temperature is almost in phase with the electric field, and since the ionization rate is more sensitive to electron temperature than to electron density, ionization is increased in these regions of field enhancement. Thus, the sinusoidal variation of the ionization rate is 90° out of phase from that of the charge density variations and in general the striations are in motion [*Raizer,* 1991, pg. 234]. While the phase velocity of these charge density striations is generally pointed in the direction of the ambient electric field, the group velocity is always pointed in the opposite direction from that of the ambient field [*Allis,* 1976]. This property means that even though the striations themselves may be traveling in the direction of the electric field, the enhanced regions of glow viewed by an observer are seen to be traveling in the opposite direction [*Raizer,* 1991, pg. 236]. In the case of a glow discharge tube, the bright regions are observed to travel from cathode to anode while in the case of sprites they would travel towards the ionosphere (in a field set up by a positive CG) as is indeed observed to be the case in Figure 4.5.

Studies of breakdown phenomena in liquids have shown that shock waves can be created by streamers forming rings of ripples emanating from the streamer tips. These shock waves have been found to have slower velocities than the causative streamers [*Devins et al.,* 1981; *Yamada et al.,* 1990]. A similar phenomenon may be present in the upper atmospheric breakdowns such as that observed in this example.

4.2 Beading

Falling neither into the category of streamers nor diffuse glow, beads are frequently observed in sprites. Telescopic images of beads show them to sometimes move up or down pre-existing streamer channels and at other times to remain stationary. The beads may persist for less than a video field ($\sim$17 ms) or for hundreds of milliseconds. Beads observed thus far by the telescope range in radius from $25 - 200$ m. Current sprite theories do not account for the existence or underlying cause of beads. In the following, we study two examples of beading in sprites observed using the Stanford telescopic imager.

4.2.1 Case I: 04:33:10 UT July 19, 1998

This sprite event exhibits the fine beading that often occurs in the middle regions of sprites. In the wide FOV images, the event is made up of a series of sprites, which move from right to left. The image shown in Figure 4.6 depicts the second sprite in the series. The beads are strung along upward-branching channels at fairly regular intervals and range in size from $\sim 70 - 150$m. Most of the beads last $2 - 3$ video fields but remain stationary from field to field.

It has been proposed that beads and other structures found in sprites may in fact be initiated by dust particles [*Zabotin and Wright,* 2001; *Wescott et al.,* 2001]. Dust particles of meteoric origin in the mesosphere and stratosphere most likely have many "microspires", or small spikes, that locally enhance the quasi-static electric field which appears after a CG discharge. Microscopic protrusions are also found on massive cathodes and it has been observed that the electric fields on these protrusions

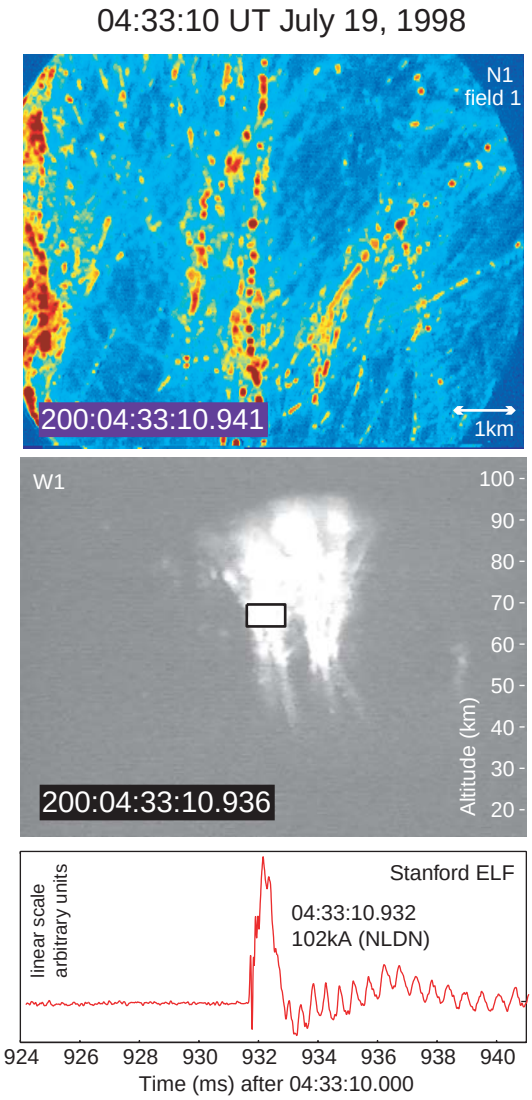

Figure 4.6: Example of fine beading in negative streamers during a large sprite at 04:33:10 UT July 19, 1998. The beads may have been initiated by meteoric dust. It may be that dust particles initiate streamers at altitudes lower than that predicted for a dust-free environment.

are enhanced by a hundredfold or more. The current caused by thermionic emissions at the protrusion tip can create enough Joule heating to explode the metal of the cathode [*Raizer,* 1991, pg. 264]. In the case of sprites, a similar thermal explosion of meteoric dust particles would create an effective plasma source that in turn could initiate a streamer. This mechanism may be responsible for sprite initiation, and the branching, discontinuous streamers, and bright beading observed in telescopic imagery of sprites [*Zabotin and Wright,* 2001].

The charge moment change at the time of the sprite in this example is calculated to be $\sim 700 - 2000$ C-km (the accuracy of the calculation is limited by the time resolution of a video field). While a 2000 C-km charge moment change could be sufficient to initiate a negative streamer at 70 km altitude, a 700 C-km charge moment most likely would be below the threshold [*Pasko et al.,* 2001]. Additionally, since the streamers are upward branching, they presumably originated below the FOV of the telescope at a lower altitude, requiring a larger charge moment change. If indeed the streamers were initiated in an electric field below the breakdown threshold, it may be that dust particles initiate streamers at altitudes lower than that predicted for a dust-free environment. A similar phenomenon has been experimentally recorded in laser breakdown of liquids where beading occurred along the breakdown axis as a result of defects such as microscopic bubbles, contaminants, or soot [*Teslenko,* 1982].

Another closely-related phenomenon is that of beading in cloud-to-ground lightning channels. Beads in cloud-to-ground lightning have been found to exist $75 - 300$ ms after the decay of the lightning channel, having diameters ranging from 50 cm to several meters [*Boichenko,* 1996]. *Boichenko* [1996] has developed a theoretical explanation for the observations of persistent beads in cloud-to-ground lightning suggesting that inhomogeneities of the atmosphere or of some parts of the lightning bolt could cause energy to be irregularly deposited within the channel. Such inhomogeneities may in fact be dust-related.

Beading appears to be primarily a negative streamer phenomenon since little beading has been observed in the positive streamers of sprites. This asymmetry in bead formation has also been found experimentally in laboratory pulsed gas discharges [*Zobov and Siderov,* 1990]. As was discussed in Chapter 3, models of positive and

negative streamers in air have shown that positive streamers have a higher electric field in their head and a higher electron density, but a lower channel electric field [*Babaeva and Naidis,* 1997]. In studies of breakdown in dielectric liquids it has been found that positive streamers appeared with a lower crest voltage, lower light emission and higher velocity than negative streamers [*Yamada et al.,* 1990; *Massala and Lesaint,* 2001]. It is possible that the more slowly propagating negative streamer with a higher channel field allows for a greater enhancement of the electric field surrounding dust microspires, thus accounting for the asymmetry in bead formation.

4.2.2 Case II: 05:43:10UT July 19, 1998

This event is an example of a single "columniform" sprite [*Wescott et al.,* 1998] imaged by the telescope (Figure 4.7). Frames preceding and subsequent to the column shown in N1 – N7 recorded by the wide FOV camera (only selected fields are shown in W1 – W4 of Figure 4.7) indicate that this sprite is the middle part of a sequence of "dancing" sprites moving from right to left across successive frames. The wide FOV recordings reveal that first, a collection of ∼15 columniform sprites occurs at approximately the same altitude (∼80 km) as the telescopically imaged column. Next, several large carrot-shaped structures form beneath the wake of fading columns and some of the columns are re-ignited. The "carrot" sprites [*Winckler,* 1995] are about fives times the height of the columns. A couple of the columns appear to become part of the carrot structures. As the carrots fade over the subsequent frames, the single columniform sprite shown in the telescopic images emerges. This column exists by itself for three successive frames. Finally, five frames later a collection of ∼10 columniform sprites appears at ∼70 km altitude and then subsequently fades away.

Figure 4.7 displays four fields from the wide FOV camera at the top. The middle two fields (W2 and W3) show a bright column in the center of the image with the wake of the carrots on the right. The middle row of panels (N1 – N7) shows a sequence of slices through the narrow FOV containing the bright single columniform sprite. As shown in these panels, the columniform sprite starts as a faint positive streamer, which branches once in the field of view and has a slightly brighter segment on the

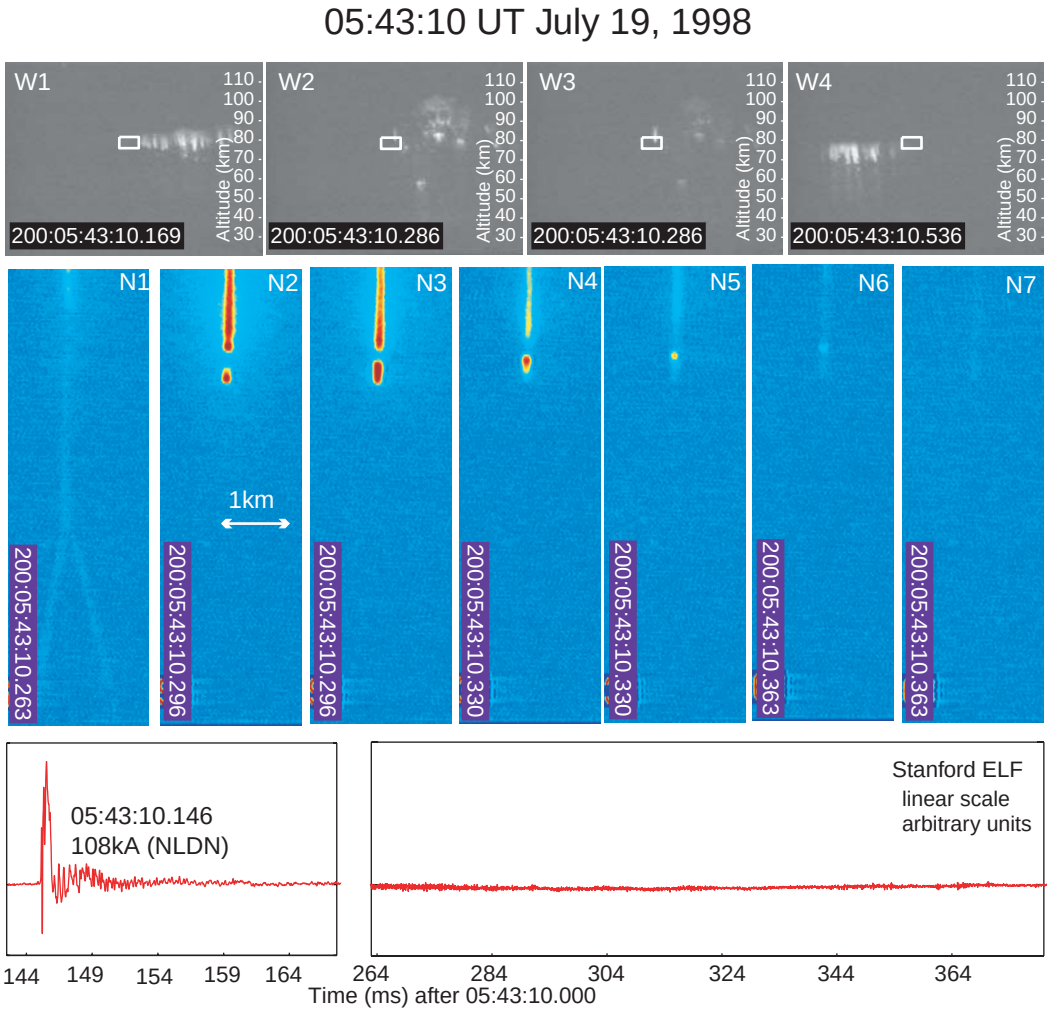

Figure 4.7: Example of a columniform sprite with initial downward branching and a slowly moving bead at 05:43:10 UT July 19, 1998. The wide FOV panels on top of the figure (W1 - W4) are selected frames containing bright features from the dancing sprite sequence of which the column sprite was a part. The telescopic images sequentially range from 05:43:10.263 - 05:43:10.380 UT. The sferic record at the bottom left shows the sferic related to the causative cloud-to-ground lightning stroke, which occurred over 100 ms prior to the column sprite. The sferic record at the bottom right shows the recording during the interval of the column sprite as displayed in the telescopic images.

top. In the subsequent fields the branching streamer is not present and the upper segment becomes much brighter, extends downward, and develops a single bead at its base with a dark space occurring between the bead and the bright segment. This bead and the dark space above travel upward along the channel as the bright segment fades and contracts upward. The bead has the longest lifetime of any features present and travels upward at a rate of $\sim 10^4$ m/s. The entire sequence has a long lifetime lasting $\sim$120 ms, which could either be the result of chemical changes or persistent electric field/current flow. The tapering of the column at its top is inconsistent with the expected profile variation of a streamer with respect to altitude [*Pasko et al.,* 1998]. A similar contraction phenomenon is observed in positive glow discharges when the current is increased [*Raizer,* 1991]. The column width of 150 m is slightly larger than predicted for this altitude [*Pasko et al.,* 1998] and has been previously documented [*Gerken et al.,* 2000]. The column appears to have boundaries that are sharper than the resolution of the camera.

This form of column/bead structure has been previously documented [*Wescott et al.,* 1998; *Gerken et al.,* 2000]. Observations with high-speed imagers suggest that columniform sprites initiate the so-called carrot sprites [*Stanley et al.,* 1999; *Stenbaek-Nielsen et al.,* 2000], and appear to originate from downward positive streamers which subsequently move upwards in branching negative streamers following the original channel. However, it is unclear as to why in some instances collections of bright columniform sprites occur while in others only a few large carrots form [*Wescott et al.,* 2001].

Although previously documented [*Wescott et al.,* 1998], it is unusual to find a single columniform sprite as exemplified by the case in hand. Columniform sprites are most frequently observed in clusters. *Cho and Rycroft* [2001] investigated the distribution of energy deposition from an electromagnetic pulse (EMP) due to a horizontal lightning discharge. They found that the EMP formed local maxima due to interference between direct waves radiated by the discharge current, those reflected by the ground, and those reflected from the ionosphere. These maxima caused the formation of "stalactites" of ionization enhancements spread $\sim$10 km apart between $\sim 75 - 85$ km altitude. *Cho and Rycroft* [2001] suggest that it would be possible to

initiate clusters of columniform sprites from field enhancements due to these stalactites thus accounting for the high altitude at which columniform sprites are found and possibly also the fact that they have been observed as the first stage in carrot sprite formation. In general a positive streamer requires a lower voltage since its electron avalanche propagates in the direction along which the electric field becomes stronger [*Bazelyan and Raizer,* 1998, pg. 253].

The bottom panel in Figure 5 displays the sferic record associated with this sprite event. While there is a sferic at the time of the initial sprite of the sequence (left bottom panel), no sferic activity is present during the interval in which the lone column exists (right bottom panel). The entire sequence lasts ∼450 ms. The long delay between sferic and much of the sprite activity suggests the presence of continuing currents either within the thunderstorm cell [*Bell et al.,* 1998] or to ground [*Cummer and Füllekrug,* 2001].

Chapter 5

Photometry and charge moment estimations

5.1 Introduction

A key concept necessary for understanding the underlying physics involved in sprite processes is the knowledge of the amount of charge produced and moved during a sprite discharge. Unfortunately, *in situ* measurements within the body of the sprite are not practical due to the random nature of the discharges, their fleeting time scales, and the fact that their altitude lies in between that of normal airplane travel and satellite orbits. However, it is possible to measure the charge and current moment of the causative CG discharge and in some cases of the sprite itself and in this way indirectly gain information about sprite processes. Additionally sprite brightness can be measured and related to current flow within the sprite. Thus the two primary means of determining sprite charge formation and movement from the ground are the measurement of sprite brightness and the waveforms of radio atmospherics of causative lightning discharges.

5.1.1 Charge moment estimation

Both CG lightning strokes and sprite discharges involve the flow of time-varying electrical currents, which radiate electromagnetic fields. In the case of CG lightning radiation, these radiated electromagetic impulses are called "sferics" and can propagate long distances in the Earth-ionosphere waveguide with relatively little attenuation. At frequencies below ∼1.5 kHz, only the quasi-transverse electromagnetic (QTEM) waveguide mode propagates with all other modes being evanescent [*Davies,* Sections 10.3 – 10.4, 1965]. The QTEM mode is inefficiently excited by horizontal current sources, so that sferic observations of frequencies less than ∼1.5 kHz primarily represent vertical currents [*Cummer and Inan,* 2000].

The sferic received by a VLF antenna several hundreds of kilometers away from the discharge is much different from the waveform originally radiated due to the propagation effects of dispersion and attenuation. The original waveform can be mostly recovered by deconvolving the observed sferic waveform with the impulse response of the earth-ionospheric waveguide system. However, since information is inherently lost in the process of convolution, the original lightning current waveform can in general not be fully recovered [*Cummer and Inan,* 2000].

Since the field radiated by a time-varying current is proportional to the product of the amplitude of the current and the length of the channel it flows in, or "current moment" [*Kraus,* 1992, pg. 717], there is an inherent ambiguity present in determining current amplitudes flowing in discharge channels. The charge moment of the discharge can be determined by integrating the current moment waveform in time. If a length is assumed for the current channel (e.g., 7 km is a reasonable approximation for a CG lightning stroke channel [*Marshall et al.,* 2001]) then the amount of charge deposited by the discharge over time can be calculated.

VLF sferic observations show that sprite discharges are frequently associated with so-called "slow-tail" or ELF pulse waveforms [*Reising et al.,* 1996]. Slow-tails are observed in data received at distances of over 10,000 km away from the sprite. In these long-range observations, the ELF peaks are separated from the VLF waveform due to dispersion and are easily identifiable. These slowly-varying waveforms have

been interpreted as evidence for continuing currents in sprite-producing cloud-to-ground lightning discharges [*Reising et al.,* 1996; *Bell et al.,* 1998]. The presence of continuing currents allows a much greater amount of charge to be lowered to the ground than would normally occur in CG lightning. The magnitude and duration of the charge lowered play a significant role in determining whether or not a sprite is produced, the altitude range in which it is produced, and its morphology (e.g., spatial extent and streamer content) [*Pasko et al.,* 1997].

There exist multiple methods by which we can calculate lightning-associated charge moments, each leading to a somewhat different result [e.g., *Burke,* 1996; *Huang et al.,* 1999; *Füllekrug and Constable,* 2000; *Greifinger and Greifinger,* 1986; *Bell et al.,* 1998; *Cummer and Inan,* 2000]. In this chapter, charge moments are estimated using the the charge moment model developed by *Cummer and Inan* [2000]. The *Cummer and Inan* [2000] method of estimating charge moment treats the earth-ionosphere waveguide between the sferic and the receiver as a linear time-invariant system. An impulse response is derived for the system using an impulsive ELF source current. Observed sferics are then deconvolved with the impulse response to find the source current moment waveform. The assumption of a time-invariant system is reasonable on the millisecond time scale of a sferic since the nighttime ionosphere typically varies over time scales of seconds to hours.

The first step in estimating the charge moment of a discharge using this method is to record the VLF sferic waveform. The sferic waveforms are typically recorded on Betamax magnetic tapes (with PCM encoding) in 16-bit digital form. The playback from the magnetic tapes is in the form of an analog voltage, which is first low-pass filtered by a "brickwall "filter (flat filter response with a very sharp high-order cutoff) at 16 kHz and subsequently sampled at a 33 kHz rate. The corresponding GPS timing signal, recorded on tape in the IRIG-B format, is also digitized and decoded. Since the frequency response of the VLF receiver extends down to $\sim$10 Hz, unwanted quasi-periodic large-amplitude 60 Hz (and harmonics) power line signals often overwhelm the low-frequency component of the VLF data, which is used in estimating charge moment. The frequency composition of this signal is not identical from one location to another due to power line frequency drift and additional noise sources. Rather

than creating a complex comb of notch filters to remove this unwanted noise during the recording of the data, we utilize a more practical solution to subtract the noise waveform from the recorded data [*Reising,* 1998]. This subtraction is accomplished by selecting several cycles of the noise waveform in a portion of the VLF data with little or no sferic activity, averaging over these cycles, and using the resultant average to generate an artificial periodic noise waveform. This waveform is then lined up with the power line harmonic fluctuations in the VLF data sample and the two time series are subtracted. The next step is to digitally low-pass filter the data with an upper cutoff frequency of 1.5 kHz to ensure that the resultant signal represents only the contributions of the QTEM mode. The data are then high-pass filtered with a lower cutoff frequency of 10 Hz to eliminate the effects due to the frequency response of the receiver system since the precise lower cutoff of the receiver is likely dominated by the frequency response of the PCM encoder used to record the signal on a Betamax tape [*Cummer,* 1997].

After filtering the data, the sferic is deconvolved with the impulse response of the earth-ionosphere waveguide system. The required impulse response is generated by propagating the signal output from an impulsive current source through an Earth-ionosphere waveguide model known as the Long Wavelength Propagation Capability (LWPC), developed by the U. S. Navy [*Ferguson et al.,* 1999] and modified by Stanford University [*Cummer,* 1997]. Deconvolution is accomplished using the CLEAN algorithm [*Teuber,* 1993], which iteratively places current peaks in a reconstructed current signal, which is then convolved with the impulse response to form a reconstructed sferic. The residual between this reconstructed sferic and the original sferic is calculated and more current pulses are added to the input signal until a pre-determined tolerance (or error criteria) is met. This input signal is the current moment waveform. The final step is the integration of the calibrated current moment waveform determined to arrive at the time-varying charge moment. Using this method it has been found that while sprites can initiate with a charge moment as low as 120 C-km, the probability for sprite generation for lightning with >1000 C-km charge moment change in <6 ms is 90% and the probability for lightning with <600 C-km in <6 ms is less than 10% [*Hu and Cummer,* 2002].

5.1.2 Photometry measurements

The method outlined in the previous section for determining charge deposition assumes currents to be flowing in one particular discharge process, namely the CG lightning stroke. On the other hand, waveforms of sferics indicate that ELF radiation due to currents flowing in the sprite discharge are superimposed on the VLF waveform in addition to the radiation originating from the CG discharge [*Reising et al.,* 1996]. In many cases, sprite brightness peaks are observed to coincide in time with peaks in the associated ELF recordings. These coincident peaks are observed by comparing photometric observations of sprites with VLF sferic waveforms and have been interpreted as definitive evidence of ELF radiation produced by electrical currents flowing within the luminous body of the sprite [*Cummer et al.,* 1998].

Sprite brightness is a nonlinear function of the amplitude of the local quasi-electrostatic field $\mathbf{E}$ present in the high altitude discharge region caused by the removal of thundercloud charge by a CG [*Pasko et al.,* 1997]. Due to the fact that the conduction current density is given by $\mathbf{J} = \sigma\mathbf{E}$, where σ is equal to the local conductivity, sprite brightness is also a function of the current density flowing in the sprite [*Cummer et al.,* 1998]. Although the relationship between $\mathbf{J}$ and sprite brightness is highly nonlinear, larger sprite currents are associated with higher luminosities, simply because of the fact that both ionization (current flow) and optical emission processes are more intense for higher electric fields. Thus, coincident peaks in photometric data and ELF in the absence of VLF sferic activity are indeed strong indications of radiating currents existing in sprites.

5.2 Two-storm case study: July 2 and July 4, 2000

Typically, large mesoscale convective system (MCS) storms are associated with sprite production [*Lyons,* 1994]. MCS's are frequently observed drifting east over the Great Plains of the central United States. Sprites are generally produced in the decaying part of the storm over the trailing stratiform region [*Lyons,* 1994], which develops as the thunderstorm anvil descends. Although it is less electrically active, this region

of the storm is where the bulk of positive CG's are located [*Lyons,* 1994]. While less common, it is also possible for sprites to be produced by storms of a smaller scale. On occasion, a small storm may produce a single sprite as it decays. A rarer type of storm is one that produces an extremely high rate of unusually small and dim sprites. Only a few cases of this sort of sprite producing storm have been recorded during several sprite campaigns conducted during the summers of 1998 to 2000. One such storm was observed during the summer 2000 campaign. In this section, we compare and contrast the characteristics of sprites produced by a typical MCS and a small but high-sprite-rate storm.

5.2.1 Meteorology of the July 2 and July 4, 2000 storms

A large MCS occurred on July 4, 2000 and 28 sprite events were observed by the Stanford imager during the two hour period of 04:00 - 07:00 UT. By contrast, during a much smaller storm on July 2, 2000, as many as 276 sprites were observed in the same amount of time (04:00 - 07:00 UT). Photometric and VLF data presented in this section were recorded at the Yucca Ridge Field Station in Fort Collins, Colorado (see Chapter 2 for more details on the Yucca Ridge site). Not only was there a substantial difference in the number of sprites produced by the two storms, but the sprites themselves exhibited very different characteristics. Those produced in the July 2 storm were consistently very small in both altitude and lateral extent, produced a sharp peak of optical brightness in photometric data. The luminous structure of the sprites of the July 4 storm varied widely with many large and intense events as well as smaller less intense events. The photometric signatures of these events were generally complex, with several peaks of brightness exhibited. A substantial amount of ELF radiation was observed in the waveforms of sferics associated with sprites produced by the July 4 storm (i.e., pulses coincident with the sferic onset and pulses correlated in time with peaks in sprite brightness). Figures 5.1 and 5.2 show representative sprites from the two storms under study.

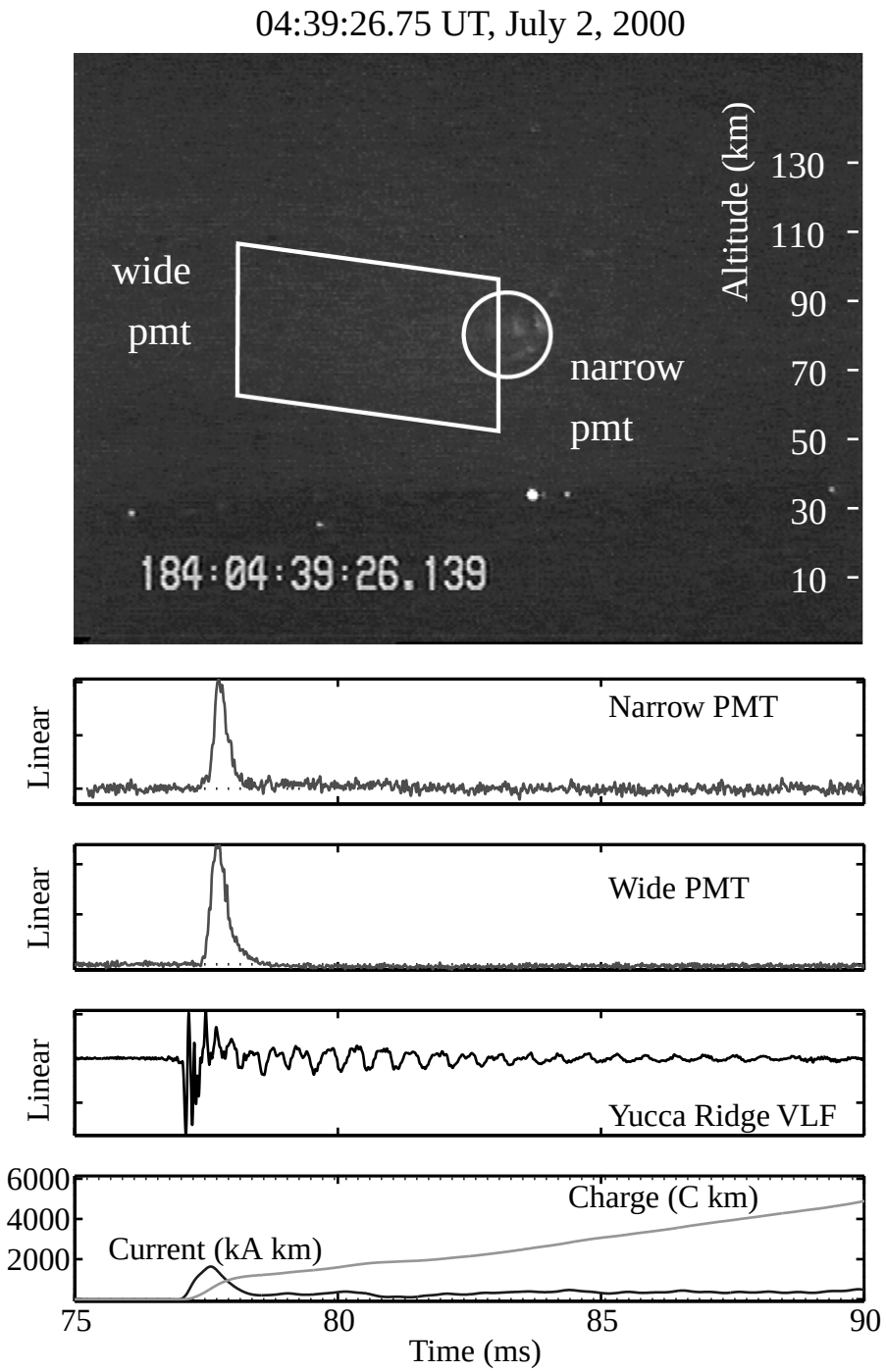

Figure 5.1: Representative sprite event from the July 2, 2000 storm. The sprites were consistently smaller and briefer than those of the July 4 storm.

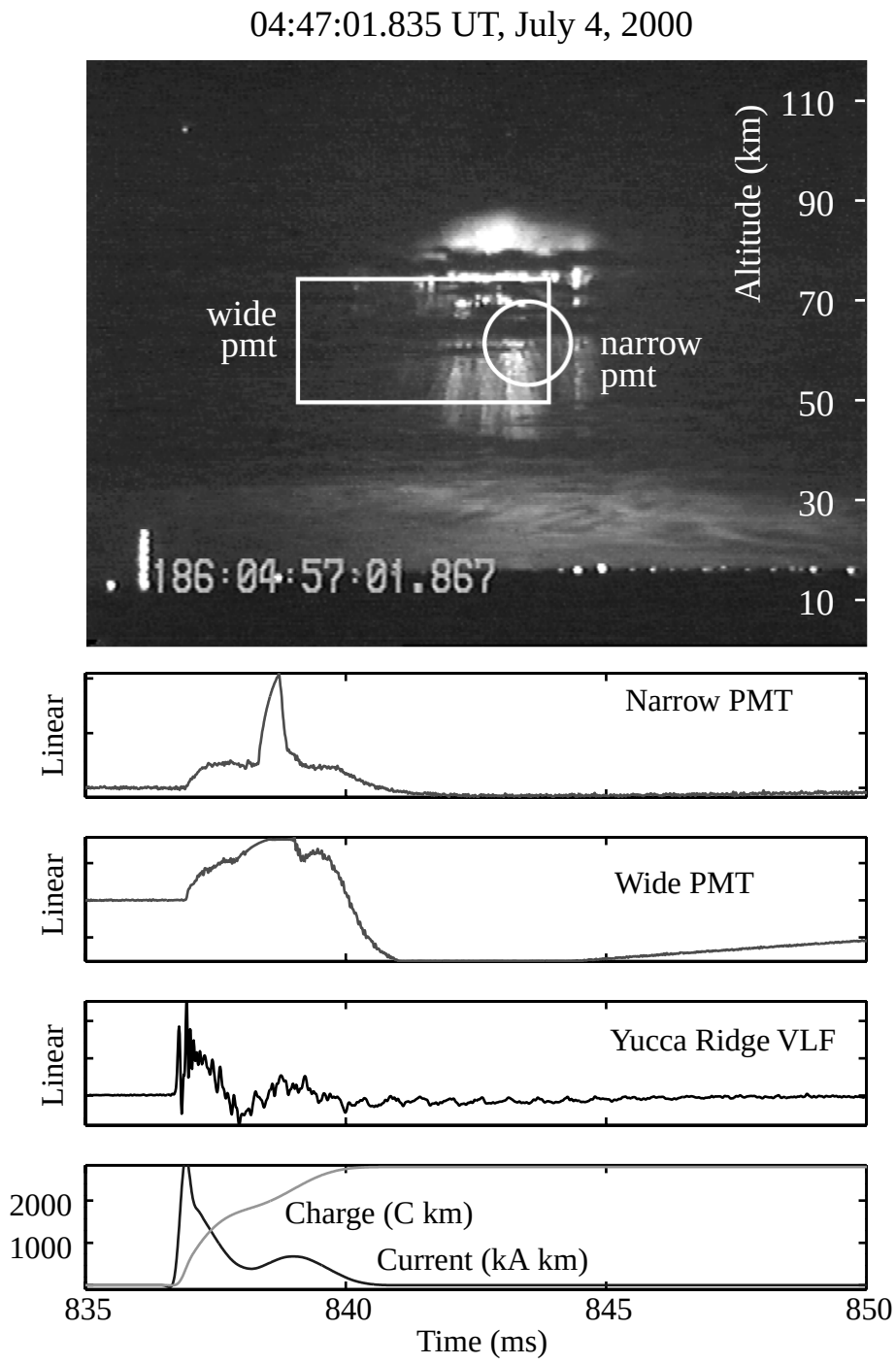

Figure 5.2: Representative sprite from the July 4, 2000 storm. The sprites of this storm varied widely, and both large and small sprites were produced. Photometric signatures are complex and many of the sprites have substantial ELF components in their associated sferics (i.e., pulses coincident with the sferic onset and pulses correlated in time with peaks in sprite brightness).

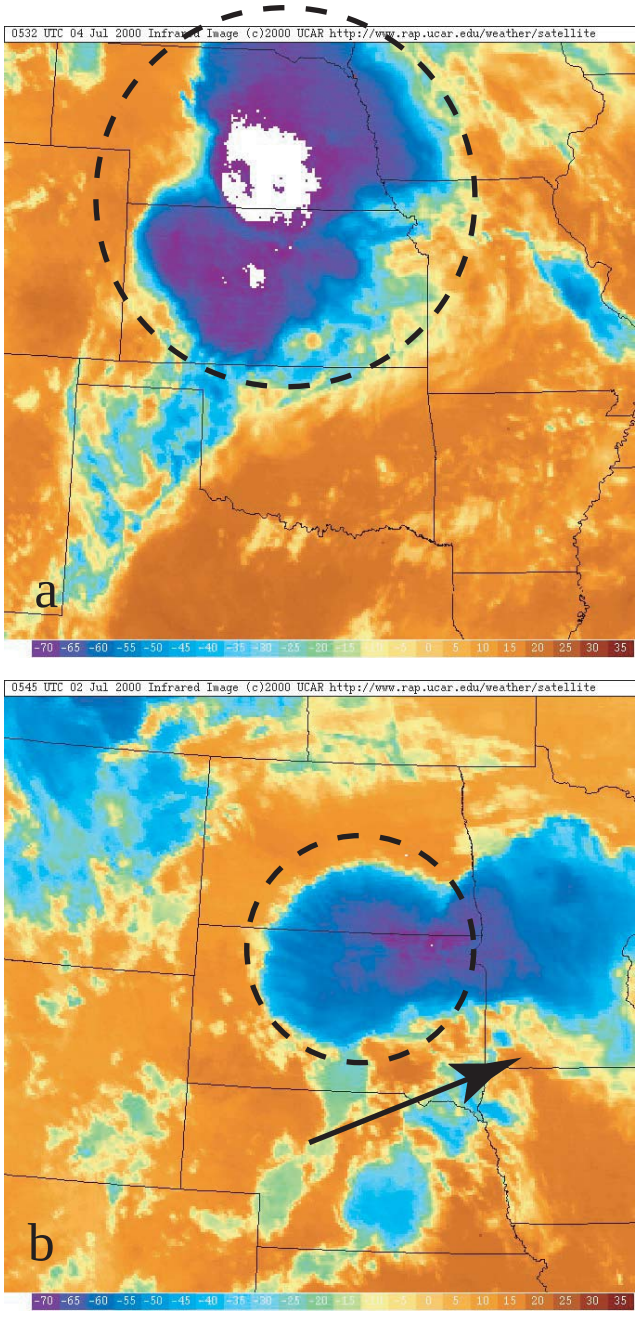

Figure 5.3: GOES satellite infrared imagery for a) the July 4, 2000 storm taken at 06:15 UT, and b) the July 2, 2000 storm taken at 06:15 UT. Temperature ranges from 35° (red) to -75° C (white). The arrow in the lower panel (b) indicates the direction the July 2 storm was traveling.

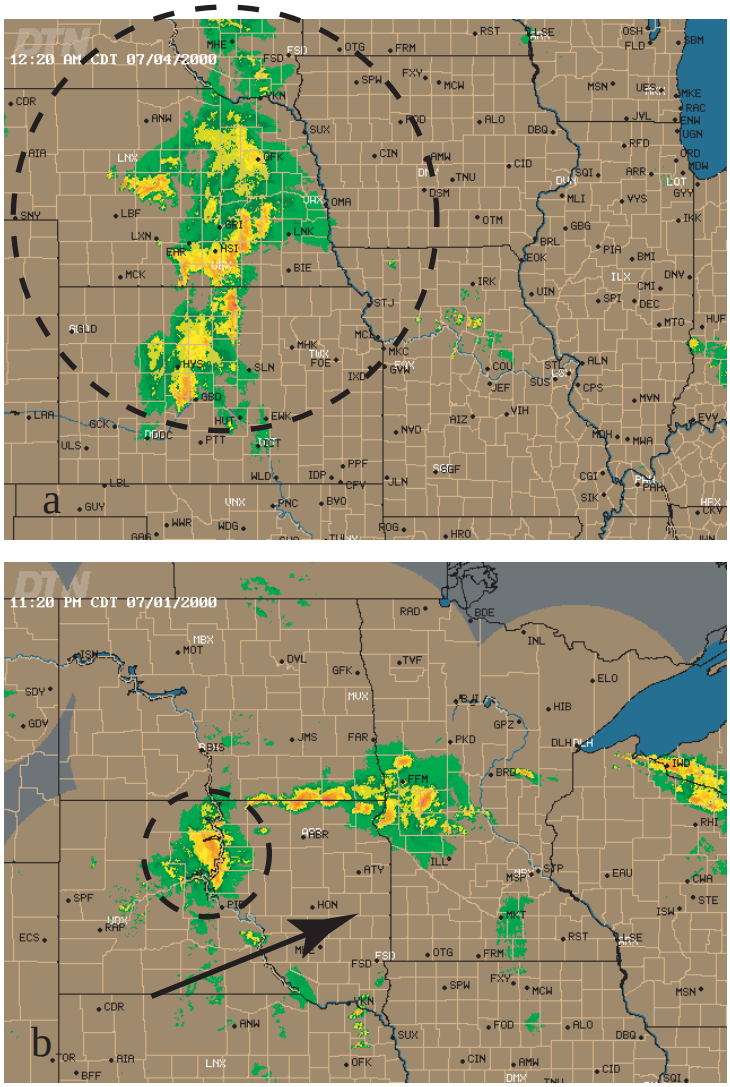

Figure 5.4: Composite radar map from www.weatherTAP.com for the a) July 4, 2000 storm and the b) July 2, 2000 storm. The highest reflectivity is plotted in red and the surrounding less-reflective stratiform region appears in green. The arrow in the lower panel (b) indicates the direction the July 2 storm was traveling.

Radar and GOES satellite data

Figure 5.3a shows infrared imagery from a GOES (Geostationary Operational Environmental Satellite) satellite (see Chapter 2) of the storm on July 4, 2000 at 06:15 UT. The storm clouds cover most of Kansas and Nebraska and extend over South Dakota, Minnesota, Iowa, Missouri, and Oklahoma. The color scale represents measured temperature and ranges from red to white, corresponding to 35° to -75° C respectively. Typically, the colder a cloud top is, the taller it is [*Arking,* 1985]. In Figure 5.4a, a composite radar map (obtained from http://www.weatherTAP.com, courtesy Tom Nelson, FMA Inc.) shows that the highest reflectivity (red) in the storm is localized with a surrounding stratiform region (green). Figures 5.3b and 5.4b show the corresponding GOES infrared and radar imagery for July 2, 2000. The storm covers the borders of North Dakota, South Dakota, and Minnesota. This storm has a smaller cloud cover area than that of July 4 and also has much warmer cloud tops. The fact that the July 4 storm had cooler cloud tops indicates that this storm extended to significantly higher altitudes than the July 2 storm.

National Lightning Detection Network Data

Examination of NLDN lightning stroke data also reveals distinct differences between the two storms. In Figure 5.5, maps are displayed with the NLDN lightning from both storms superimposed. The gray dots show the locations of all the lightning strokes occurring between 04:00 - 07:00 UT while the colored dots indicate those strokes associated with sprite events. The color scale is a function of time and progresses from blue (04:00 UT) to red (07:00 UT). It is evident that in the July 2 storm (upper panel) the majority of the sprite-associated strokes were tightly clustered in time and moved toward the northeast along with the storm (see Figure 5.4). On the other hand, the July 4 storm (lower panel) remained relatively stationary and the sprite-associated lightning strokes were scattered throughout the storm.

Histograms of the NLDN-reported currents for the two storms are shown in Figure 5.6. The number of negative CGs recorded during July 4 storm (lower panel) is about an order of magnitude greater than that on July 2. Otherwise, the intensity

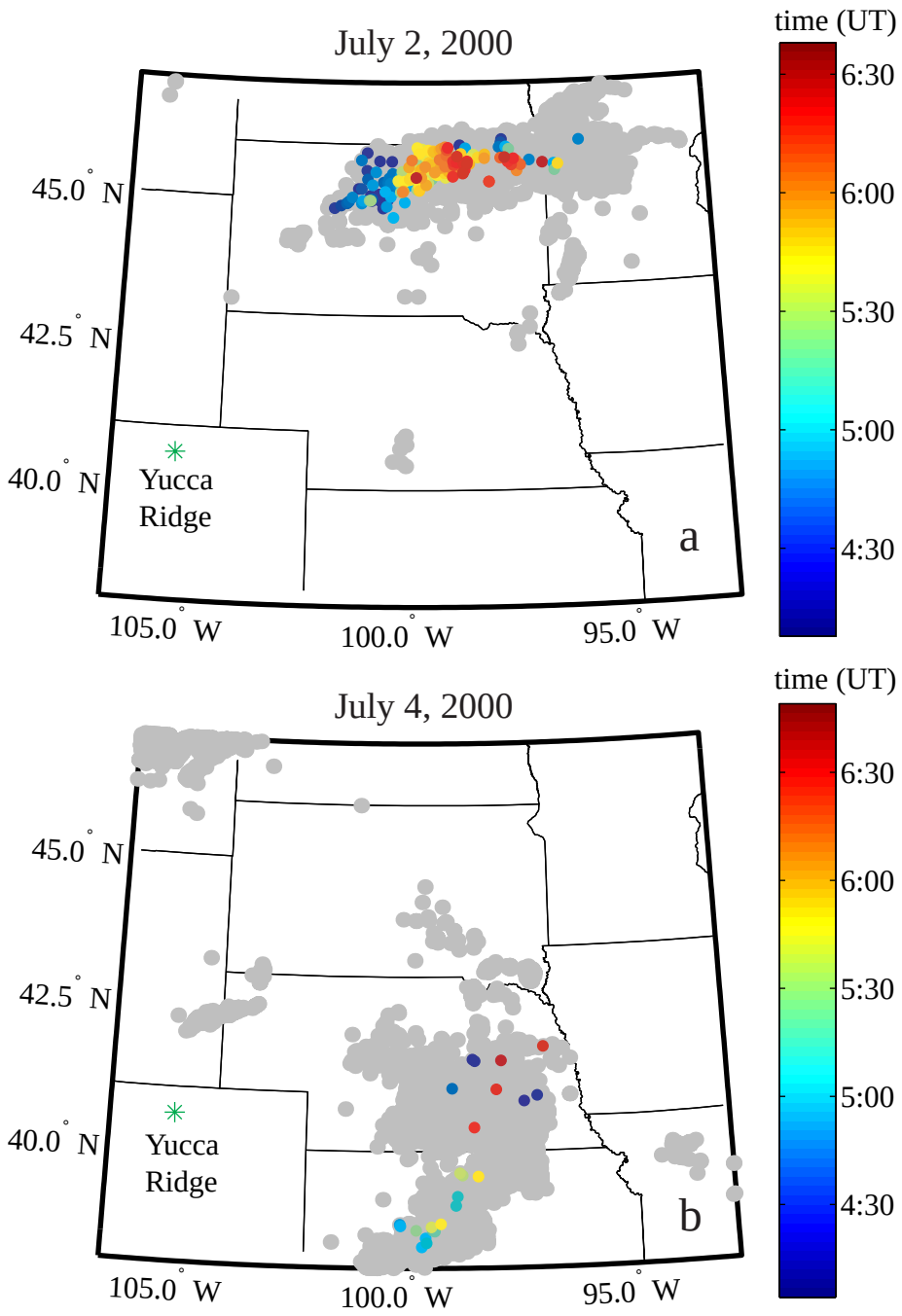

Figure 5.5: NLDN lightning stroke data for the a) July 2 and b) July 4, 2000 storms. All the NLDN-recorded strokes during 04:00 - 07:00 UT are plotted in gray on the maps. Those strokes associated with sprite events are plotted in color. The color scale is a function of time with the blue dots occurring earlier than the red dots. As can be seen the sprite-associated strokes in the July 2 storm progress to the northeast in time while sprite events in the July 4 storm are scattered in time throughout the storm.

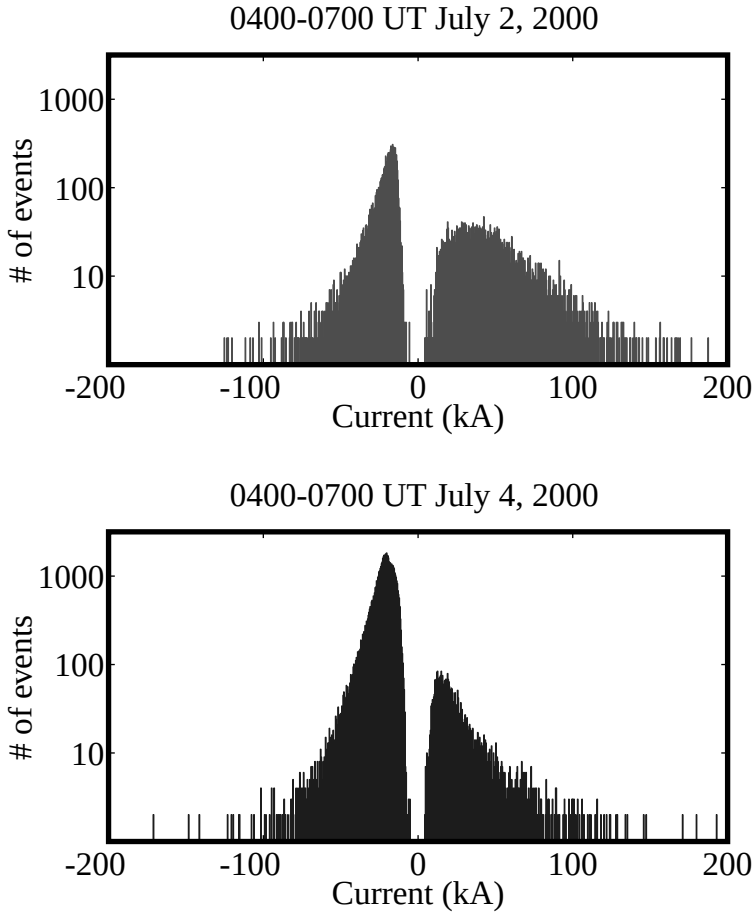

Figure 5.6: Histogram of NLDN lightning currents recorded during the July 2 and July 4 storms. Note the events are plotted using a log scale. While the July 4 storm has about an order of magnitude more negative CGs than the July 2 storm, the number of positive CGs is comparable in the two storms. The distribution of positive currents in the July 2 storm is shifted to higher values than the July 4 storm.

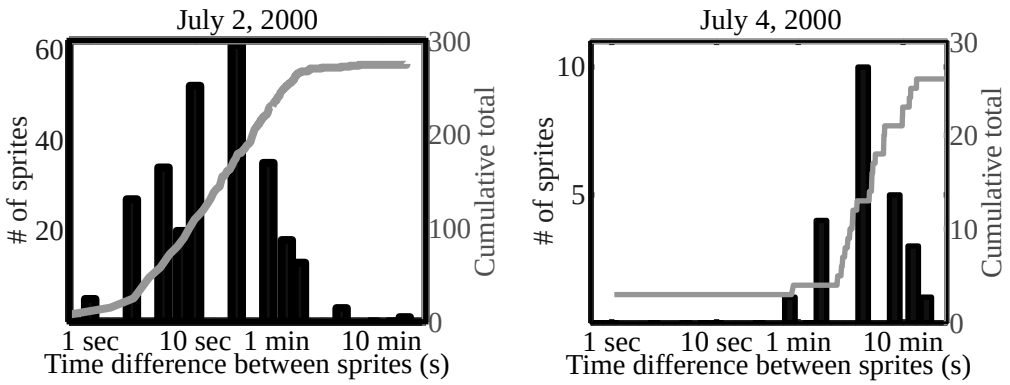

Figure 5.7: Time difference between sprite events on July 2 and July 4. The histogram shows that the distribution of time differences on July 2 peaks in the tens of seconds while on July 4 the peak is on the order of minutes. As demonstrated by the cumulative total, the majority of sprites on July 2 occurred with a time delay less than a couple minutes while on July 4 there were delays of tens of minutes between sprites.

distributions of negative discharges appear similar. By contrast, comparable numbers of positive CGs were recorded in both storms. The distribution of positive currents during the July 2 storm appears to be shifted to somewhat higher current values than those for the July 4 storm. Since sprites are commonly associated with strong positive CGs [e.g., *Boccippio et al.,* 1995], it is not suprising that the July 2 storm produced more sprites than the July 4 storm despite the much lower overall (i.e., including both negative and positive discharges) flash rate of the storm.

5.2.2 Sprite altitudes and rates

The sprite occurrence rates and altitudes also varied widely between the two storms that occurred on July 2 and July 4. As shown in Figure 5.7 the sprites on July 2 typically occurred with a time difference of tens of seconds with the smallest difference being only 1 s. By contrast, the storm on July 4 had much greater delays between sprites - typically on the order of 5 min and ranging up to ∼30 min. The altitude spans of selected sprite events (inferred on the basis described in Section 2.4) from both storms are shown in Figure 5.8. The sprites on July 2 were similar to each other and were primarily confined to altitudes of $\sim 75-85$ km. In contrast, there was wide

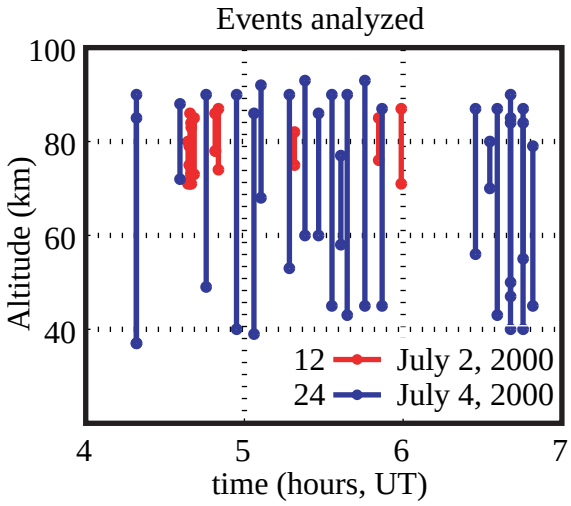

Figure 5.8: Sprite altitudes for selected events on July 2 and 4. The sprites on July 2 were primarily confined to $\sim 75-85$ km altitude while the July 4 storms had high variability and ranged from $\sim 40-95$ km.

variability in the luminous structure of sprites in the case of July 4, which occurred over altitudes of $\sim 40-95$ km.

5.2.3 Charge moment estimations

Charge moments for selected sprite events from the July 2 and July 4, 2000 storms were estimated in order to better understand the underlying cause of the different sprite morphologies observed in the two storms. Although the uncertainties involved in charge moment estimation should be minimized and should ideally be limited to an imperfect knowledge of the ionospheric profile, in practice other uncertainties are also present. In the case of the particular measurement setup used for the July 2000 observations, the largest error introduced is that of timing. When imaging sprites with standard video resolution, a $\sim$17 ms ambiguity is inherently present. Charge moment ranges over this interval can be calculated, but the error bars on such a calculation can become so large that the results may be of little use. In general, the use of photometer recordings (which were recorded onto the audio channel of VHS videotapes) of sprites allows microsecond timing resolution [*Inan et al.*, 1997].

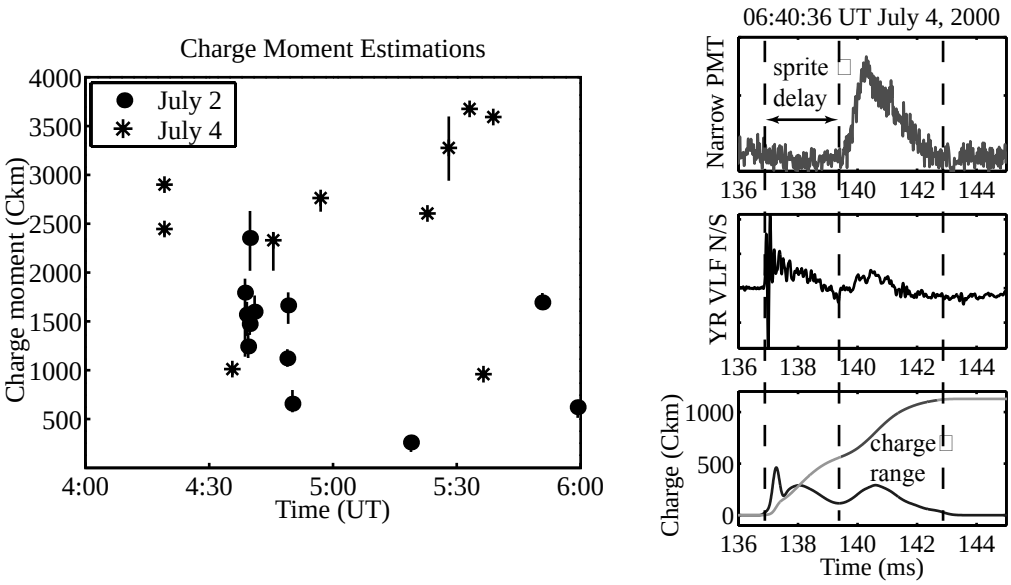

Figure 5.9: Charge moment versus time. The sprites observed on July 2 mainly had charge moments ranging from 1000-2000 C-km. On July 4, however, the measured charge moments ranged from 1000-3700 C-km. The panels on the right show the relative timing of photometer and antenna signals and the charge moment estimation for one sprite event.

However, in the case of the Stanford sprite data recorded on July 2 and July 4, 2000, IRIG-B GPS timing was used for the photometric recordings allowing for a time a resolution of only 1 ms.

In reporting and comparing cumulative charge moment estimations with that of other methods it is also important to specify the point at which the cumulative charge moment was estimated (i.e., at the end of the sferic, at the beginning of the sprite, or at the end of the sprite). Other timing uncertainties can be introduced by an imperfect knowledge of the propagation delay from the source to the recording device. In the case of the July 2000 data, however, the photometers and the VLF antennas were co-located at Yucca Ridge and the propagation delays for the light and VLF signals were within 1 ms of one another.

Figure 5.9 shows charge moment estimates using the *Cummer and Inan* [2000] model for selected sprite events in the July 2 and 4 storms. Reported charge estimates are those calculated at the end of the sprite event as observed in the photometers

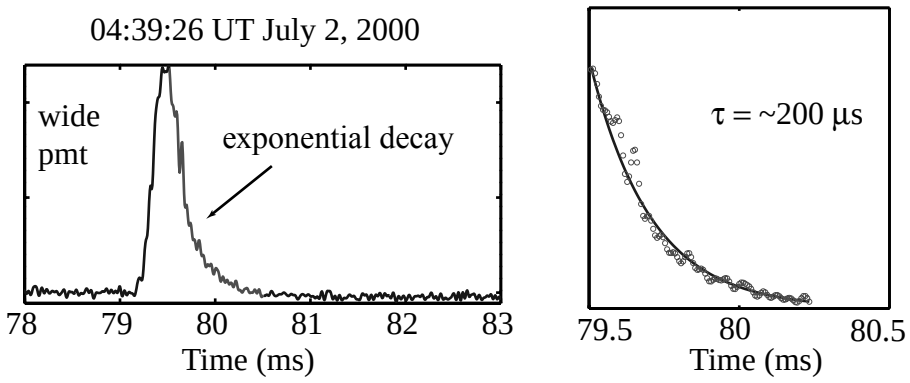

Figure 5.10: Exponential curves fitted to the data are used to determine time constants of decay.

within a 1 ms error. The right hand column of panels shows an example of the relative timing of the photometer and VLF data and the charge moment calculation. In this example an ELF pulse is observed coincident with the light pulse observed by the photometer. This pulse generates a further increase in the charge moment curve and can be attributed to currents flowing within the sprite itself. A delay between the onset of the sferic and the sprite is evident. The majority of sprites observed on July 2 had a sferic-to-sprite delay of 1 ms or less while those on July 4 were highly variable with delays ranging from less than 1 ms to greater than 30 ms. As shown in Figure 5.9, the sprites observed on July 2 mainly had charge moments ranging from 1000-2000 C-km. On July 4, however, the measured charge moments were higher, ranging from 1000-3700 C-km.

5.2.4 Decay time constants

The optical emission intensities of sprites observed by photometers do not rise and fall instantaneously. Although sprites frequently emit complex optical signals, exponential decay is often observed as the sprite brightness fades away [*Barrington-Leigh et al.,* 2002]. Selected sprites from the storms of July 2 and July 4, 2000 were examined to assess the presence and rate of exponential decay. Exponential curves fitted to the

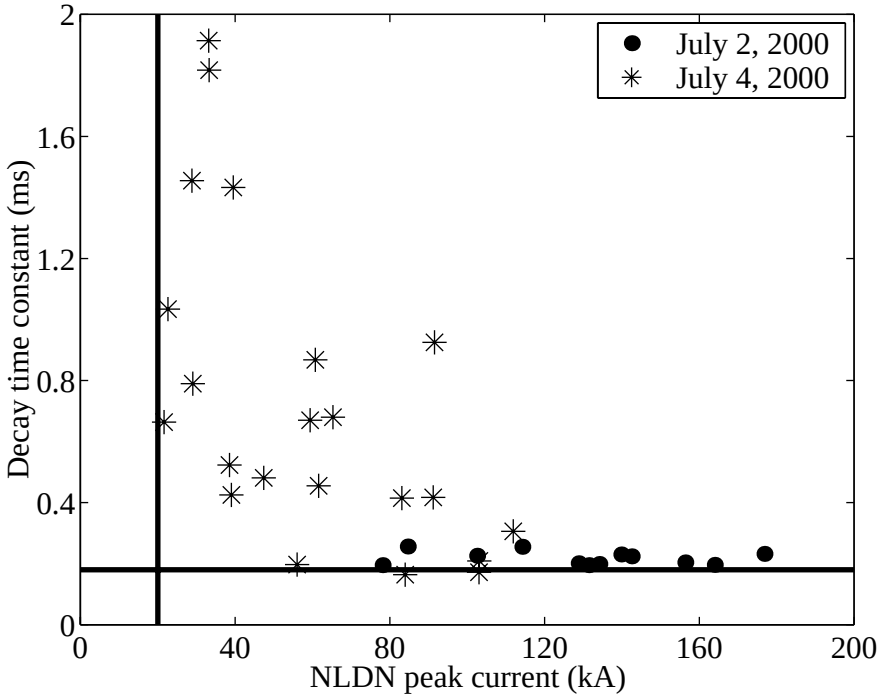

Figure 5.11: Decay time constants versus NLDN peak current for selected sprite events during the July 2 and July 4 storms. When looking at the data set as a whole, it appears that the data points are following a curve with two asympotes: a 200 μs time constant and a 20 kA peak current.

data are used to determine time constants of decay as shown in Figure 5.10 with the fitted curves having the form:

$$y = A + Ce^{-t/\tau} \tag{5.1}$$

where τ is the decay time constant and A and C are constants to be determined by the fit.

Figure 5.11 shows a plot of decay time constants versus NLDN peak current for selected sprite events during the July 2 and July 4 storms, revealing several interesting relationships between time constants and peak current in these two storms. Firstly, the July 2 sprites are associated with the NLDN peak currents greater than 80 kA. The sprites on July 4 are associated with peak currents ranging from $20-120$ kA the majority of which being less than 80 kA. Secondly, all of the time constants measured on July 2 were less than 400 μs while those on July 4 ranged from 200 μs to almost

2 ms with the majority of events being greater than 400 μs. Viewing the results in Figure 5.11 as a whole, it appears that the data points follow a curve with two asymptotes; $\sim$200 μs time constant and 20 kA peak current. These asymptotic values also are in good agreement with those found in other data sets [e.g., *Barrington-Leigh et al.,* 2002].

Barrington-Leigh et al. [2002] showed that in streamer discharges, the exponential decay of optical brightness may possibly be explained by the presence of quasi-constant electric fields inside of the sprite streamers. A quasi-constant electric field (which remains approximately constant) would lead to exponential decay of the electron density within the streamer body and it can be shown that in a quasi-constant electric field, optical emission intensity is approximately proportional to the electron density [*Barrington-Leigh et al.,* 2002]. At streamer altitudes, when the ambient electric field remains constant, an enhanced electron density (as is present in a streamer) would thus be expected to decay approximately with the minimum attachment time constant (corresponding to the maximum attachment rate) for that particular altitude. In such cases, the optical brightness of sprites observed at streamer altitudes should decay with a time scale exceeding the minimum attachment time constant [*Barrington-Leigh et al.,* 2002].

Figure 5.12 shows a plot of time constants versus altitude measured for the same selected sprite events shown in Figure 5.11 for the July 2 and July 4 storms. While the sprite events of July 4 are widely distributed both in altitude and decay time constant, the events of July 2 are tightly clumped in an altitude range of $\sim 75 - 85$ km and time constant range of $\sim$ 200 $-$ 400 μs. For comparison, the minimum attachment time constant versus altitude is superimposed on the data set. When the error bars are taken into consideration, all but two of the events of the July 4 storm decay with a time constant greater than the minimum attachment time constant at that altitude as predicted for streamer discharges [*Barrington-Leigh et al.,* 2002]. Even with error bars, however, *all* of the July 2 events decay with a time scale less than the minimum attachment time constant and are more closely associated with the dielectric relaxation time constant. This result is consistent with the fact that the quasi-static electric fields driving these diffuse glow discharges observed at these high

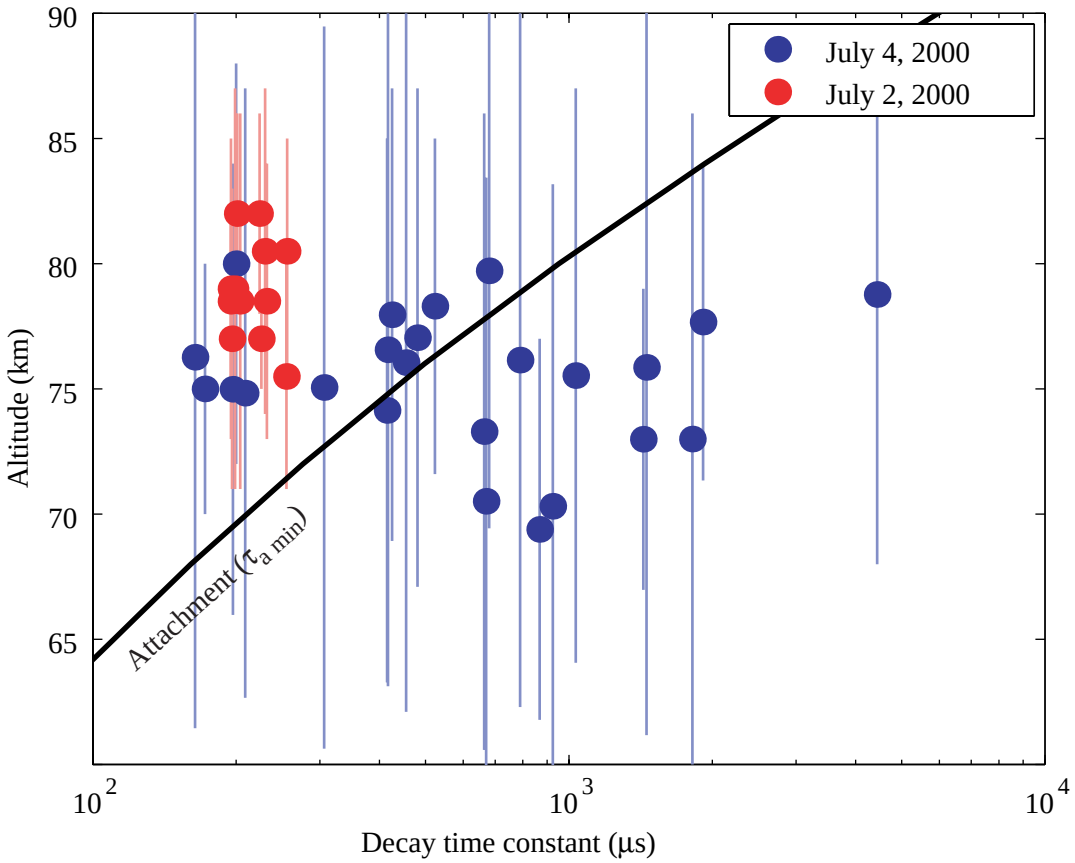

Figure 5.12: Time constants versus altitude measured for the same selected sprite events as in Figure 5.11 in the July 2 and July 4 storms. The minimum attachment time constant is superimposed for reference.

altitudes likely dissipate rapidly (due to relatively high conductivity) at the dielectric relaxation rate.

5.2.5 Summary and discussion

We have compared two storms using Yucca Ridge data in order to highlight the range of variations in sprite properties between different types of sprite-producing storms. On July 2, 2000 a relatively small storm was observed moving northwest over the Dakotas. Between 04:00 - 07:00 UT, 275 sprites were sighted by the Stanford telescopic imager. These sprites occurred at a high rate with generally only $\sim$10 s time delay between sprite events. The sprites themselves were very small, diffuse, and dim, and located at relatively high altitudes of $70-85$ km with short peaks of brightness in photometric data. These sprites followed CG discharges with strong peak currents ($120-180$ kA), which typically corresponded to charge moments of $1000-2000$ C-km. The majority of the sprites showed strong exponential decay in photometer recordings with relatively short time constants of $\sim$200 μs. The observed time constants were determined to be less than the minimum attachment time constant at these altitudes and were more closely associated with the dielectric relaxation time constant.

By contrast, the storm observed between 04:00 - 07:00 UT on July 4, 2000 was a relatively large MCS type storm covering Nebraska and Kansas, that remained almost stationary in the course of its development. Only 27 sprites were observed by the Stanford telescopic imager during this interval and there was an average of $\sim$5 min time delay between sprites. The sprites had a wide variety of shapes and sizes and spanned $40-90$ km in altitude. These sprites were associated with CG discharges with much smaller peak currents ($20-120$ kA), but which nevertheless corresponded to charge moments of $1000-3700$ C-km. Slower optical decay time constants were observed in the photometric data ($\sim 0.2-2$ ms) and almost none of the events decayed with time constants less than the minimum attachment time constant.

Our comparative study demonstrates that storm geometry may play a significant role in determining the type of sprite discharge produced. A key difference between

the two storms is evident in the GOES satellite infrared imagery (Figure 5.3). The cloud tops in the July 4 storm were significantly cooler than those of the July 2 storm, and thus it is likely the thunderclouds in this storm extended to a higher altitude. The charges moved by +CGs from higher altitudes would produce higher electric fields at mesospheric heights. The altitude variation between the two storms likely explains why the July 4 storm had sprites with a full altitude extent while the July 2 storm mainly produced diffuse glow. Additionally, the MCS-type storm on July 4 may have had a much larger charge pool to draw from. While peak currents in this storm were low, ELF components coincident with the sferic onset were frequently present in electromagnetic recordings indicating the existence of continuing currents [*Reising et al.,* 1996], possibly drawing charge from distant parts of the storm through horizontal intracloud processes. On the other hand, the associated sferics of the July 2 storm produced less ELF energy, but had high peak currents indicating fast charge removal processes. Since this storm covered a much smaller area, it would not have been able to draw charge from distant charge pools and would thus be less likely to produce the long continuing currents observed in the case of the July 4 storm.

The most important parameter in sprite initiation is believed to be the charge moment which is equal to the charge removed from the thundercloud times the altitude from which the charge was removed [e.g., *Pasko et al,* 1997; *Hu et al.,* 2002, and references cited therein]. Accordingly, there do exist two means of sprite initiation - short duration and high peak currents, or long continuing and lower peak currents [*Bell et al.,* 1998]. Fast charge removal leads to diffuse glow breakdown at higher altitudes and longer continuing currents with large charge removal allow sufficient electric field to initiate streamers at lower altitudes [*Barrington-Leigh and Inan,* 2001]. It appears that those sprites observed in the July 2 storm were mostly diffuse glow discharges (sprite "halos") while those of the July 4 storm primarily involved both diffuse glow and streamer processes.

Due to the wide FOV of the photometer (Figure 5.2), the photometric recordings during the July 4 storms are likely dominated by bright streamer processes at lower altitudes. Hence, the fact that the observed optical decay time constants are slower than minimum attachment time constants is in accordance with that expected for

streamer processes [*Barrington-Leigh et al.,* 2002]. On the other hand, the optical decay time constants observed in the July 2 storm appear to be solely due to diffuse glow discharge. At the high altitudes of diffuse glow processes, the dielectric relaxation rate is much faster than that of attachment and is the dominant time constant. It may thus be possible to use photometric recordings of sprites to distinguish between streamer and diffuse glow processes by examining the optical brightness decay time constants. Precise measurements of these time constants may potentially be used for remote sensing of atmospheric parameters such as conductivity and minimum attachment time constants.

Chapter 6

Summary and suggestions for future research

6.1 Summary

We have presented results of the first telescopic imaging of streamer and diffuse glow dynamics in high altitude electrical discharges known as sprites. During the summers of 1998 – 2000, Stanford University deployed a telescopic imaging system at Langmuir Laboratory (Socorro, New Mexico) and Yucca Ridge Field Station (Fort Collins, Colorado). This system consists of telescopic and wide FOV CCD cameras and photometers. Electromagnetic signatures of causative lightning discharges are recorded using crossed-loop magnetic antennas and ELF/VLF receiving systems located at Stanford and in Colorado. Hundreds of sprites have been observed by the Stanford University telescopic imager. Telescopic imaging shows that decameter-scale structure in sprites can assume a wide variety of shapes, sizes, and time scales, but that certain structures such as beading, faint downward branching, bright upward branching, propagating diffuse glows, and columns appear repeatedly.

Sprites exhibit a bewildering range of fine structure, much like the spectacular and varying structures exhibited by tropospheric lightning discharges. Nevertheless, many of the observed features can be explained using theories of streamer and diffuse glow electrical breakdown. Upon removal of charge from a thundercloud by a

(typically positive) CG, a quasi-static electric field is set up at high altitudes between the cloud and the ionosphere [*Pasko et al.,* 1997]. In the altitude range where the air is thin enough, this field may exceed the conventional breakdown field, leading to electrical discharge. In the course of the discharge, electrons are accelerated and collide with neutral particles. The excited neutral particles emit photons as they relax to lower energy states and these photons are observed as a luminous sprite event. Since neutral atmospheric density decreases exponentially with altitude while the free electron density increases exponentially, the electrical discharge mechanism is altitude-dependent. Streamers are observed at lower altitudes where the dielectric relaxation time scale is large in comparison with the time needed to form a streamer. At higher altitudes where the dielectric relaxation time scale becomes small in comparison with the streamer formation time, the diffuse glow mechanism is more commonly observed [*Pasko et al.,* 1998].

Telescopic images show a transition region between streamer activity and diffuse glow occurring at ∼80 km [*Gerken and Inan,* 2002]. Streamer widths measured during one storm on July 13, 1998 are about an order of magnitude greater than that predicted using a ground level radius of 0.02 cm, although a slight dependence on the altitude is observed as expected. While diffuse glow is indeed observed as predicted at the tops of sprites, propagating diffuse glow striations are also observed in the streamer regions of sprites. These striations have not been predicted to occur by any current sprite models, but they may be related to those that have long been observed in glow discharge tubes. In addition to streamer and diffuse glow features, beads are also observed in sprites. Currently there is no accepted theory to explain the existence of these beads. Beads observed by the telescopic imager range from $\sim 20 - 250$ m in radii and have been found to last less than one video field (∼17 ms) up to 240 ms.

A two-storm case study of data from the summer of 2000 demonstrates that storm geometry can play a large role in determining sprite properties. On July 2, 2000, up to 275 small diffuse sprites occurring between 04:00 - 07:00 UT were observed above a small storm, while only 27 sprites were observed during an equivalent time period over a large storm on July 4, 2000. The July 4 sprites occurred in a wide range of

shapes and time scales spanning $40 - 90$ km altitude, but the July 2 sprites were largely confined to $70 - 85$ km altitude. The sprites of the July 2 storm were typically associated with very high peak currents, short time duration. Those of July 4 were produced by $20 - 120$ kA CG's, had complex optical signatures, and frequently were associated with sferics which had significant ELF radiation (i.e., pulses coincident with the sferic onset and pulses correlated in time with peaks in sprite brightness). Examination of optical decay time constants reveals that the July 4 sprites relaxed with time constants exceeding the minimum attachment time constants as expected when the streamer mechanism is dominant. On the other hand, the July 2 sprites had time constants smaller than the minimum attachment time constant and their decay rates were more closely associated with the dielectric relaxation rate. The July 2 sprites appear to mainly consist of diffuse glow. These observations suggest that it may be possible to distinguish between diffuse glow and streamer mechanisms on the basis of photometric measurements of decay rates.

6.2 Suggestions for future research

6.2.1 High-speed telescopic imagery

As demonstrated in this dissertation, both telescopic imagery and photometric recordings can provide valuable information about the electrical discharge processes occurring at high altitudes. The streamers exhibit very fine structure and propagate with high velocities. The obvious drawbacks of the existing telescopic measurement system are that the imaging is recorded at the low resolution of video rate ($\sim$17 ms/field) and that while the photometric data has very high time resolution, a photometer is essentially a one-pixel "camera". One way of reducing these limitations is to incorporate a high-speed CCD camera with the telescope. High-speed cameras have been used to image sprites in the past [*Stanley et al.,* 1999; *Stenbaek-Nielsen et al.,* 2000], using wide fields of view. While these data sets provide excellent observations of the overall temporal development of a sprite, the fine structure is not readily resolvable. By combining a high speed camera and a telescope it would be possible

to measure individual streamer velocities (or at least set an upper bound on them) and compare these measurements to results of laboratory experiments. While measurements of streamer radii are difficult to compare accurately from one system to another, streamer velocities are the most commonly reported measurement in both laboratory and modeling results. Since at present it is not possible to generate such long spark discharges in laboratories, such high-resolution measurement of streamer velocity and morphology would be instrumental in advancing our understanding of the spark discharge physics community as well as the sprites community.

6.2.2 Triangulation on fine structure in sprites

While much information about high altitude discharge processes can be gleaned from a single site telescopic system, even more information would be acquired by triangulation using a two-site system. Currently, altitude estimates in sprite images obtained with the telescopic imager are made by assuming the sprite to occur directly above the associated NLDN-reported CG. It is possible however for sprites to be located as far as 40 km from the causative CG [*Winckler et al.,* 1996; *Lyons et al.,* 1996]. This possible displacement frequently corresponds to error bars of ± 5 km on altitude estimates in images from Stanford's telescopic imager [*Gerken et al.,* 2000]. While this error is quite small on the scale of a sprite (often 50 km tall), it definitely limits our ability to quantitatively determine the physical mechanisms underlying the fine structure. As has been shown in previous chapters, streamer radius should vary rapidly with altitude and the transition boundary can occur over a very narrow altitude range. With triangulation, the location of sprite features could be determined much more precisely. The limiting source of error would be the ability to accurately fit the star fields in images and to account for atmospheric effects such as refraction and scintillation. This error could be reduced by observing sprites relatively close to both sites and with optimal triangulation geometry. Once the altitude uncertainty of streamer features is reduced, it would be easier to use sprites to determine background atmospheric properties such as neutral density, electron density, or attachment rates. Possible multiple sites for imaging Mexican sprites would be Langmuir Laboratory in

New Mexico and Kitt Peak Observatory in Arizona. Theoretically, once triangulated images have been gathered it would then also be possible to construct 3D images of the fine structure features in sprites. Such images would provide critical new information about the distribution of the fine structure features within sprites as well as allowing more accurate volumetric estimates to be made and possibly leading to more accurate estimates of the current flowing through sprite streamers.

6.2.3 Streamer measurements using a telescopic array

A telescopic imager is inherently limited in the region of space within its field of view. While the observed region can be well studied, it is not possible to know the larger scale discharge dynamics occurring in the space surrounding this region. As discussed in the previous chapters, electrical discharges at high altitudes transition from a streamer regime to a diffuse glow regime. A solution to this limitation would be to use multiple telescopes and construct a co-aligned array of high-resolution imagers. Such a system would immediately allow the altitude dependence of streamer radius to be measured and would allow the assessment of sprite-to-sprite and storm-to-storm variability. The ultimate telescopic imaging system would use high-speed CCD cameras for each telescope in the array in order to also measure the altitude dependence of the streamer velocity. A database of altitude profiles of such sprite parameters as streamer radius and velocity would greatly enhance the potential usefulness of sprites as atmospheric probes. Sprites occur in a region of the atmosphere that is difficult to measure, falling in between the altitudes reachable by airplanes and those at which satellites can orbit. Rocket measurements, expensive both in time, manpower, and money, provide only single data point altitude profiles and are inherently unsuited for measurements of transient short duration phenomena such as sprites. By contrast, sprites occur frequently and can be observed on many nights throughout a summer. As we have shown in this dissertation, a single storm can produce over 100 sprites. Such high occurrence rates would allow studies of nightly variability of altitude profiles of atmospheric properties (e.g. electron density) on an hourly or minute-to-minute basis.

Bibliography

[*Allis,* 1976] Allis, W. P., Review of glow discharge instabilities, *Physica, 82C,* 43, 1976.

[*Arking,* 1985] Arking, A. and J. D. Childs, Retrieval of cloud cover parameters from multispectral satellite images, *J. Clim. Appl. Meteor., 24,* 322, 1985.

[*Armstrong et al.,* 2000] Armstrong, R. A., D. M. Suszcynsky, and W. A. Lyons, Multi-color photometric measurements of ionization and energies in sprites, *Geophys. Res. Lett., 27,* 653, 2000.

[*Babaeva and Naidis,* 1997] Babaeva, N. Y. and G. V. Naidis, Dynamics of positive and negative streamers in air in weak uniform electric fields, *IEEE Trans. Plasma Sci., 25,* 375, 1997.

[*Barrington-Leigh et al.,* 1999] Barrington-Leigh, C. P., U. S. Inan, M. Stanley, and S. A. Cummer, Sprites triggered by negative lightning discharges, *Geophys. Res. Lett., 26,* 3605-3608, 1999.

[*Barrington-Leigh and Inan,* 2001] Barrington-Leigh, C. P. and U. S. Inan, Identification of sprites and elves with intensified video and broadband array photometry, *J. Geophys. Res., 106,* 1741, 2001.

[*Barrington-Leigh et al.,* 2002] Barrington-Leigh, Christopher P., Victor P. Pasko, and Umran S. Inan, Exponential relaxation of optical emissions in sprites, *J. Geophys. Res., 107,* SIA 6-1, 2002.

[*Bazelyan and Raizer,* 1998] Bazelyan, E. M. and Yu. P. Raizer, Spark Discharge, *CRC Press LLC*, 1998.

[*Bell et al.,* 1998] Bell, Timothy F., Steven C. Reising, and Umran S. Inan, Intense continuing currents following positive cloud-to-ground lightning associate with red sprites, *Geophys. Res. Lett., 25,* 1285, 1998.

[*Boccippio et al.,* 1995] Boccippio, Dennis J., Earle R. Williams, Stan J. Heckman, Walter A. Lyons, Ian T. Baker, and Robert Boldi, Sprites, ELF transients, and positive ground strokes, *Science, 269,* 1088, 1995.

[*Boichenko,* 1996] Boichenko, A. M., On the nature of bead lightning, *Plasma Phys. Reports, 22,* 917, 1996.

[*Burgess and Inan,* 1993] Burgess, W. C. and U. S. Inan, The role of ducted whistlers in the precipitation loss and equilibrium flux of radiation belt electrons, *J. Geophys. Res., 98,* 15,643, 1993.

[*Burke,* 1996] Burke, M. W., *Image acquisition,* Chapman and Hall, London, 1996.

[*Cho and Rycroft,* 2001] Cho, M. and M. J. Rycroft, Non-uniform ionisation of the upper atmosphere due to the electromagnetic pulse from a horizontal lightning discharge, *J. Atmos. Sol. Terr. Phys., 63,* 559, 2001.

[*Cummer,* 1997] Cummer, Steven Andrew, Lightning and ionospheric remote sensing using VLF/ELF radio atmospherics, *thesis,* 1997.

[*Cummer et al.,* 1998] Cummer, S. A., U. S. Inan, T. F. Bell, and C. P. Barrington-Leigh, ELF radiation produced by electrical currents in sprites, *Geophys. Res. Lett., 25,* 8, 1998.

[*Cummer and Inan,* 2000] Cummer, Steven A. and Umran S. Inan, Modeling ELF radio atmospheric propagation and extracting lightning currents from ELF observations, *Radio Sci., 35,* 385, 2000.

[*Cummer and Füllekrug,* 2001] Cummer, Steven. A, and Martin Füllekrug, Unusually intense continuing current in lightning produces delayed mesospheric breakdown, *Geophys. Res. Lett., 28,* 495, 2001.

[*Cummins et al.*, 1998] Cummins, Kenneth L., Martin J. Murphy, Edward A. Bardo, William L. Hiscox, Richard B. Pyle, and Alburt E. Pifer, A Combined TOA/MDF Technology Upgrade of the U.S. National Lightning Detection Network, *J. Geophys. Res., 103*, 9035, 1998.

[*Davies,* 1965] Davies, Kenneth, Ionospheric radio propagation, *National Bureau of Standards Monograph 80,* Washington D. C., 1965.

[*Dejnakarintra and Park,* 1974] Dejnakarintra, M. and C. G. Park, Lightning-induced electric fields in the ionosphere, *J. Geophys. Res., 79,* 1903, 1974.

[*Devins et al.,* 1981] Devins, J. C., S. J. Rzad, and R. J. Schwabe, Breakdown and prebreakdown phenomena in liquids, *J. Appl, Phys., 52,* 4531, 1981.

[*Dhali and Williams,* 1987] Dhali, S. K., and P. F. Williams, Two-dimensional studies of streamers in gases, *J. Appl, Phys., 62,* 4696, 1987.

[*Ferguson et al.,* 1999] Ferguson, J. A., F. P. Snyder, D. G. Morfitt, and C. H. Shellman, Long-wave propagation capability and documentation, *Tech. Doc. 1518,* Naval Ocean Systems Center, San Diego, Calif., 1989.

[*Fishman et al.,* 1994] Fishman, G. J., P. N. Bhat, R. Mallozzi, J. M. Horack, T. Koshut, C. Kouveliotou, G. N. Pendleton, C. A. Meegan, R. B. Wilson, W. S. Paciesas, S. J. Goodman, and H. J. Christian, Discovery of intense gamma-ray flashes of atmospheric origin, *Science, 264,* 1313, 1994.

[*Franz et al.,* 1990] Franz. R. C., R. J. Nemzek, and J. R. Winckler, Television image of a large upward electrical discharge above a thunderstorm, *Science, 249,* 48, 1990.

[*Fukunishi et al.,* 1996a] Fukinishi, H., Y. Takahashi, M. Kubota, K. Sakanoi, U. S. Inan, and W. A. Lyons, Elves: Lightning-induced transient luminous events in the lower ionosphere, *Geophys. Res. Lett, 23,* 2157, 1996a.

[*Fukunishi et al.,* 1996b] Fukinishi, H., Y. Takahashi, M. Fujito, Y. Wanatabe, and S. Sakanoi, Fast imaging of elves and sprites using a framing/streak camera and a multi-anode array photometer, *EOS Trans. AGU, 77, Fall Meet. Suppl.,* F60, 1996b.

[*Füllekrug et al.,* 1996] Füllekrug, Martin, Steven C. Reising, and Walter A. Lyons, On the accuracy of arrival azimuth determination of sprite-associated lightning flashes by Earth-ionosphere cavity resonances, *Geophys. Res. Lett., 23,* 3691, 1996.

[*Füllekrug et al.,* 1998] Füllekrug, Martin, Antony C. Fraser-Smith, and Steven C. Reising, Ultra-slow tails of sprite-associated lightning flashes, *Geophys. Res. Lett., 25,* 3497, 1998.

[*Füllekrug and Constable,* 2000] Füllekrug, Martin and Steven Constable, Global triangulation of intense lightning discharges, *Geophys. Res. Lett., 27,* 333, 2000.

[*Gerken et al.,* 2000] Gerken, E. A., U. S. Inan, and C. P. Barrington-Leigh, Telescopic imaging of sprites, *Geophys. Res. Lett., 27,* 2637, 2000.

[*Gerken and Inan,* 2002] Gerken, E. A. and U. S. Inan, A survey of streamer and diffuse glow dynamics observed in sprites using telescopic imagery, *J. Geophys. Res., 107,* SIA 4-1, 2002.

[*Gerken and Inan,* 2003] Gerken, Elizabeth A. and Umran S. Inan, Observations of decameter-scale morphologies in sprites, *J. of Atmos. and Sol. Terr. Phys., 65,* 567, 2003.

[*Gerken et al.,* 2003] Gerken, E. A., U. S. Inan, T. R. Pedersen, C. A. Selcher, M. McCarrick, J. Pau, Temporal development of HAARP-induced magnetic zenith airglow enhancements, *Geophys. Res. Lett., in review,* 2003.

[*Hale,* 1994] Hale, Leslie C., Coupling of ELF/ULF energy from lightning and MeV particles to the middle atmosphere, ionosphere, and global circuit, *J. Geophys. Res., 99,* 21,089, 1994.

[*Hardman et al.,* 2000] Hardman, Simon F., Richard L. Dowden, James B. Brundell, and John L. Bahr, Sprite observations in the Northern Territory of Australia, *J. Geophys. Res., 105,* 4689, 2000.

[*Holzworth et al.,* 1985] Holzworth, R. H., M. C. Kelley, C. L. Siefring, L. C. Hale, and J. D. Mitchell, Electrical measurements in the atmosphere and the ionosphere over an active thunderstorm: 2. Direct current electric fields and conductivity, *J. Geophys. Res., 90*, 9824, 1985.

[*Hu and Cummer,* 2002] Hu, Wenyi and Steven A. Cummer, Lightning charge moment changes for the initiation of sprites, *Geophys. Res. Lett., 29,* 120-1, 2002.

[*Inan et al.,* 1985] Inan, U. S., D. L. Carpenter, R. A. Helliwell, and J. P, Katsufrakis, Subionospheric VLF/LF phase perturbations produced by lightning-whistler induced particle precipitation, *J. Geophys. Res., 90,* 7457, 1985.

[*Inan et al.,* 1991] Inan, U. S., T. F. Bell, and J. V. Rodriuez, Heating and ionization of the lower ionosphere by lightning, *Geophys. Res. Lett., 18*, 705, 1991.

[*Inan et al.,* 1995] Inan, U. S., T. F. Bell, V. P. Pasko, D. D. Sentman, E. M. Wescott, and W. A. Lyons, VLF signatures of ionospheric disturbances associated with sprites, *Geophys. Res. Lett., 22,* 3461, 1995.

[*Inan et al.,* 1996] Inan, U. S., A. Slingeland, V. P. Pasko, and J. V. Rodriguez, VLF and LF signatures of mesospheric/lower ionospheric response to lightning discharges, *J. Geophys. Res., 101,* 5219, 1996.

[*Inan et al.,* 1997] Inan, U. S., C. Barrington-Leigh, S. Hansen, V. S. Glukhov, T. F. Bell, and R. Rairden, Rapid lateral expansion of optical luminosity in lightning-induced ionospheric flashes referred to as 'elves', *Geophys. Res. Lett., 24,* 583, 1997.

[*Inan and Inan,* 2000] Inan, Umran S. and Aziz S. Inan, Electromagnetic Waves, *Prentice Hall:Upper Saddle River, NJ,* 2000.

[*Kraus,* 1992] Kraus, J. D., Electromagnetics, *McGraw-Hill:New York,* 1992.

[*Kulikovsky,* 1997] Kulikovsky, A. A., Positive streamer between parallel plate electrodes in atmospheric pressure air, *J. Phys. D: Appl, Phys., 30,* 441, 1997.

[*Lehtinen et al.,* 2001] Lehtninen, N.G., U.S. Inan, and T.F. Bell, Effects of thunderstorm-driven runaway electrons in the conjugate hemisphere: purple sprites, ionization enhancements, and gamma rays, *J. Geophys. Res., 106*, A12, 28, 841, 2001.

[*Lyons,* 1994] Lyons, Walter A., Low-light video observations of frequent luminous structures in the stratosphere above thunderstorms, *Monthy Weather Rev., 122,* 1940, 1994.

[*Lyons,* 1996] Lyons, W.A., Sprite observations above the U. S. High Plains in relation to their parent thunderstorm systems, *J. Geophys. Res., 101*, 29641, 1996.

[*Lyons et al.,* 2003] Lyons, Walter A., CCM, Thomas E. Nelson, Russell A. Armstrong, Victor P Pasko, and Mark A. Stanley, Upward electrical discharges from thundercloud tops, *Am. Meterological Soc.,* 445, 2003.

[*Marshall et al.,* 2001] Marshall, Thomas C., Maribeth Stolzenburg, W. David Rust, Earle R. Williams, and Robert Boldi, Positive charge in the stratiform cloud of a mesoscale convective system, *J. Geophys. Res., 106,* 1157, 2001.

[*Massala and Lesaint,* 2001] Massala, G. and O. Lesaint, A comparison of negative and positive streamers in mineral oil at large gaps, *J. Phys. D: Appl, Phys., 34,* 1525, 2001.

[*Mishin,* 1997] Mishin, Evgeny, Ozone layer perturbation by a single blue jet, *Geophys. Res. Lett., 24,* 1919, 1997.

[*Morrill et al.,* 2002] Morrill, J., E. Buscela, C. Siefring, M. Heavner, S. Berg, D. Moudry, S. Slinker, R. Fernsler, E. Wescott, D. Sentman, and D. Osborne, Electron energy and electric field estimates in sprites derived from ionized and neutral N2 emissions, *Geophys. Res. Lett., 29,* 100-1, 2002.

[*Neubert et al.,* 2001] Neubert, T., T. H. Allin, H. Stenbaek-Nielsen, and E. Blanc, Sprites over Europe, *Geophys. Res. Lett., 28,* 3585, 2001.

[*Pasko and Inan*, 1994] Pasko, V. P., and U. S. Inan, Recovery signatures of lightning-associated VLF perturbations as a measure of the lower ionosphere, *J. Geophys. Res., 101*, 15,737, 1994.

[*Pasko et al.,* 1996] Pasko, V. P., U. S. Inan, and T. F. Bell, Blue jets produced by quasi-electrostatic pre-discharge thundercloud fields, *Geophys. Res. Lett., 23,* 301, 1996.

[*Pasko et al.,* 1997] Pasko, V. P., U. S. Inan, and T. F. Bell, Sprites produced by quasi-electrostatic heating and ionization in the lower ionosphere, *J. Geophys. Res., 102,* 4529, 1997.

[*Pasko et al.,* 1998] Pasko, V. P., U. S. Inan, and T. F. Bell, Spatial structure of sprites, *Geophys. Res. Lett., 25,* 2123, 1998.

[*Pasko et al.,* 1999] Pasko, V. P., U. S. Inan, and T. F. Bell, Mesospheric electric field transients due to tropospheric lightning discharges, *Geophys. Res. Lett., 26,* 1247, 1999.

[*Pasko et al.,* 2000] Pasko, V. P., U. S. Inan, and T. F. Bell, Fractal structure of sprites, *Geophys. Res. Lett., 27,* 497, 2000.

[*Pasko et al.,* 2001] Pasko, Victor P., Umran S. Inan, and Timothy F. Bell, Mesospheric-troposphere coupling due to sprites, *Geophys. Res. Lett., 28,* 3821, 2001.

[*Pasko and Stenbaek-Nielsen,* 2002] Pasko, Victor P. and Hans C. Stenbaek-Nielsen, Diffuse and streamer regions of sprites, *Geophys. Res. Lett., 29,* 82-1, 2002a.

[*Pasko et al.,* 2002] Pasko, Victor P., Mark A. Stanley, John D. Matthews, Umran S. Inan, and Troy G. Wood, Electrical discharge from a thundercloud top to the lower ionosphere, *Nature, 416,* 152, 2002b.

[*Pasko and George,* 2002] Pasko, Victor P. and Jeremy J. George, Three-dimensional modeling of blue jets and blue starters, *J. Geophys. Res., 107,* SIA 12-1, 2002c.

[*Pedersen et al.,* 2001] Pedersen, Todd R., and Herbert C. Carlson, First observations of HF heater-produced airglow at the High Frequency Active Auroral Research Program facility: thermal excitation and spatial structuring, *Radio Sci., 36,* 1013, 2001.

[*Petrov and Petrova,* 1999] Petrov, N. I. and G. N. Petrova, Physical mechanisms for the development of lightning discharges between a thundercloud and the ionosphere, *Tech. Phys., 44,* 472, 1999.

[*Raizer,* 1991] Raizer, Y. P., Gas Discharge Physics, *Springer-Verlag Berlin Heidelberg,* 1991.

[*Raizer et al.,* 1998] Raizer, Y. P., G. M. Milikh, M. N. Shneider, and S. V. Novakovski, Long streamers in the upper atmosphere above thundercloud, *J. Phys. D: Appl, Phys., 31,* 3255, 1998.

[*Reising et al.,* 1996] Reising, Steven C., Umran S. Inan, Timothy F. Bell, and Walter A. Lyons, Evidence for continuing current in sprite-producing cloud-to-ground lightning, *Geophys. Res. Lett., 23,* 3639, 1996.

[*Reising,* 1998] Reising, Steven Craig, Remote sensing of the electrodynamic coupling between thunderstorm systems and the mesosphere/lower ionosphere, *thesis*, 1998.

[*Reising et al.,* 1999] Reising, Steven C., Umran S. Inan and Timothy F. Bell, ELF sferic energy as a proxy indicator for sprite occurrence, *Geophys. Res. Lett., 26,* 987, 1999.

[*Sentman et al.,* 1995] Sentman, D. D., E. M. Wescott, D. L. Osborne, D. L. Hampton, and M. J. Heavner, Preliminary results from the Sprites94 aircraft campaign: Red sprites, *Geophys. Res. Lett., 22,* 1209, 1995.

[*Sentman et al.,* 1996] Sentman, D. D., E. M. Wescott, M. J. Heavner, and D. R. Moudry, Observations of sprite beads and balls, *EOS Trans. AGU, 77, Fall Meet. Suppl.,* F61, 1996.

[*Stanley et al.,* 1996] Stanley, M., P. Krehbiel, W. Rison, C. Moore, M. Brook, and O. H. Vaughn, Observations of sprites and jets from Langmuir Laboratory, New Mexico, *EOS Trans, AGU, 77, Fall Meet. Suppl.,* F69, 1996.

[*Stanley et al.,* 1999] Stanley, M. P., P. Krehbiel, M. Brook, C. Moore, and W. Rison, High speed video of initial sprite development, *Geophys. Res. Lett., 26,* 3201, 1999.

[*Stenbaek-Nielsen et al.,* 2000] Stenbaek-Nielsen, H. C., D. R. Moudry, E. M. Wescott, D. D. Sentman, and F. T. Sao Sabbas, Sprites and possible mesospheric effects, *Geophys. Res. Lett., 27,* 3829, 2000.

[*Stewart,* 1956] Stewart, A. B., Oscillating glow discharge plasma, *J. Appl, Phys., 27,* 911, 1956.

[*Su et al.,* 2003] Su, H. T., R. R. Hsu, A. B. Chen, Y. C. Wang, W. S. Hsiao, W. C. Lai, L. C. Lee, M. Sato, H. Fukunishi, Gigantic jets between a thundercloud and the ionosphere, *Nature, 423,* 974, 2003.

[*Sukhorukov et al.,* 1996] Sukhorukov, A. I., E. V. Mishin, P. Stubbe, and M. J. Rycroft, On blue jet dynamics, *Geophys. Res. Lett., 23,* 1625, 1996.

[*Taranenko et al.,* 1992] Taranenko, Y. N., U. S. Inan, and T. F. Bell, Optical signatures of lightning-induced heating of the D region, *Geophys. Res. Lett., 19,* 1815, 1992.

[*Taranenko et al.,* 1993] Taranenko, Y. N., U. S. Inan, and T. F. Bell, The interaction with the lower ionosphere of electromagnetic pules from lightning: Excitation of optical emissions, *Geophys. Res. Lett., 20,* 2675, 1993.

[*Taranenko and Roussel-Dupré,* 1996] Taranenko, Yuri and Robert Roussel-Dupré, High altitude discharges and gamma-ray flashes: a manifestation of runaway air breakdown, *Geophys. Res. Lett., 23,* 571, 1996.

[*Taylor and Clark,* 1996] Taylor, M. J., and S. Clark, High resolution CCD and video imaging of sprites and elves in the N2 first positive band emission, *EOS Trans. AGU, 77, Fall Meet. Suppl.,* F60, 1996.

[*Teslenko,* 1982] Teslenko, V. S., Effect of stimulated scattering on the spatial structure of laser breakdown in liquids, *Sov. Tech. Phys. Lett., 8,* 33, 1982.

[*Teuber,* 1993] Teuber, J., *Digital Image Processing,* New York: Prentice Hall, 1993.

[*Uman,* 1969] Uman, Martin A., Lightning, *Dover Publications, Inc.,* 1969.

[*Valdivia et al.,* 1997] Valdivia, J. A., G. Milikh, and K. Papadopoulos, Red sprites: lightning as a fractal antenna, *Geophys. Res. Lett., 24,* 3169, 1997.

[*van Veldhuizen et al.,* 2002] van Veldhuizen, E. M., A. H. F. M. Baede, D. Hayashi, and W. R. Rutgers, Fast imaging of streamer propagation, *Spring Meeting on Diagnostics of Non-Equilibrium High Pressure Plasmas*, Bad Honnef, Germany, 2001.

[*Veronis et al.,* 1999] Veronis, Georgios, Victor P. Pasko, and Umran S. Inan, Characteristics of mesospheric optical emissions produced by lightning discharges, *J. Geophys. Res., 104,* 12,645, 1999.

[*Vitello et al.,* 1994] Vitello, P. A., B. M. Penetrante, and J. N. Bardsley, Simulation of negative-streamer dynamics in nitrogen, *Phys. Rev. E, 49,* 5574, 1994.

[*Wescott et al.,* 1995] Wescott, E. M., D. Sentman, D. Osborne, D. Hampton, and M. Heavner, Preliminary results from the Sprites94 aircraft campaign: 2. Blue jets, *Geophys. Res. Lett., 22,* 1209, 1995.

[*Wescott et al.,* 1998] Wescott, E. M., D. D. Sentman, M. J. Heavner, D. L. Hampton, W. A. Lyons, and T. Nelson, Observations of 'Columniform' sprites, *J. Atmos. Sol. Terr. Phys., 60,* 733, 1998.

[*Wescott et al.,* 2001] Wescott, E. M., H. C. Stenbaek-Nielsen, D. D. Sentman, M. J. Heavner, D. R. Moudry, and F. T. Sao Sabbas, Triangulation of sprites, associated halos, and their possible relation to causative lightning and micrometeors, *J. Geophys. Res., 106,* 10,467, 2001.

[*Winckler,* 1995] Winckler, J. R., Further observations of cloud-ionosphere electrical discharges above thunderstorms, *J. Geophys. Res., 100, 14,* 335, 1995.

[*Winckler et al.,* 1996] Winckler, J. R., W. A. Lyons, T. E. Nelson, R. J. Nemzek, New high-resolution ground- based studies of sprites, *J. Geophys. Res., 101,* 6997, 1996.

[*Yamada et al.,* 1990] Yamada, H., T. Sato, and T. Fujiwara, High-speed photography of prebreakdown phenomena in dielectrc liquids under highly non-uniform field conditions, *J. Phys. D: Appl, Phys., 23,* 1715, 1990.

[*Yi and Williams,* 2002] Yi, Won J. and P. F. Williams, Experimental study of streamers in pure N_2 and N_2/O_2 mixtures and a $\sim$13 cm gap, *J. Phys. D: Appl. Phys., 35,* 205, 2002.

[*Yukhimuk et al.,* 1998] Yukhimuk, V., R. A. Roussel-Dupré, E. M. D. Symbalisty, and Y. Taranenko, Optical characteristics of blue jets produced by runaway air breakdown, simulation results, *Geophys. Res. Lett., 25,* 3289, 1998.

[*Zabotin and Wright,* 2001] Zabotin N. A. and J. W. Wright, Role of meteoric dust in sprite formation, *Geophys. Res. Lett., 28,* 2593, 2001.

[*Zobov and Siderov,* 1990] Zobov, E. A. and A. N. Siderov, Beaded structure of discharge during breakdown in a nonuniform field, *J. Appl. Mech. And Tech. Phys., 31,* 16, 1990.